NASA CONTRACTOR REPORT 166442 - vol. I

ADVANCED PREDICTION TECHNIQUE FOR THE LOW SPEED AERODYNAMICS OF V/STOL AIRCRAFT, VOL. I

(NASA-CR-166442-Vol-1) ADVANCED PREDICTION TECHNIQUE FOR THE LOW SPEED AERODYNAMICS OF V/STOL AIRCRAFT. VOLUME 1: TECHNICAL DISCUSSION Final Report, Mar. 1982 - Mar 1983 (Vought Corp., Dallas, Tex.) 148 p G3/02

N84-26662

Unclas 13928

T. D. Beatty and M. K. Worthey

CONTRACT NAS2- 11156

March 1983

NASA

NASA CONTRACTOR REPORT 166442

ADVANCED PREDICTION TECHNIQUE FOR THE LOW SPEED AERODYNAMICS OF V/STOL AIRCRAFT, VOL. I

T. D. Beatty
M. K. Worthey

Vought Corporation
P. O. Box 225907
Dallas, TX 75265

Prepared for
Ames Research Center
under Contract NAS2-11156

National Aeronautics and
Space Administration

Ames Research Center
Moffett Field, California 94035

FORWARD

A study was conducted for the NASA AMES Research Center by the Vought Corporation to develop improved methodologies for predicting the propulsive induced aerodynamics of V/STOL aircraft in Transition/STOL flight. The study was performed under NASA AMES as a contract monitor. The Vought efforts in this program were accomplished under the direction of Mr. T.D. Beatty who was the Principal Investigator for this contract. He was assisted on the contract by Mr. M.K. Worthey. Both personnel are from the Flight Technologies directorate of the Vought Corporation.

The authors are particularly indebted to Mrs. D.L. Lewis and Mr. J.W. McCharen for their support in the programming of the computer code.

This report consists of two volumes. The technical discussion of the methodology, verification of the techniques and conclusions and recommendations are presented in Volume I. Volume II is a detailed user's manual for the computer code developed.

TABLE OF CONTENTS

TABLE OF CONTENTS (Cont.)

LIST OF ILLUSTRATIONS

Page intentionally left blank

LIST OF SYMBOLS

SYMBOLS	DEFINITION
a	Constant used in equation 3.3.2-1
AR	Aspect ratio of lifting surface
A_R	Aspect ratio of rectangular jet nozzle length/width
b	Constant used in equation 3.3.2-1
b/2	Semi span of wing
c	Constant used in equation 3.3.2-1
c	Chord length local
c_{mac}	Mean aerodynamic center chord length
C_L	Lift coefficient
C_m	Pitching moment coefficient
C_N	Total normal force coefficient
C	Local normal force coefficient
CP	Control point
Cp	Specific heat at constant pressure
C_p	Pressure coefficient
C_R	Wing root chord length
C_T	Wing tip chord length
C_V	Specific heat at constant volume
d, D	Jet diameter or equivalent jet diameter - diameter of jet with area equal to total area of all jets
E	Mass entrainment per unit length
H	Height above ground
h	Specific enthalpy
ho	Lateral spacing, equation 3.3.2-2
L	Lift
L/T	Ratio of lift to thrust

SYMBOLS	DEFINITION
M	Mach number
R	Jet velocity ratio V_{JET}/V
r	Radius
R_X	Reynolds number based on surface distance
R_N	Reynolds number based on chord
$R_{\theta_{TR}}$	Reynolds number based on boundary layer momentum thickness
S	Surface distance
T	Thrust
u	Velocity inside boundary layer
U_e	Velocity at edge of boundary layer
U	Velocity
U, U'	Induced velocity vectors in axial direction
V	Velocity
V_t	Total inviscid tangential velocity
V, V'	Induced velocity vector in vortical direction
X_1	Location of max derivative in jet equation (3.3.2-5)
X	Distance in downstream direction
Xo	X location where Weston jet curve is tangent to δ_j
Y	Distance in lateral direction
Yo	Y location where Weston jet curve is tangent to δ_j
Y_1	Location at max derivative in jet equation (3.3.2-5)
Z	Distance in vertical direction

GREEK SYMBOLS

α	Angle of Attack
αJET_{IM}	Angle of Jet Relative to Ground Plane At Impingement
βho	Term Used in Equation 3.3.2-2
γ	Ratio of Specific Heats Cp/Cv
Λ	Sweep Angle
η	Percent Semispan
λ	Taper Ratio C_T/C_R
δ^*	Boundary Layer Displacement Thickness
δ_J	Jet Injection Angle
ν	Kenematic Viscosity

SUBSCRIPTS

Symbol	Definition
J	Jet Exit, Jet
N	Normal Direction
S	Separation
∞	Freestream Conditions
T.E.	Trailing Edge

1.0 SUMMARY

A computerized prediction method for propulsive induced forces and moments in transition and short takeoff and landing (STOL) flight has been improved and evaluated for the NASA AMES Research Center under Contract Number NAS 2-11156. Earlier development of this method was funded under IR and D and by the Naval Air Development Center (NADC) and is known as the Vought V/STOL Aircraft Propulsive Effects computer program (VAPE).

The VAPE program is capable of evaluating:

- Effects of relative wind about an aircraft
- Effects of propulsive-lift jet entrainment, vorticity, and flow blockage
- Effects of engine inlet flow on the aircraft flow field
- Engine inlet forces and moments including inlet separation
- Ground effects in the STOL region of flight
- Viscous effects on lifting surfaces

The effects of relative wind about an aircraft with or without jets and/or inlet effects is determined by a three-dimensional potential flow panel method.

The effects of the propulsive lift jets are determined by one of three different jet models which have been extensively modified and/or developed at Vought.

The effects of engine inlet flow on the aircraft is determined by a NASA Lewis code for axisymmetric inlets which has been modified and automated at Vought. This method determines the pressures on the inlet face and nacelle inlet lips. The VAPE program then utilizes these pressures to determine the forces and moments acting on the inlet. Calculations may also be done to determine when and where separation occurs on the inlet lip.

The effects of viscosity on the lifting surfaces is determined by using a two-dimensional finite difference boundary layer code in a "strip" approach.

The various options of the VAPE program have been verified by comparisons between calculated and experimental values.

A computer code was delivered to NASA AMES and made operational on the NASA CDC 7600 computer. A user's manual for this program is contained in Volume II of this report.

2.0 INTRODUCTION

Configuration concepts for STOL and/or V/STOL missions employ various arrangements of deflected thrust devices to obtain the required vertical force increment. The experimental data on STOL and V/STOL configurations indicate that sizable propulsion induced force and moment characteristics on the vehicle can occur due to the reaction between these deflected thrust vectors and the freestream air. The induced flow around a jet V/STOL aircraft depends upon the flight speed of the vehicle, its height above the ground, and the deflection and placement of the jets on the aircraft.

During flight of a V/STOL aircraft in the transition mode, jet induced pressures and downwash on the aircraft can cause a significant change in lift. This lift tends to increase with increasing forward velocity. A nose-up pitching moment is often caused by the jet induced effects, and this moment also increases with increasing speed. Downwash induced at the horizontal tail and on the wing can cause trim changes and stability problems. In addition, the low pressures which cause a nose-up pitching moment also produce a rolling moment in a sideslip or crosswind condition.

The presence of these jet induced effects poses a problem to the aircraft designer in the conceptual or preliminary design stage, since the designer must account for all these propulsive induced effects to obtain the best performance.

These propulsive induced effects have caused considerable efforts to be expended throughout the aircraft industry to develop analytical and empirical prediction methods. Most of these efforts have been concentrated into two basic categories: (1) In Ground Effect (IGE), and (2) Out of Ground Effect (OGE). Various techniques have been developed to simulate the propulsive jet and its influence upon the aircraft.

The objectives of this contract effort were to improve and evaluate a computational aerodynamic method for predicting the flow field about a V/STOL aircraft in the transition or STOL regions of flight. The tasks proposed consisted of the following:

(1) Addition of viscous effects capability for lifting surfaces to the VAPE system.

(2) Evaluation of this viscous capability.

(3) Verification of the Vought STOL model by comparisons of experimental data to calculated results.

(4) Determination of VAPE applicability to VATOL configurations.

(5) Substantiation of the VAPE rectangular Jet model.

The method to be improved was originally developed by Vought IR and D and under contract to the Naval Air Development Center and is known as the Vought V/STOL Aircraft Propulsive Effects program (VAPE).

The objectives were accomplished through modifications and extensions of the VAPE program and through extensive evaluation of the program options. This improved VAPE contains a combination of programs that provides a reliable, accurate and versatile design procedure for V/STOL and STOL aircraft.

3.0 V/STOL AIRCRAFT PROPULSIVE EFFECTS PROGRAM (VAPE)

The Vought Aircraft Propulsive Effects program (VAPE), Reference 3.0-1 has been improved under this contracted effort by the addition of a capability to determine viscous effects on lifting surfaces. Thus, VAPE is now a union of seven computational techniques: (1) The Hess Three-Dimensional Analysis Program, (2) The Vought/Stockman Inlet Analysis Program, (3) The Vought/Wooler Jet Model, (4) The Vought/Weston Jet Model (5) The Thames Rectangular Jet Model, (6) The Vought STOL Module, and (7) The Viscous Module. A short description of VAPE is presented in Section 3.1 through 3.4. A more detailed description may be found in Reference 3.0-1.

These programs are used in conjunction with geometry models to form a very general and efficient program for determining the propulsive induced effects. A schematic of the program options and the basic program logic is presented in Figure 3.0-1. The geometry module is a separate system of computer programs which are linked to the VAPE program by data transfer files. The configuration geometry is digitized using the geometry module which is then input to the Hess potential flow program where the actual aerodynamic characteristics of the aircraft are determined.

Inlet effects are based on inlet velocities determined in one of two ways. The first is simply to input one value of inlet velocity which is then used at all of the inlet panel control points. The second requires that the nacelle geometry be input to the Vought/Stockman inlet module. The inlet module determines the velocity on the inlet face needed to obtain the specified mass flow through the nacelle. These velocities are then transferred to the Hess program to be used as boundary conditions on the inlet face.

Jet induced aerodynamic effects are determined by computing the velocities induced on the model panels by one of the available jet models. These velocities are then converted to a normal velocity acting at the centroid of each panel to be used as boundary conditions in Hess. The Vought STOL module is used when the aircraft is near the ground. This model determines induced velocities on the ground plane produced by the wall jet formed when the jet impinges the ground. These induced velocities are input to the Hess program together with the induced velocities on the aircraft panels. The Hess solution is then executed with the above boundary conditions producing the aerodynamic forces on the aircraft which include inlet jet exhaust effects, and if necessary, the ground plane effects. In the program presented in this document, the predicted pressures on the lifting surfaces are input to a boundary layer code where the displacement thickness distribution, δ^*, is determined. These displacement thickness values are then used to generate a "viscous" solution as discussed in section 4.0

Reference

3.0-1 Beatty, T. D. and Kress, S. S., "Prediction Methodology or Propulsive Induced Forces and Moments of V/STOL Aircraft in Transition/STOL Flight", Naval Air Development Center Report NADC-77119-30, July 1979.

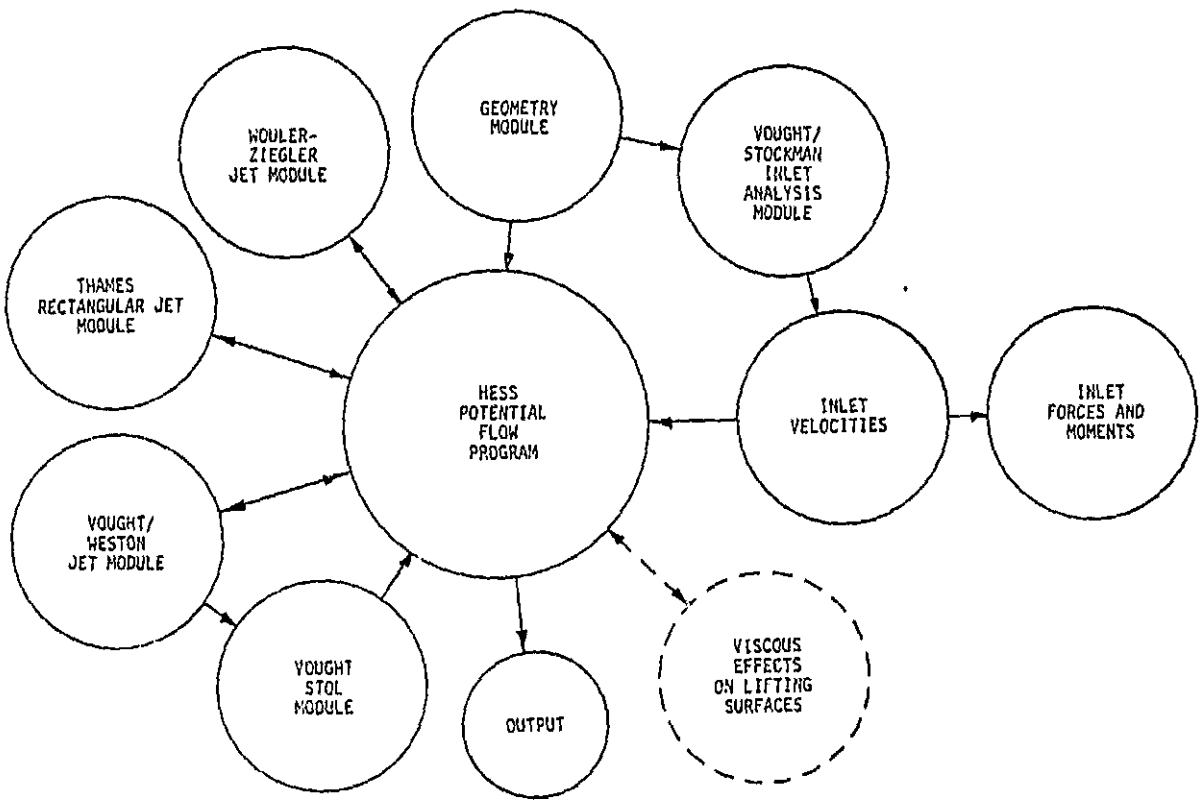

FIGURE 3-1 VAPE PROGRAM STRUCTURE

3.1 POTENTIAL FLOW SOLUTION

The calculation of propulsive induced effects requires a sophisticated three-dimensional potential flow technique due to the importance of properly modeling fuselage geometry. In the VAPE system, the method selected is the Hess three-dimensional lifting potential flow program, references 3.1-2 and 3.1-3. This program is well documented and has proven to be very accurate and reliable through several years of usage. The code has been selected for use by several government agencies and industrial companies due to versatility and ease of application. The formulization of the Hess program is fairly well known throughout the industry and so no detail will be presented in this document. If further details are desired they can be obtained from references 3.1-1 through 3.1-3.

The Hess program has been modified at Vought in order to improve computational efficiency. The input and output have been modified and the machine storage space has been reduced. In addition, the computational time has been reduced due to various changes in the program code. None of these changes, however, effect the basic formulation of the program. Also, the Gothert compressibility algorithm has been incorporated into the Hess program along with an option to allow flow-through boundary conditions, i.e., V_N at the control point may be different than zero on any panel. This latter option is necessary for modeling inlets and accounting for jet induced effects.

In summary, the Hess program contained in the VAPE system is a powerful tool for analysing V/STOL configurations with or without jets operating.

REFERENCE

3.1-1 Beatty, T.D., and Kress, S. S., "Prediction Methodology for Propulsive Induced Forces and Moments of V/STOL Aircraft In Transition/STOL Flight," Naval Air Development Center Report, NADC-77119-30, July 1979.

3.1-2 Hess, J.L., "The Problem of Three-Dimensional Lifting Potential Flow and its Solution by Means of Surface Singularity Distribution," Computer Methods in Applied Mechanics and Engineering, Vol. 4, 1974, North Holland Publishing Co.

3.1-3 Hess, J. L., "Calculation of Potential Flow about Arbitrary Three-Dimensional Lifting Bodies," Final Technical Report, McDonnell Douglas Report No. MDC 55679-01, Oct. 1972, also AD755480.

3.2 INLET ANALYSIS METHOD

In order to properly model the entire flow field about a V/STOL aircraft, the effects produced by the flow entering the inlet and the forces and moments on the inlet itself must be determined. Several years ago, N. O. Stockman of NASA Lewis Research Center developed an analytical technique to calculate the flow in and around subsonic axisymmetric inlets, reference 3.2-1, including first order viscous effects.

This technique provides a valuable tool for estimating the performance and optimization of lip shapes for V/STOL and conventional inlets. In Stockman's approach, the potential flow solution was performed and the resulting pressures on the internal surfaces were corrected for compressibility. These pressures, along with the original geometry, were then input to the boundary layer program to obtain the desired viscous parameters. The displacement thickness, δ^*, was then added, by hand, to the original geometry and the process repeated to obtain the viscous effects on the flow field.

As shown in Figure 3.2-1, these programs were combined by Vought into a single iterative computer code, reference 3.2-2. This code has proven to be an excellent way to screen preliminary inlet designs and, thereby, to reduce the scope of expensive inlet parametric test programs. This code has been modified further to calculate the inlet ram forces and moments.

Results from analytical studies and from limited test data indicate the forces and moments induced by the inlets can significantly influence the aerodynamic control power requirements for V/STOL aircraft, specifically during transitional flight and at high angles of inlet incidence such as with tilt nacelle configurations. Thus, correct estimation of these forces and moments is important.

Inlet forces and moments due to the entering stream tube are a vector sum of the forces and moments created by ram drag and additive drag at a specified engine power setting, angle of inlet incidence, and flight speed.

The force and moment analysis for each inlet operating condition is conducted in two specific steps. First, the combined inlet analysis routine in VAPE is used to calculate pressures on the inlet lip and velocities of the fluid within the inlet duct. Forces and torques imposed on the lip by these pressures, as well as effluxes of momentum and angular momentum in the duct across a plane normal to the axis at the throat, are calculated by the inlet force and moment subroutines in VAPE. Proper accounting of these parameters yields the inlet forces and moments for specific configurations.

REFERENCES:

3.2-1 Stockman, N. O., "Potential and Viscous Flow in VTOL, STOL, or CTOL Propulsion System Inlets," AIAA Paper No. 75-1186, Sept. 1975.

3.2-2 Ybarra, A. H., Rhoades, W. W. and Stockman, N. O., "A Combined Potential and Viscous Flow Solution for V/STOL Engine Inlets," AIAA Paper No. 78-142, Jan. 1978.

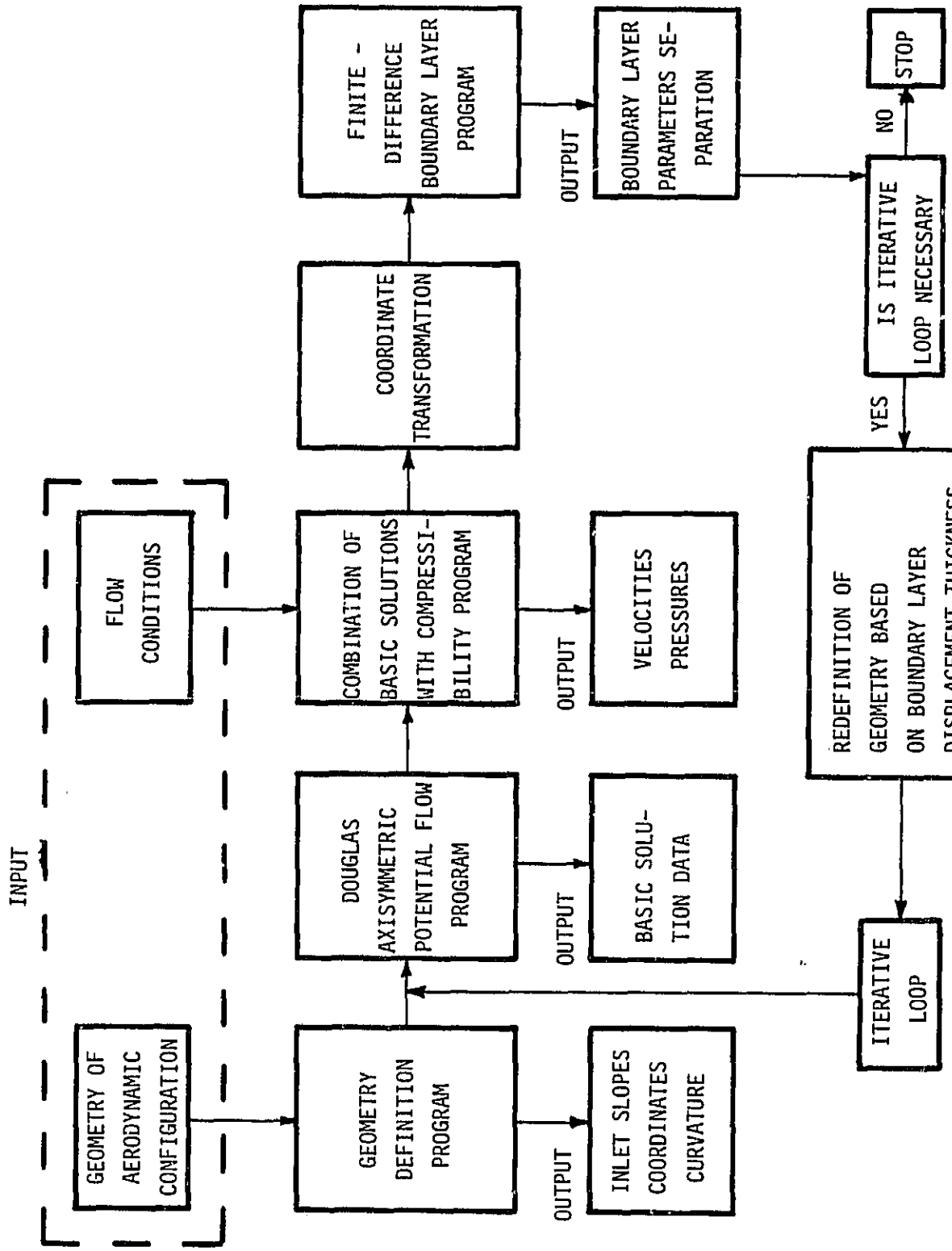

FIGURE 3.2-1 VOUGHT COMBINED POTENTIAL FLOW AND BOUNDARY LAYER PROGRAM

3.3 JET METHODS

The high velocity airstream exiting from a jet nozzle into a subsonic crosswind has a high level of momentum which enables the jet to penetrate the crossflow in essentially an inviscid fashion. At this point, the jet appears to be a solid obstruction to the crossflow. However, as the jet penetrates the crossflow further, it entrains low momentum fluid. In addition, viscous effects begin to erode momentum of the primary jet flow. As velocity in the jet plume falls off, the jet decays in the direction of crossflow and eventually becomes parallel to the crossflow. This flow field is shown in Figure 3.3-1. This interaction basically results in the jet spreading, deforming, and deflecting, while the crossflow is displaced and entrained into the jet. In addition, a wake region is formed behind the jet at the jet exit.

There have been several jet models developed which are applicable to this flight regime. The method of Weston, Wooler and Wu are described in references 3.3-1 through 3.3-4.

All of these methods predict the jet induced flow fields, flow outside the jet efflux, based on some empirical information. These models have the common feature of using a potential flow representation for the jet induced flow field. They differ in how the flow effects caused by the jet are represented and in which factors (i.e., blockage, entrainment or wake effect) received the most attention in the analysis.

Among the best of these techniques from the viewpoint of simplicity and applicability are the methods of Wooler, reference 3.3-5 and Fearn, Dietz, Sellers and Weston, references 3.3-6 through 3.3-9. The VAPE system contains these jet simulation techniques, along with a new method developed by Thames (reference 3.3-10) for rectangular jets. Any of these methods may be selected to be used simply by setting an input flag to a different value. The jet methods and modifications made to them will be discussed in the following sections.

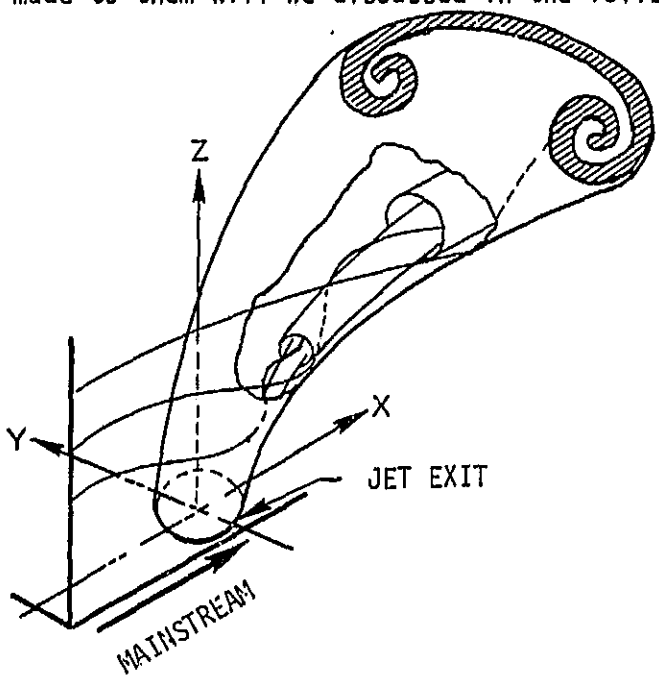

FIGURE 3.3-1 SCHEMATIC OF FORMATION OF CONTRA-ROTATING VORTICES CREATED BY THE JET ISSUING INTO A CROSSFLOW

REFERENCES:

3.3-1 Weston, R. P., "A Description of the Vortex Pair Associated with a Jet in a Crossflow," presented at Navy Workshop on Prediction Methods for Jet V/STOL Propulsion Aerodynamics, Washington, D.C., July 28-31, 1975.

3.3-2 Wooler, P.T., Kao, H.C., Schwendemann, M.F., Wasson, H.R. and Ziegler, H., "V/STOL Aircraft Aerodynamic Prediction Methods Investigation, Volume I. Theoretical Development of Prediction Methods," Air Force Flight Dynamics Laboratory, AFFDL-TR-72-26, Volume I, January 1972.

3.3-3 Wooler, P.T., Burghart, G.H. and Gallagher, J.T., "Pressure Distribution on a Rectangular Wing with a Jet Exhausting Normally into an Airstream," Journal of Aircraft, Vol. 4, No. 6, pp. 537-543, Nov.-Dec. 1967.

3.3-4 Wu, J.C., McMahon, H.M., Mosher, D.K. and Wright, M.A., "Experimental and Analytical Investigations of Jets Exhausting into a Deflecting Stream," Journal of Aircraft, Vol. 7, No. 1, pp. 44-51, Jan.-Feb. 1970.

3.3-5 Wooler, P.T. and Ziegler, H., "An Analytical Model for the Flow of Multiple Jets into an Arbitrary Directed Crossflow in Ground Effect," AIAA Paper 70-545 presented at the AIAA Atmospheric Flight Mechanics Conference, Tullahoma, Tenn., 1970.

3.3-6 Fearn, R. and Weston, R.P., "Vorticity Associated with a Jet in a Crossflow," AIAA Journal, Vol. 12, Number 12, Dec. 1974.

3.3-7 Sellers, W.L., "A Model for the Vortex Pair Associated with a Jet in a Crossflow," Masters Thesis, University of Florida, 1975.

3.3-8 Dietz, W.E., "A Method for Calculating the Induced Pressure Distribution Associated with a Jet in a Crossflow," Masters Thesis, University of Florida, 1975.

3.3-9 Fearn, R.L., Drausche, D. and Weston, R.P., "A Round Jet in a Crossflow - The Influence of Jet Injection Angle on Vortex Properties," to be published by AIAA.

3.3-10 Thames, F.C., "Development of an Analytical Model to Predict Induced Effects on Aspect Ratio 4.0 Rectangular Nozzles in a Subsonic Crossflow," Vought Report No. 2-53110/9R-52268, October 1979.

3.3.1 Wooler Jet Method

The version of the Wooler jet model contained in VAPE is basically that presented in references 3.3.1-1 and 3.3.1-2 with two modifications added by Vought personnel: (1) the method is limited to two jets per system, and (2) an intermediate ground effects algorithm has been included. It should be noted that in VAPE more than two jets may be treated by utilizing multiple systems. There is no interaction assumed between systems. Although this is not absolutely correct, in actual practice the results obtained are good. The Wooler program is well documented in the references cited.

Reference 3.3.1-1 shows that when a jet exhausts into a crossflow it is deflected and modified by entrainment. Wooler assumed that deflection is due partly to viscous entrainment and partly due to forces on the jet surface resulting from pressure distributions around the jet. He also assumed that the flow is incompressible and that viscous effects other than entrainment may be neglected. This latter effect is accounted for by an empirical expression for mass entrainment per unit length on the jet.

Net forces acting on the boundary as a result of pressure differentials around the jet are accounted for by a crossflow drag analogy. This force, along with the mainstream momentum contribution, supplies the force necessary to produce a centrifugal acceleration of the local jet mass, thus causing the jet to bend.

To obtain the jet induced velocity field, Wooler assumed entrained fluid to be represented by a uniform sink distribution placed orthogonal to the plane of the jet and the mainstream (see Figure 3.3.1-1) and by a distribution of doublets with their axis perpendicular to the jet centerline to represent the so-called jet 'blockage' phenomenon. The strength of the

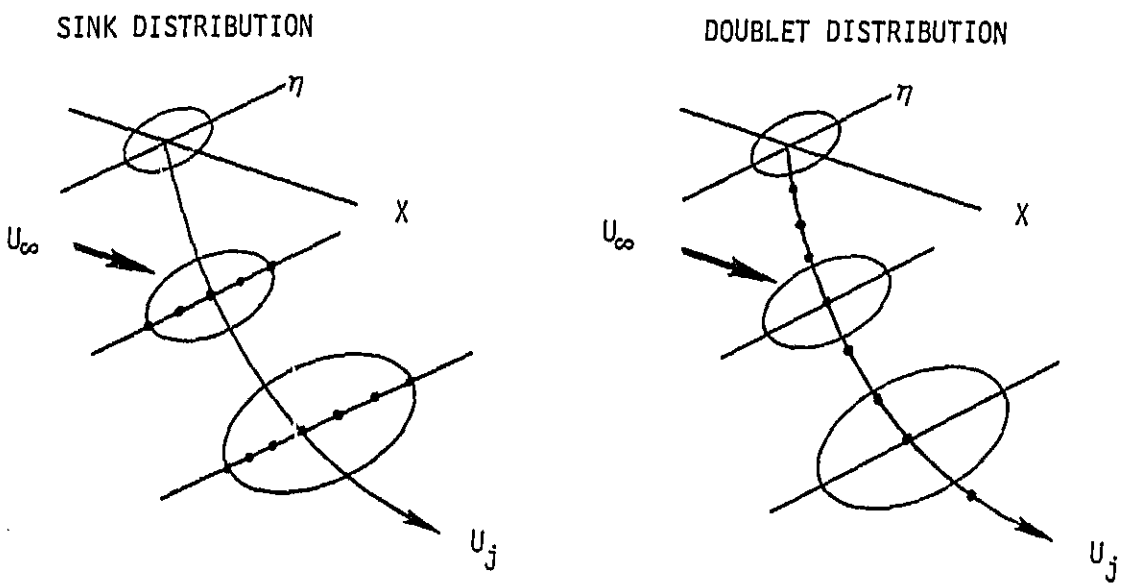

FIGURE 3.3.1-1 WOOLER JET MODEL SINK AND DOUBLET DISTRIBUTIONS

doublet distribution is obtained from a two-dimensional analogy. In effect, the flow considered is that past an equivalent circular cyliner and the strength is obtained from the 1/z term in the complex velocity expansion w(z) for two-dimensional flow past an ellipse. In addition to the sink and doublet distributions, Wooler introduced a third set of singularities which are also distributed along the calculated jet centerline. This latter is a set of point sources which are added to compensate for the invalidity of the hypothesized entrainment expression. Source strength is made proportional to local curvature, which is justified by Wooler mainly through comparison with experimental results. The total jet induced velocity at a point (x, y, z) in space can be obtained by integrating the effects of all singularities. Details of the calculation procedure are given in reference 3.3.1-1.

The single jet analytical model can be applied to the computation of the interaction flow field due to multiple exhausting jets. A multiple jet configuration is treated as a combination of discrete jets, with each jet (including jets resulting from coalescence of jets) being replaced by its representative singularity distribution to obtain the induced velocity field. The development of the two-jet model is discussed below.

Two assumptions are made for the two jet model:

a. The leading (or upstream) jet develops independently of the downstream jet.

b. The downstream jet exhausts into a free stream of reduced dynamic pressure due to blockage by the upstream jet.

These assumptions have been substantiated by wind tunnel tests.

Figure 3.3.1-2 shows a plan view of three two-jet configurations in relation to the free stream flow. Arrangements (a) and (c) represent limiting cases. Arrangement (a) allows each jet to develop independently to the point where growth of the jets in the direction normal to the flow causes them to intersect. Arrangement (c) places the downstream jet entirely in the zone of influence of the upstream jet. Arrangement (b) shows the downstream jet as partially in the zone of influence of the upstream jet.

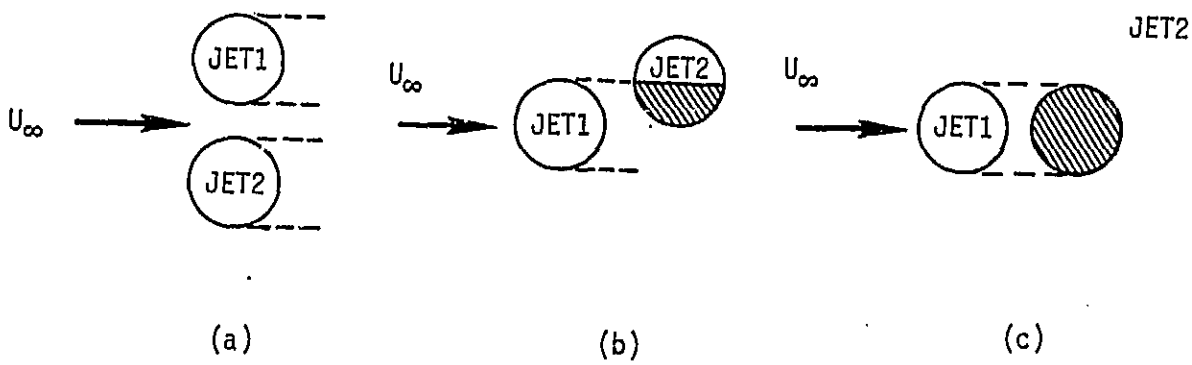

FIGURE 3.3.1-2 MULTIPLE JET INTERACTION IN THE WOOLER JET MODEL

Although Figure 3.3.1-2 shows the relationship of the jets in the plane of the jet exits, the determination of the degree of influence of the upstream jet (JET 1) on the downstream jet (JET 2) can be carried out for each element of JET 1, as shown in the general case of Figure 3.3.1-3 (Note that Jet 2 does not influence Jet 1). Plane L is defined as the plane perpendicular to the local velocity vector (U_J) of JET 1 at a selected point on the jet centerline. The intersection of Plane L with JET 2 locates the cross-section of JET 2 which is affected by the jet cross-section at the selected point on the centerline of JET 1. Plane M passes through the selected center point of JET 1 and contains the vectors U_J and the free stream velocity vector, U_∞. The intersection of Plane M with the JET 2 cross section in Plane L is determined next. From this determination, a calculation can be made of the extent to which the selected JET 1 cross section influences the JET 2 cross section.

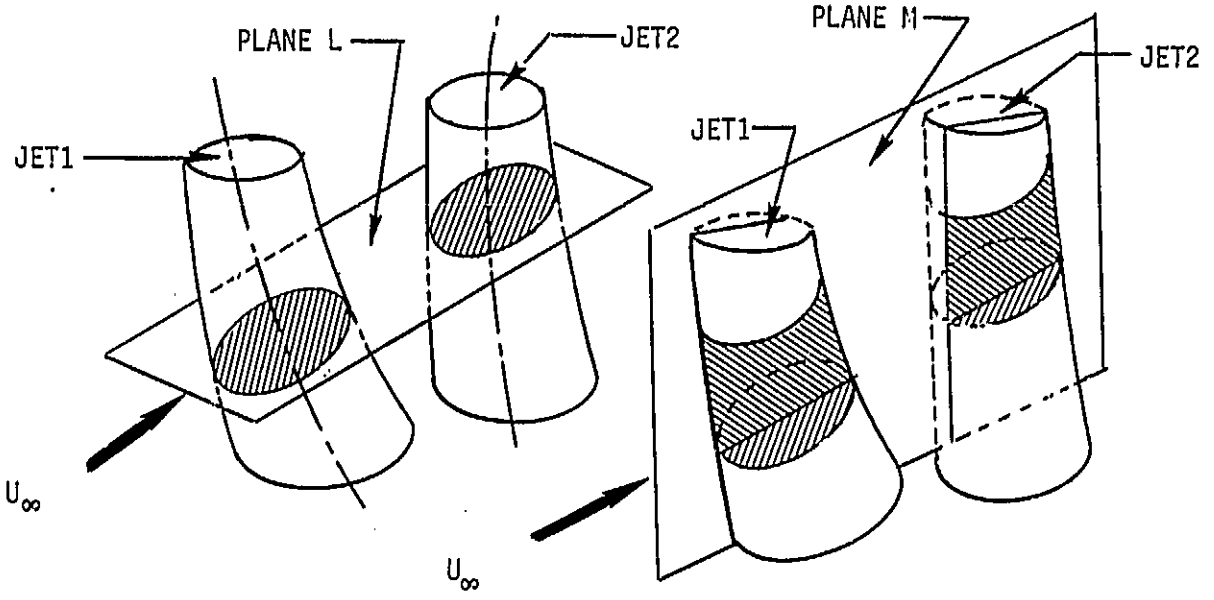

FIGURE 3.3.1-3 MULTIPLE JET INFLUENCE DETERMINATION IN WOOLER JET MODEL

Velocities induced by a two-jet configuration can now be determined by replacing each jet (including the coalesced jet) by its representative singularity distribution. The induced velocity components due to each singularity distribution are additive at every point of interest on the airframe.

The Wooler program has been modified at Vought to include ground effects at intermediate altitudes ($5 \leq h/d \leq 25$). This is done by letting the ground become an image plane. The computed flow field is assumed to be reflected by the image plane so that the combination of real and imaginary flow fields yields zero normal velocity components at the image plane. This approach is similar to that proposed by Wooler in reference 3.3.1-3.

Elementary concepts for the intermediate altitude math model are shown in Figure 3.3.1-4. As the jet approaches the ground plane, the ground plane is assumed to be an image plane. An imaginary jet can be assumed to exist below the image plane. The induced velocity flow field is composed of the contributions due to the real jet and the imaginary jet. For the simple case shown in Figure 3.3.1-4, induced velocity components in the axial and vertical directions are u and v for the real jet; since u' and v' are opposite, the sum of v and v' will vanish for control points on the ground plane (image plane).

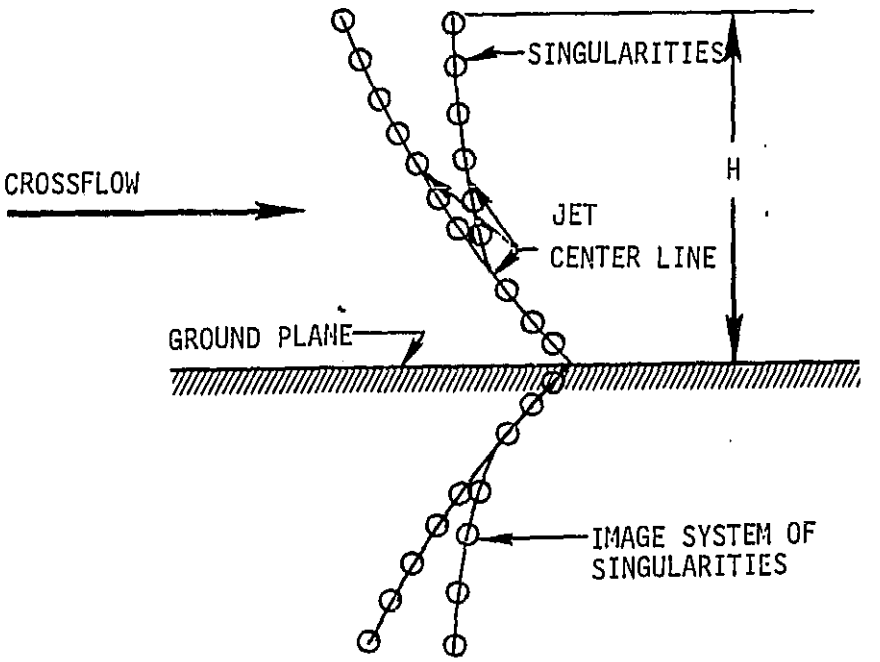

FIGURE 3.3.1-4 IMAGE SYSTEM MODEL FOR GROUND EFFECT IN WOOLER JET MODEL

The Vought-Wooler-Ziegler intermediate altitude math model uses a system of imaginary control points instead of an imaginary jet. The induced velocity components at the control point (cp) due to the jet are u and v. The induced velocity components at the imaginary control point (cp') due to the jet are u' and v'. Velocity components at the real control point and at the imaginary control point are summed (i.e., add u' to u and subtract v' from v) to obtain the combined solution.

Models used in the preceding discussions have been simplified by assuming the orientation parallel to the ground plane and treating only the x and y components of velocity. However, the basic concepts apply to any arbitrary orientation and to all three orthogonal velocity components.

REFERENCES:

3.3.1-1 Wooler, P.T., Kao, H.C., Schwendemann, M.F., Wasson, H.R. and Ziegler, H., "V/STOL Aircraft Aerodynamic Prediction Methods Investigation, Volume I. Theoretical Development of Prediction Methods," Air Force Flight Dynamics Laboratory, AFFDL-TR-72-26, Volume I, January 1972.

3.3.1-2 Wooler, P.T., Burghart, G.H., and Gallagher, J.T., "Pressure Distribution on a Rectangular Wing with a Jet Exhausting Normally into an Airstream," Journal of Aircraft, Vol. 4, No. 6, pp. 537-543, Nov.-Dec. 1967.

3.3.1-3 Wooler, P.T. and Ziegler, H., "An Analytical Model for the Flow of Multiple Jets into an Arbitrary Directed Crossflow in Ground Effect," AIAA Paper 70-545 presented at the AIAA Atmospheric Flight Mechanics Conference, Tullahoma, Tenn. 1970.

3.3.2 Vought/Weston Jet Model

As discussed earlier, the flow field produced by a jet issuing into a cross flow is dominated by two factors: (1) the jet entrainment, and (2) the flow produced by a pair of contrarotating vortices formed by the shearing action between the relative wind and the jet. Wooler's method discussed previously does a reasonable job of simulating the jet induced effects, but does not directly model the contrarotating vortices. Instead, Wooler placed singularities, which simulated the vortex pair, along the jet centerline rather than along the true vortex trajectories. In addition, Wooler's singularity strengths were obtained from assumptions concerning the growth of the jet plume rather than from an experimental description of the actual vortex pair.

Recently, Fearn and Weston (reference 3.3.2-1) have obtained experimentally a very good quantitative description of the vorticity associated with a jet in a crossflow. This data was used by Sellers, reference 3.3.2-2, to formulate a mathematical model of the vortex flow. Dietz, reference 3.3.2-3, used these two results to develop a method for predicting jet induced effects on a flat plate. Dietz's method was limited to a 90 degree jet injection angle, one value of jet velocity ratio, R, and one jet.

The method contained in VAPE was developed at Vought using the above references in addition to a recent report by Fearn, reference 3.3.2-4, on jet injection angle effects. This method is applicable to various injection angles, various values of R, and to multiple jets.

The method based on the above references uses experimental data to define a diffuse vortex model which assumes that the distribution of vorticity within each of the contrarotating vortices is Gaussian in nature.

Paths of the jet streamline and vortex curves were determined from the experimental data for a 90° injection angle to obey a power law of the form

$$\frac{Z}{D} = aR^{b}\,(X/D)^{c} \qquad (3.3.2\text{-}1)$$

where Z = Z coordinate in jet coordinate system
X = X coordinate in jet coordinate system
D = Jet Diameter
$R = V_{Jet}/V_{\infty}$
a, b, c, are empirically derived coefficients

The jet coordinate system is presented in Figure 3.3.2-1

The values of a, b, c are given in Table 3.3.2-1

TABLE 3.3.2-1
Coefficients For Equation 3.3.2-1

CURVE	a	b	c
Jet Centerline	1.2583	0.6200	0.4060
Vortex Curve	0.3067	1.1513	0.4492

The lateral spacing, y, for the vortex curve is

$$y = \frac{h_o}{\text{erf}(\beta h_o)} \qquad (3.3.2\text{-}2)$$

where $h_o = (D)\ 2.04 \left(1 - e^{\frac{-s/d}{R}}\right)$

s = Surface distance along jet

and $$\text{erf}(\beta h_o) = \frac{2}{\sqrt{\pi}} \int_{o,}^{\beta h_o} e^{-t^2} dt \qquad (3.3.2\text{-}3)$$

Fearn, Drausche and Weston, reference 3.3.2-4, modified this equation based on further wind tunnel results, to account for injection angles other than 90°. The equation formulated is quite similar and is given by,

$$\frac{Z - Z_1}{D} = aR^b \frac{(x - x_1)^c}{D} \qquad (3,3,2\text{-}4)$$

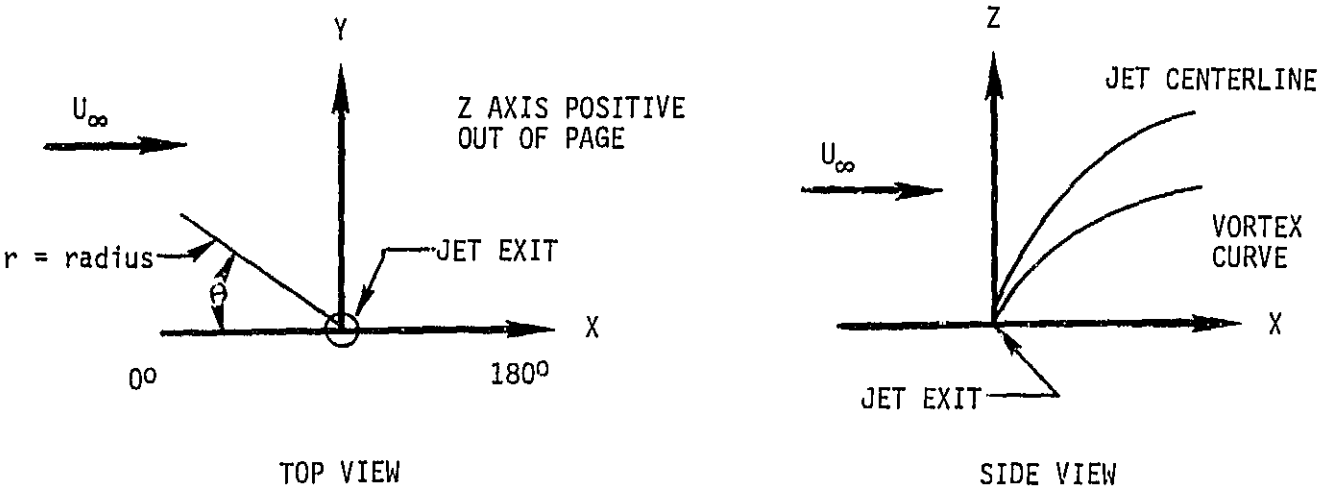

FIGURE 3.3.2-1 WESTON JET EXIT COORDINATE SYSTEM

This curve is defined as being the same shape as the 90 degree injection curve but displaced from the origin of the jet exit coordinate system. Figure 3.3.2-2 shows a schematic that is applicable on both the jet centerline and the vortex curve showing the relationship between (X_1, Z_1) and (X_0, Z_0) and δ_j. By definition, (X_0, Z_0) is the point where the tangent of the curve is the injection angle δ_j and X_1, Z_1, is the point where the curve is perpendicular to the crossflow.

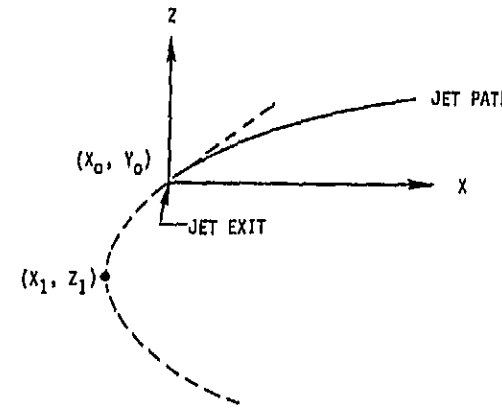

FIGURE 3.3.2-2 FEARN/WESTON MODEL FOR ARBITRARY JET INJECTION ANGLE

The description of the jet model formulated from the above information is presented in detail in reference 3.3.2-5.

The above approach has been modified at Vought to be applicable to multiple jets using a procedure similar to that employed by Wooler, as explained earlier. In this approach, the front jet in a jet pair is assumed to act independently of the aft jet, therefore the equation for both the jet centerline and the vortex curves, as well as the associated singularity strengths for a single jet, are used. For the aft jet, it is assumed that the front jet alters the dynamic pressure field into which the aft jet issues. A description of the variation in the dynamic pressure as a function of jet spacing is given in reference 3.3.2-5.

Using the experimental data on which Wooler based his multiple jet method, reference 3.3.2-6, a modification was obtained to the equation of the aft jet penetration which produced excellent agreement with this data. The equation obtained for the aft jet is given by:

$$\frac{Z - Z_1}{D} = a(R'^{b}) \frac{(x - x_1)^c}{D} \qquad (3.3.2\text{-}5)$$

where a and b are given in Table 3.3.2-1 and c is set equal to .4 for the jet centerline calculation. The value of c for the vortex curve is left unchanged due to a lack of experimental data upon which to base any modification. The value R' is a jet velocity ratio based on the reduced freestream dynamic pressure at the aft jet. R' is determined in the program by the following relationship

$$R' = R \frac{V_\infty}{V'_\infty} \qquad (3.3.2\text{-}6)$$

where V'_∞ is determined as shown in reference 3.3.2-5 or 3.3.2-7.

Figure 3.3.2-3 presents a comparison of the jet centerline locations as calculated by the above approach to those calculated by Wooler's method and to the experimental data. The above technique gives a good description of the jet centerline and the vortex curves for a two jet system.

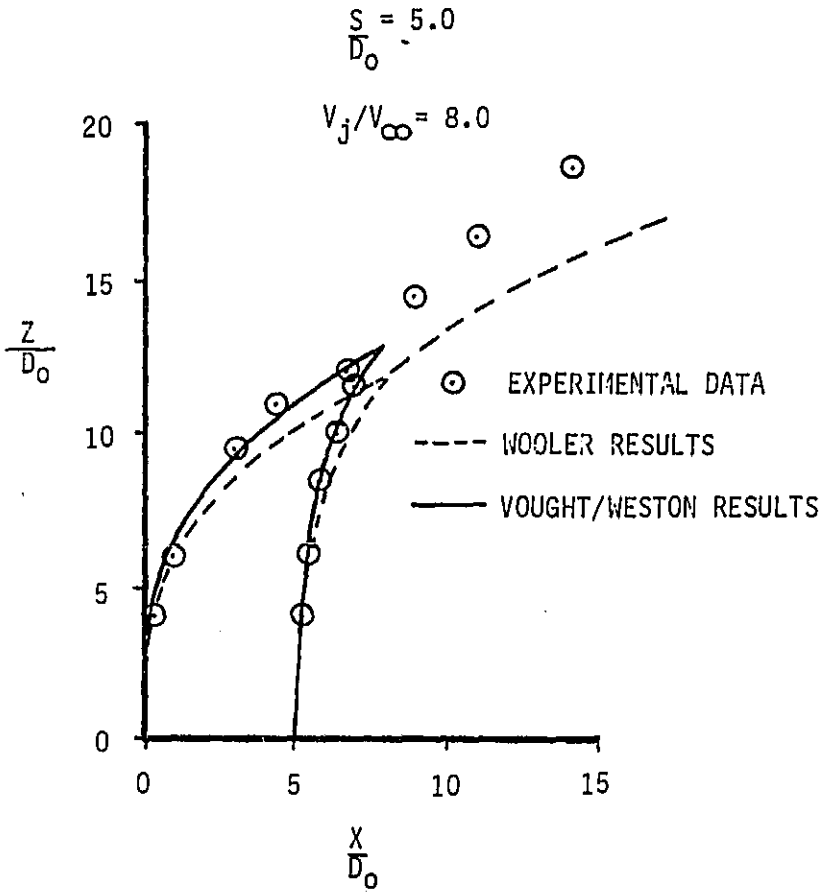

FIGURE 3.3.2-3 COMPARISON OF CALCULATED AND EXPERIMENTAL JET PATH CENTERLINES, JET SPACING = 5.0 DIAMETERS, JET VELOCITY RATIO, R = 8

The question which now arises is "what happens if these two jets intersect as shown in Figure 3.3.2-3. Wooler uses a technique for merging the two jets in his method which suggests a method for use in the approach presented above. Wooler used continuity and momentum considerations to develop a merged jet as discussed earlier. This same approach is used in the Weston model contained in VAPE with some modifications as discussed in reference 3.3.2-5.

REFERENCES:

3.3.2-1 Fearn, R. and Weston, R.P., "Vorticity Associated with a Jet in a Crossflow," AIAA Journal, Vol. 12, Number 12, Dec. 1974.

3.3.2-2 Sellers, W.L., "A Model for the Vortex Pair Associated with a Jet in a Crossflow," Masters Thesis, University of Florida, 1975.

3.3.2-3 Dietz, W.E., "A Method for Calculating the Induced Pressure Distribution Associated with a Jet in a Crossflow," Master's Thesis, University of Florida, 1975.

3.3.2-4 Fearn, R.L., Drausche, D. and Weston, R.P., "A Round Jet in a Crossflow - The Influence of Jet Injection Angle on Vortex Properties," to be published by AIAA.

3.3.2-5 Beatty, T.D., and Kress, S.S., "Prediction Methodology for Propulsive Induced Forces and Moments of V/STOL Aircraft In Transition/STOL Flight," Naval Air Development Center Report, NADC-77119-30, July 1979.

3.3.2-6 Fricke, L.B., Wooler, P.T. and Ziegler, H., "A Wind Tunnel Investigation of Jets Exhausting into a Crossflow," Air Force Flight Dynamics Laboratory Technical Report, AFFDL-TR-70-154, Volumes I-IV, Dec. 1970.

3.3.2-7 Wooler, P.T. and Ziegler, H., "An Analytical Model for the Flow of Multiple Jets into an Arbitrary Directed Crossflow in Ground Effect," AIAA Paper 70-545 presented at the AIAA Atmospheric Flight Mechanics Conference, Tullahoma, Tenn., 1970.

3.3.3 Thames Rectangular Jet Model

A method has been developed, reference 3.3.3-1, to calculate the propulsive induced effects produced by an aspect ratio 4 rectangular jet oriented with the major axis either parallel or perpendicular to the cross-flow. The approach selected parallels that used by Weston and Dietz, references 3.3.3-2 and 3.3.3-3. This required that an extensive data base be generated to define the vortex strengths for the two nozzle orientation and various jet-to-freestream velocity ratios and nozzle injection angles that the model was to simulate. Thames conducted a wind tunnel test to generate the required data base and then used this to develop the analytical model.

The model has two principal components:

- A pair of variable strength potential filament vortices lying along the experimentally determined vortex trajectories, and
- One or more source/sink lines lying along (and parallel to) the experimentally determined jet centerline curve.

The vortices are included to model the real contrarotating vortex pair. The vortex strength distributions were determined from the experimental data. The source/sink lines are used to simulate the blockage/entrainment of the jet. Since there was no direct experimental procedure for measuring the source/sink strengths, these were determined analytically to give the best approximation to the experimentally measured flat plate pressure distributions. Figure 3.3-9 presents a schematic of the rectangular jet model showing the vortex and source/sink lines for both a blunt and streamwise orientation of the jet.

Since the strength of each filament vortex varies along its path, each vortex is subdivided into a specified number of constant strength vortex segments, N_{VS}, as illustrated in Figure 3.3.3-1. The segment lengths are stretched cubically to compensate for the rapid variation in Z immediately downstream of the jet exit.

To simulate the blockage/entrainment effects of the jet, the model uses one or more segmented source/sink lines lying along (or parallel to) the experimentally determined jet centerline (Figure 3.3.3-1). The source/sink strength along a given line is a constant. However, if more than one line is used, the strengths may vary from line to line. In addition, if multiple lines are used, the strengths must be symmetric about the symmetry plane (only an odd number of lines is allowed) for blunt oriented jets. However, non-symmetric strengths may be used for streamwise oriented nozzles. As mentioned before, the number and strengths of the source/sink lines were determined analytically. The strength distributions were determined by interpolation in the model assuming that the source/sink strength is a function of nozzle orientation, velocity ratio, and jet incidence angle. However, the model does allow the user to specify these quantities if desired.

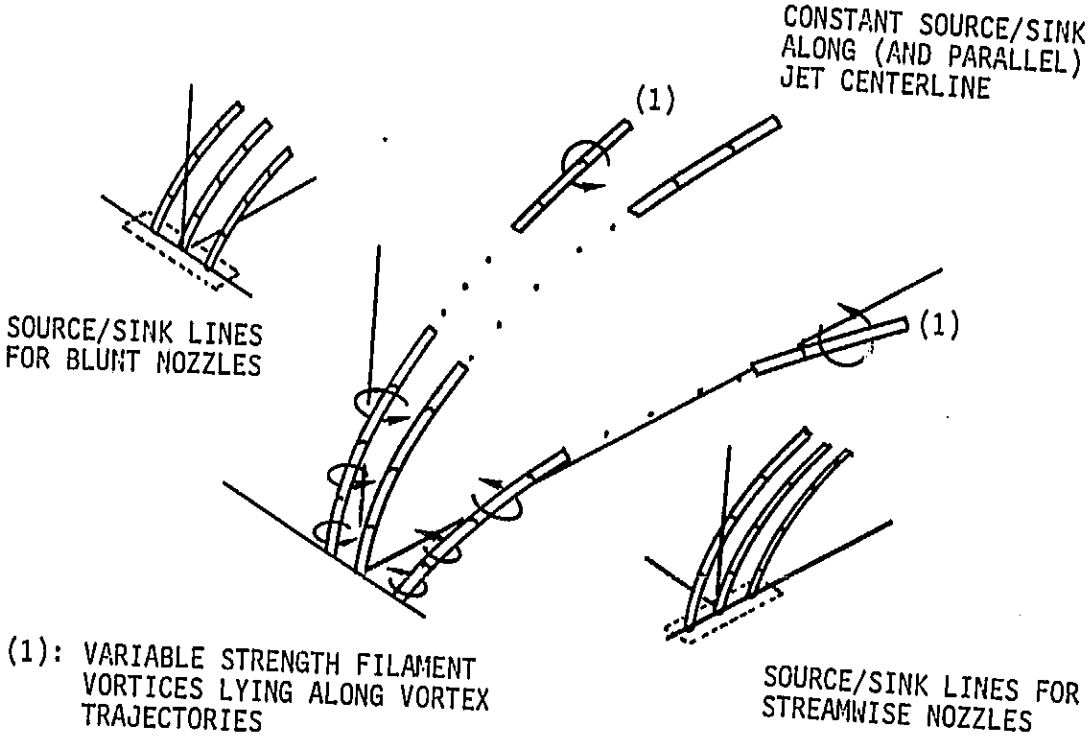

FIGURE 3.3.3-1 THAMES' RECTANGULAR JET MODEL FORMULATION

This model gives reasonable results for nozzle and jet flow conditions within the following application ranges:

- Nozzle aspect ratio: $3.0 \leq A_R \leq 5.0$
- Nozzle equivalent diameter: $3.5 \leq D \leq 4.5$
- Nozzle orientations: Blunt, streamwise
- Velocity ratio: $3.0 \leq R \leq 12.0$
- Jet Deflection:
- - Blunt Nozzles: $45^0 \leq \delta j \leq 90^0$
  - Streamwise Nozzles: $60^\circ \leq \delta j \leq 90^\circ$

The detailed development and implementation of this method is contained in references 3.3.3-1 and 3.3.3-4.

REFERENCES:

3.3.3-1 Thames, F.C., "Development of an Analytical Model to Predict Induced Effects or Aspect Ratio 4.0 Rectangular Nozzles in a Subsonic Cross-flow," Vought Report No. 2-53110/9R-52268, October 1979.

3.3.3-2 Fearn, R. and Weston, R.P., "Vorticity Associated with a Jet in a Crossflow," AIAA Journal, Vol. 12, Number 12, Dec. 1974.

3.3.3-3 Dietz, W.E., "A Method for Calculating the Induced Pressure Distribution Associated with a Jet in a Crossflow," Masters Thesis, University of Florida, 1975.

3.3.3-4 Beatty, T.D. and Kress, S.S., "Prediction Methodology for Propulsive Induced Forces and Moments of V/STOL Aircraft In Transition/STOL Flight," Naval Air Development Center Report, NADC-77119-30, July 1979.

3.4 STOL CALCULATIONS

The jet methods discussed so far are for the transitional area of flight which was defined as the regime between normal horizontal flight and vertical hovering. There are several methods which have been developed for the vertical hovering region, references 3.4-1 and 3.4-2. Discussed next is the STOL region of flight which is defined as the region where the aircraft is taking off or landing and very close to the ground, at a reasonable forward speed. The lift jets are deflected such that they impinge the ground forming wall jets, which are not reflected back to the aircraft. The wall jets increase entrainment and thus increase the "suck-down" effect of the jets on the aircraft. A technique to predict this effect has been developed and incorporated into the Weston jet model contained in the VAPE program. The details of this approach are given below.

Consider a STOL aircraft with its lift jets deflected and moving close to the gound as shown in Figure 3.4-1. The jet flow between the aircraft and the ground plane is assumed to be represented by the flow model in the Weston jet model. When the jet intersects the ground, an impingement region is formed where the jet flow direction is changed to be parallel to the ground plane, forming a radial wall jet. A radial wall jet in a cross-flow creates a rather complex flow field. At some distance ahead of the jet impingement point, the flow along the wall jet separates from the wall and curves back on itself. The loci of these separation points is referred to as the separation line of the wall jet (Figure 3.4-2).

A strong vortex is formed between the sources of the wall jet and the separation line of the two flows.

In the approach used in VAPE, the separation line is modeled, but the vortex is ignored. The algorithm used in VAPE is to (1) determine the impingement point; (2) define the wall jet; (3) find the separation line, and (4) determine the entrainment due to the wall jet aft of the separation line. These entrainment values are then used to calculate a normal velocity at control points on the ground plane which are used as boundary conditions in the Hess program.

The jet impingement location is determined by finding the intersection point of the ground plane with the jet centerline path.

Once the impingement point is found, then the velocity of the jet at this point is determined. In addition, the angle of the jet relative to the ground plane at impingement is determined. This angle is calculated in the following manner.

$$\alpha JET_{IM} = TAN^{-1}\left(\frac{dz}{dx}\right)_{JET_{IM}} \qquad (3.4\text{-}1)$$

Where:

αJET_{IM} = Impingement angle

$\left(\frac{dz}{dx}\right)_{JET_{IM}}$ = Tangent of jet centerline path at impingement point

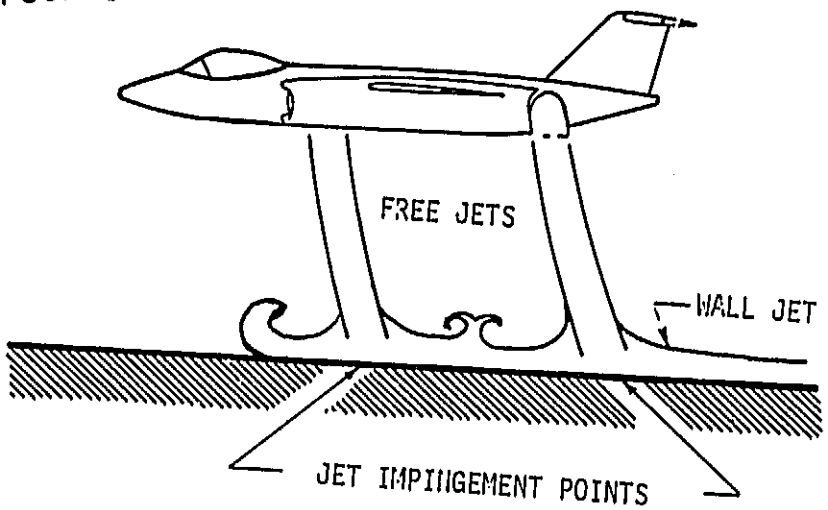

FIGURE 3.4-1 AIRCRAFT IN STOL FLIGHT

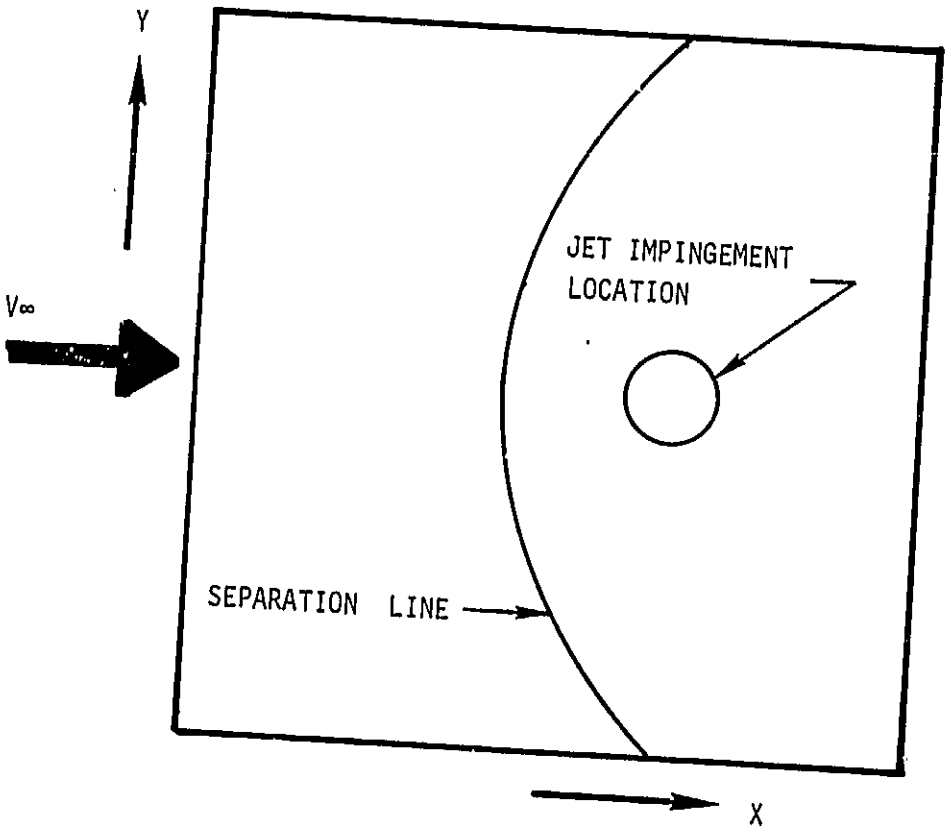

FIGURE 3.4-2 GROUND PLANE MODEL

The separation line is now determined based on an empirical equation developed by Colin, reference 3.4-3.

Again, the details of this analysis are contained in reference 3.4-4.

REFERENCES:

3.4-1 Kotansky, D.R., Durando, J.A. and Bristol, D.R., "Multi-Jet Induced Forces and Moments on VTOL Aircraft Hovering In and Out of Ground Effect," Naval Air Development Center, Report No. NADC-77-229-30, June 1977.

3.4-2 Siclari, M.J., Barche, J. and Migdal, D., "V/STOL Aircraft Prediction Technique Development for Jet-Induced Effects," Naval Air Propulsion Test Center Report No. PDR-623-18, April 1975.

3.4-3 Colin, P.E. and Olivari, D., "The Impingement of a Circular Jet Normal to a Flat Surface With and Without Crossflow," AD688953, Jan. 1969.

3.4-4 Beatty, T.D. and Kress, S.S., "Prediction Methodology for Propulsive Induced Forces and Moments of V/STOL Aircraft In Transition/STOL Flight," Naval Air Development Center Report, NADC-77119-30, July 1979.

4.0 VISCOUS SIMULATION

The presence of a boundary layer on a body causes the irrotational flow outside of the boundary layer to be the same as the flow about a surface, which has been displaced into the fluid by a distance δ^*, the displacement thickness of the layer.

This can be explained, reference 4.0-2, by considering the entire flow field about the body. Inside the boundary layer region the flow velocity reduction due to the presence of rotational flow in this viscous area is given by

$$\Delta U = U_e - u \qquad (4.0\text{-}1)$$

where U_e = Velocity at edge of boundary layer
u = Velocity inside of boundary layer as a function of distance from the surface z.

Then the total reduction in volume flow per unit span is

$$\int_0^\infty (U_e - u)\, dz \qquad (4.0\text{-}2)$$

Now between the body surface and any streamline outside the boundary layer there must be a constant volume flow per unit span. This can only be true if the flow reduction inside the boundary layer is compensated for by displacing the streamline out from the body by an appropriate amount. Defined as δ^* the displacement thickness. The magnitude of δ^* is determined from the following:

(1) If the external streamline is displaced outward by the value δ^* then the volume flow increase per unit span is $\delta^* U_e$ (since the velocity is U_e where the displacement occurs).

(2) Then

$$\delta^* U_e = \int_0^\infty (U_e - u)dz \qquad (4.0\text{-}3)$$

so the displacement thickness must be

$$\delta^* = \int_0^\infty \left(1 - \frac{u}{U_e}\right) dz$$

where U_e = velocity at edge of boundary layer
u = velocity in boundary layer.

This displacement thickness is then used as described later to formulate a correction to the inviscid technique which will permit an inviscid code to determine, with some limitation, a "viscous" solution about a given geometry.

In the past few years, several programs have been developed to simulate viscous effects on a given geometry by coupling a boundary layer code, to calculate the displacement thickness, with a potential flow code. A very good review of this work is presented in reference 4.0-1. In several of these programs, the potential flow code was essentially the same Hess code as contained in VAPE. The boundary layer routines used varied from simple two-dimensional integral methods to fairly sophisticated three-dimensional methods. Reference 4.0-1 showed how the various programs compared and gave an

insight into some of the areas of concern. When efforts were initiated to add viscous effects to VAPE, the following concerns were investigated in depth:

- o Determination of boundary layer parameters on three dimensional wing surface,
- o Selection of boundary layer method,
- o Simulation of viscous effects, and
- o Numerical implementation of simulation model

Each of these items is discussed in some detail in the following sections.

The modifications to VAPE under this contract added the capability to determine the viscous effects to the lifting surfaces only since it was felt that this was the most important part of the aircraft to consider initially..

REFERENCES:

4.0-1 Kjelgaard, S.O. and Thomas, J.L., "Comparison of Three-Dimensional Panel Methods with Strip Boundary Layer Simulations to Experiment," NASA TM 80088, July 1979.

4.0-2 Lighthill, M.J.: "On Displacement Thickness," Journal of Fluid Mechanics, Part 4, 1958.

4.1 BOUNDARY LAYER PARAMETER ESTIMATION

There are several ways of determining the boundary layer parameters required to simulate the viscous flow about a wing. The standard approaches are:

- o Two-dimensional strip theory in which velocity distributions on streamwise strips on the wing upper and lower surfaces are analyzed by a two-dimensional or infinite swept wing boundary layer method.

- o Quasi-three dimensional boundary layer approaches such as the method of reference 4.1-1, which is based on the assumption of small cross flow normal to the streamlines.

- o Full three-dimensional boundary layer methods which are based on either integral or finite-difference techniques.

The full three-dimensional methods were eliminated from consideration during this study period due to availability, generality and computer operation cost. The quasi-three dimensional methods such as the small cross flow technique (reference 4.1-1) were also eliminated for several reasons. Most of these techniques require solving the boundary layer equations along streamlines. This requires a considerable effort not only to find the streamlines, but also to project the boundary layer results back to the potential flow control points. A technique of this type was used in reference 4.1-2 with only a slight improvement over the simpler strip theory approach. Another quasi-three dimensional approach was used in reference 4.1-3 which was simpler in application and gave better results for some configurations. However, personal correspondence with the author has indicated that this boundary layer code is very sensitive and often requires multiple runs to obtain a solution.

The strip-theory approach selected for this program has none of the problems of the other methods discussed. There are numerous two-dimensional methods which have been well proven through several years of use. These codes are all generally easy to adapt to the type of analysis being done in this program. They solve for the boundary layer parameters at input points which directly correspond to the three-dimensional nodal points, thus eliminating any large scale multi-dimensional manipulations of the pressure data. They have been shown by several authors, including reference 4.1-2, to give good results.

REFERENCES:

4.1-1 Cebeci, T: "Calculation of Three-Dimensional Boundary Layers. I. Swept Infinite Cylinders and Small Cross Flows," AIAA Journal, Vol. 12, No. 6, June 1974.

4.1-2 Hess, J.L: "A Fully Automatic Combined Potential Flow Boundary Layer Procedure for Calculating Viscous Effects on the Lifts and Pressure Distributions of Arbitrary Three-Dimensional Configurations," McDonnel Douglas Report No. MDC 57491, June 1977.

4.1-3 Waggoner, E.G.: "Transonic Three-Dimensional Viscous-Inviscid Interaction for Wing Body Configuration Analysis", AIAA Paper No. 82-0163 presented at 20th Aerospace Sciences Meeting, Jan. 1982.

4.2 BOUNDARY LAYER METHOD

There are numerous two-dimensional boundary layer methods available that are well suited for this task. Indeed, references 4.2-1 and 4.2-2 cite several different methods that have been used for this type of analysis with very good results. The choice of which boundary layer program to use was based on the generality, accuracy, maturity, computational speed and documentation available. In the light of these guidelines, a finite difference method originally developed by Cebeci and Smith (references 4.2-3 and 4.2-4) and used in the two-dimensional approach of reference 4.2-5 and the axisymmetric approach of reference 4.2-6 was selected. This particular method, which is normally referred to as the Cebeci-Smith (CS) method, was developed over a period of several years. The theory and numerical implementation are given in reference 4.2-4. This method is very general and is as complete as any comparable method. It has been shown in several studies to be extremely accurate over a wide range of cases. An overview of the program is given in the following paragraphs (see reference 4.2-4 for a more detailed presentation).

The C-S method contained in VAPE calculates the viscous flow about both two-dimensional airfoil sections and infinite yawed wings for both laminar and turbulent flow. For laminar flows, the problem is strictly mathematical because the governing differential equations can be written exactly. For turbulent flows, however, an exact solution of the governing equations is not now possible. Thus, existing methods all must use some empiricism in their formulation.

In the past, most of the work in this area concentrated on momentum and/or energy integral methods as a means of evaluating the viscous flow parameters. The exact mathematical solution to the problems of the turbulent flow was bypassed, leading to fast and simple methods with varying degrees of accuracy. These methods usually relied heavily on empirical correlations and generally were restricted to a limited range of flow conditions.

The Cebeci-Smith program eliminates many of the disadvantages of the integral methods by proceeding to solve the full partial-differential equations governing the flow, thereby being classified as a differential method. For incompressible flows, turbulent boundary-layer equations contain terms involving time means of fluctuating velocity components known as Reynolds stress terms. The exact relationship between these terms and the mean velocity distribution in the boundary layer is currently unknown. In the C-S method, a relation based on the eddy-viscosity concept is used which provides highly satisfactory results for a great variety of flow conditions.

The C-S method in VAPE calculates accurate results for both incompressible and compressible flows. The method solves the laminar and turbulent boundary layer equations for both two-dimensional and infinite yawed configurations. Infinite yawed configurations are simply two-dimensional airfoils that have been yawed, or swept, by a fixed angle. As input data, the program needs the body surface pressure distribution as determined by the potential flow routine along with certain controling information. The boundary layer program in VAPE also indicates the point of laminar or turbulent separation, transition location and reattachment at laminar separation.

The laminar and turbulent separation points are determined by the program to be at the point where the skin friction coefficient becomes zero or where the derivative of the velocity profile becomes negative. In the laminar

case, this flow will normally reattach as turbulent flow and continue unless the flow field at that point is too adverse to permit this action. The basic C-S method does not have any way to predict whether the flow will reattach or not. Thus, an empirical relation by Gastor, reference 4.2-7, which gives reasonable results, was added to the C-S method. Figure 4.2-1 presents a curve showing the relation used in VAPE to determine whether the flow reattaches or remains separated at the laminar separation point. The point where the boundary layer transitions from laminar to turbulent flow is also predicted in the C-S method by a fairly accurate emperical equation by Cebeci. Reference 4.2-4 discusses the equation and its accuracy in some detail. This relation is based on the assumption that the variation of the transition momentum - thickness Reynolds number $R_{\theta_{TR}}$ with the surface distance - Reynolds number, R_X, is a "universal" curve. Cebeci took Michel's curve and a curve generated by Smith and Gamberoni, reference 4.2-8, and developed the following correlation formula:

$$R_{\theta_{TR}} = 1.174\,[1 + (22{,}400/R_X)]\,R_X^{0.46} \qquad .1\times10^{6} \leq Rx \leq 40\times10^{6} \qquad (4.2\text{-}1)$$

This method works fairly well when the pressure gradients are moderate to large. However, if the pressure gradient is mild, as for example on the lower surface of an airfoil, the results can be in error by a considerable amount. Therefore, the results should be checked to ensure reasonable locations of the transition point.

Most of the output data produced by the boundary layer program is presented in standard terms familiar to most users. Some of the important parameters are presented below.

The boundary layer displacement thickness is given by:

$$\delta^* = \int_0^{\infty} \left(1 - \frac{u}{ue} \right) dy \qquad (4.2\text{-}2)$$

The relationships between the pressure coefficient, C_p, and the local velocity u_e for incompressible flows is

$$C_p = 1 - \left(\frac{u_e}{u} \right)^2 \qquad (4.2\text{-}3)$$

and for compressible flow is

$$C_p = \frac{2}{\gamma m_\infty^2} \left\{ \left[1 + \frac{\gamma - 1}{2} M_\infty^2 \left(1 - \left(\frac{u_e}{u_\infty} \right)^2 \right) \right]^{\frac{\gamma}{\gamma - 1}} - 1 \right\} \qquad (4.2\text{-}4)$$

where $\gamma = 1.4$.

The fluid properties used in the C-S program are given by Sutherland's formula for the viscosity of air, reference 4.2-4.

$$\mu = \mu_\infty \left\{ \left(\frac{h}{h_\infty} \right)^{1.5} \frac{h_\infty + 1.1928 \times 10^6}{h + 1.1928 \times 10^6} \right\} \qquad 4.2\text{-}5$$

where h is the specific enthalpy, the other air properties are determined from the usual perfect gas laws.

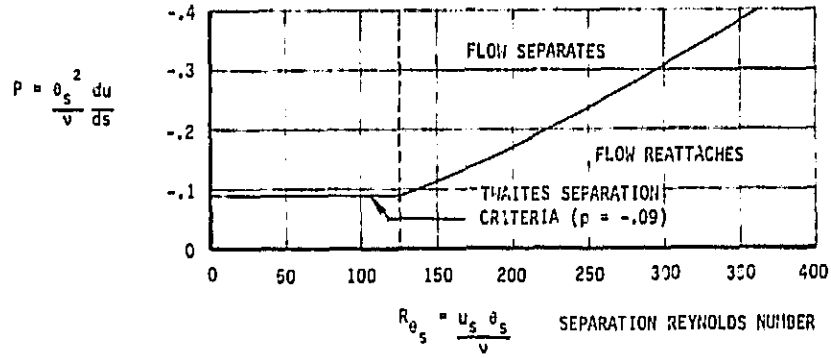

FIGURE 4.2-1 GASTOR'S CRITERION FOR LEADING EDGE LAMINAR FLOW SEPARATION AND REATTACHMENT

REFERENCES:

4.2-1 Hess, J.L.: "A Fully Automatic Combined Potential Flow Boundary Layer Procedure for Calculating Viscous Effects on the Lifts and Pressure Distributions of Arbitrary Three-Dimensional Configurations", McDonnell Douglas Report No. MDC 57491, June 1977.

4.2-2 Kjelgaard, S.L. and Thomas, J.L.: "Comparison of Three-Dimensional Panel Methods with Strip Boundary Layer Theory Simulations to Experiment", NASA TM-80088, July 1979.

4.2-3 Cebeci, T.: "Calculation of Three-Dimensional Boundary Layers. I. Swept Infinite Cylinders and Small Cross Flows," AIAA Journal, Vol. 12, No. 6, June 1974.

4.2-4 Cebeci, T. and Smith, A.M.O.: "Analysis of Turbulent Boundary Layers," Academic Press, 1974 (Applied Mathematics and Mechanics Series).

4.2-5 Beatty, T.D. and Callaghan, J.G.: "A Theoretical Method for the Analysis and Design of Multi-Element Arifoils," Journal of Aircraft, December 1972.

4.2-6 Beatty, T.D.: "A Theoretical Method for the Analysis and Design of Axisymmetric Bodies," NASA CR 2498, Sept. 1974.

4.2-7 Gaster, M: "The Structure and Behavior of Laminar Separation Bubbles," R and M No. 3595, 1969.

4.2-8 Michel, R.: "Etude de la Transition sur Les Profiles d'aile; Establishment d'un Critere de Determination de Point de Transition et Calcul de la Trainee de Profile Incompressible" Onera Rep., 1/1578A, 1951.

4.2-9 Smith, A.M.O. and Gamberoni, W.: "Transition, Pressure Gradient and Stability Theory," Procedures 9th International Congress of Applied Mechanics, Brussels, Belgium 4, 234, 1956.

4.3 SIMULATION OF VISCOUS EFFECTS

The simulation of the viscous effects using boundary layer parameters in a potential flow solution was proposed by Lighthill, reference 4.3-1. He suggested four approaches for simulating high Reynolds number viscous flow which is assumed to be essentially unseparated. Two of the four have become somewhat standard and will be discussed here. The first method, surface displacement, takes the boundary layer displacement thickness and physically adds it to the original body in the direction of the local surface normal (see Figure 4.3-1). This produces a thicker equivalent body which, when analyzed by the potential flow solution, generates a solution which approximates viscous flow. This procedure is done only on the body since the results of reference 4.3-2 indicate that no increase in accuracy is obtained by also considering the airfoil wake.

This procedure has been used quite successfully in two-dimensions, reference 4.3-3. However, the technique requires that a new geometry be run for each viscous case, which in theory means that for each angle of attack, a different geometry must be analyzed. In addition, if iterations are required, each iteration requires a new geometry. In two dimensions, this is not too time consuming, but in three dimensions where the geometry problems and the solution algorithms are much more severe, the computing costs for this approach are much too high. Also, as explained in reference 4.3-4, this approach results in a finite-thickness trailing edge which can produce problems in the three dimensional potential flow routine contained in VAPE.

The other technique that Lighthill proposed, transpiration, is much more amenable to the three-dimensional case. In this approach, a surface blowing distribution is defined which results in a dividing streamline of the flow being the same as the modified body in the first method above, Figure 4.3-1. The potential flow about the original body subject to this nonzero-velocity boundary condition on the body surface is the desired modified potential flow that approximates the viscous flow.

This procedure is much faster than the surface displacement approach because of the way potential flow solutions are formulated. In the potential flow program in VAPE, as in most panel methods, the basic calculation consists of two primary parts which account for approximately ninety percent of the total computing time. These two parts are the determination of the "influence coefficient matrix" that contains the velocities induced by the panels on each other and the solution of the linear equations for determining the singularity strength on the panels. Both of these calculations are performed on matrices which are formed entirely from geometric considerations. Therefore, if the geometry remains the same, then these parts would not have to be recalculated. The transpiration approach does not change the geometry, whereas the surface displacement technique does. Therefore, the transpiration approach requires only slightly more computing time than a single potential flow solution, while the surface displacement approach requires a new potential flow solution for each iteration and each angle of attack. Therefore, the computing time difference between the two methods is considerable.

Based on the above observations and on the results of reference 4.3-4, it was decided that transpiration was the only approach that should be used in VAPE.

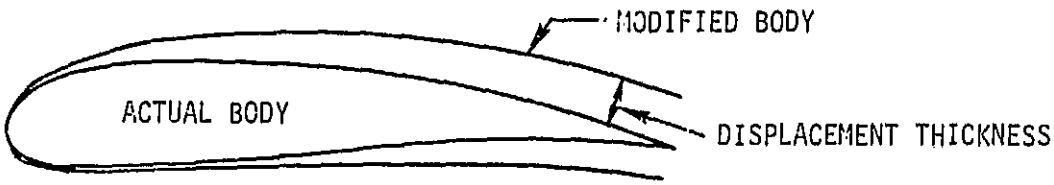

(a) SURFACE DISPLACEMENT MODEL

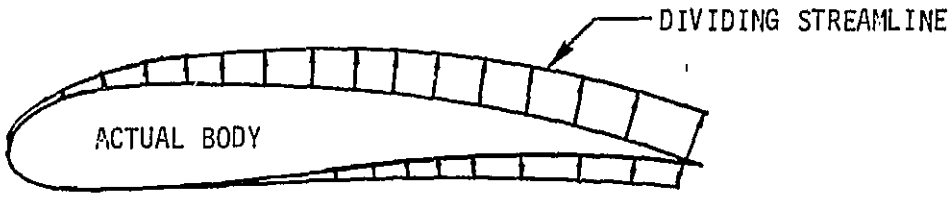

(b) TRANSPIRATION MODEL

FIGURE 4.3-1 VISCOUS SIMULATION MODELS

One other item which has been mentioned above concerns the number of passes or iterations that are required to obtain a good viscous approximation using this combined boundary layer/potential flow procedure. Typically, one iteration requires:

(1) calculate the potential flow about the actual body shape,

(2) calculate the boundary layer displacement thickness using the velocity distributions from (1) as input,

(3) use these displacement thicknesses to define a blowing distribution about the body, and

(4) calculate the potential flow solution about the body with the blowing distribution from (3) imposed on the panels.

In two dimensions, various methods require different amounts of iteration depending on the methods involved. Most techniques involve several iterations with relaxation techniques used to obtain convergence. The method of reference 4.3-3 which used a two-dimensional version of the three-dimensional potential flow program in VAPE and the same boundary layer method required only one iteration. Therefore, the question is raised as to how many iterations need to be performed in this approach. Hess, in reference 4.3-2, presents a very good argument for using one iteration only. Based on Hess's results and the authors own experience with these types of calculations, it was decided to perform only one iteration.

REFERENCES:

4.3-1 Lighthill, M.J.: "On Displacement Thickness", Journal of Fluid Mechanics, Part 4, 1958.

4.3-2 Hess, J.L.: "A fully Automatic Combined Potential Flow Boundary Layer Procedure for Calculating Viscous Effects on the Lifts and Pressure Distributions of Arbitrary Three-Dimensional Configurations," McDonnel Douglas Report No. MDC 57491, June 1977.

4.3-3 Beatty, T.D. and Callagaan, J.G. : "A Theoretical Method for the Analysis and Design of Multi-Element Airfoils," Journal of Aircraft, Vol. 9, No. 12, Dec. 1972.

4.3-4 Kjelgaard, S.L. and Thomas, J.L.: "Comparison of Three-Dimensional Panel Methods with Strip Boundary Layer Theory Simulations to Experiment", NASA TM-80088, July 1979.

4.4 NUMERICAL IMPLEMENTATION OF SIMULATION MODEL

The equivalent "viscous" body has been shown to consist of the original inviscid body modified to include the effects of the boundary layer displacement thickness δ^*. This procedure, therefore, requires that several items be addressed, including:

- a method of determining the boundary layer solutions on the wing surfaces must be formulated, and
- a relationship between the displacement thickness and the blowing rate must be determined.

The first item has several parts to consider. First, how must the surface be partitioned in order to use the two-dimensional strip theory approach. In the VAPE system, the lifting-surface coordinates are normally input along rows of streamwise airfoil shapes. Two of these rows form a lifting "strip" with panels starting at the lower surface trailing edge, proceeding forward on the lower surface to the leading edge and then back to the trailing edge along the upper surface. The potential flow program then determines velocities at the centroids of these panels. Within the accuracy of this approach, these centroids lie along a streamwise section. Thus, this streamwise distribution of centroid locations and associated velocities can be used as input to the boundary layer program. The boundary layer solution must start at the leading edge stagnation point. Therefore, the "strip" of velocities must be divided into two cases, one for the upper surface and one for the lower surface. This is accomplished by searching the velocities on the strip to determine the stagnation point at the leading edge. The strip is then divided at this point and the desired two cases formed. This procedure is formed for the entire lifting surface for each angle of attack. Thus, if the wing has ten strips and solutions for five angles of attack are desired, then:

$$(10)\,(5)\,(2) = 100$$

boundary layer solutions are required. Fortunately, the boundary layer solutions do not require very much computer time.

From the above calculation, a matrix of displacement thickness values is formed with a value for each panel defined. These values are then converted to blowing velocity values using the relationship

$$V_N = \frac{d}{dS}\,(V_t \delta^*) \qquad (4.4\text{-}1)$$

Where V_t is the total inviscid tangential velocity from the potential flow computation, S is surface length starting at the stagnation point and V_N is the required normal velocity for the blowing distribution. These values for V_N are then used to modify the right hand side values of the solution matrix. The matrix is then recombined with this new right hand side to obtain the desired solution. If a direct matrix solution had been used, this recombining would be a simple multiplication of the two matrices. This produces the desired viscous approximation.

5.0 VERIFICATION OF VISCOUS EFFECTS METHOD

The VAPE system has been developed to predict the V/STOL characteristics about arbitrarily shaped V/STOL aircraft. Therefore, the only true evaluation of the program is a direct comparison between calculated and experimental data. There is a wealth of experimental data available for this correlation for various configurations. However, certain constraints should be imposed on the data selection. There should be pressure distributions at several spanwise stations for a wide range of angle of attack. For isolating the viscous effects, they should be simple wing geometries with moderate amounts of sweep and taper. If possible, these configurations should have no body, i.e. ,wing alone, in order to minimize interference effects. These criteria were used to help in deciding what experimental data cases should be used.

Two primary configurations were selected to use in this evaluation effort. Both cases are for wing alone models tested in NASA facilities. One case is for an unswept wing with a taper ratio of 1.0, while the other is for a wing with 45° of sweep and a taper ratio of 0.5. Both have pressure distributions at various spanwise stations for several angles of attack.

The first set of data is contained in reference 5.0-1. This data was selected because it fit the criteria specified above and because it was also used in reference 5.0-2 as a correlation test. Choosing this configuration also permitted direct comparisons with other methods designed to perform the same task.

The second set of data is from reference 5.0-3. This data was selected because it is fairly recent data that fit all of the above criteria.

REFERENCES:

5.0-1 Kolbe, C.D. and Bultz, F.W.: "The Forces and Pressure Distribution at Subsonic Speeds on a Plane Wing Having 45° of Sweepback, an Aspect Ratio of 3. and a Taper Ratio of 0.5", NACA RM A51931, Oct. 1951.

5.0-2 Kjelgaard, S.L. and Thomas, J.L.: "Comparison of Three-Dimensional Panel Methods with Strip Boundary Layer Theory Simulations to Experiment", NASA TM 80088, July 1979.

5.0-3 Yip, L.P. and Shubert, S.L.: "Pressure Distribution on a 1- by 3-Meter Semi-Span Wing at Sweep Angles from 0° to 40° in Subsonic Flow", NASA TN D-8307, Dec. 1976.

5.1 VISCOUS VERIFICATION - CASE 1

The first test case considered was an aspect ratio 3, 45 degree swept wing with a taper ratio of 0.5, reference 5.1-1. This reference contains a very comprehensive set of data on this wing. The airfoil section was a NACA 64A010 perpendicular to the quarter-chord. This data set was one used in reference 5.1-2 to evaluate several "viscous" calculation methods. Figure 5.1-1 presents a schematic of the wing showing the geometric features as well as the spanwise location of the chordwise pressure taps. This configuration was first run through VAPE in an inviscid mode.

Figures 5.1-2 through 5.1-4 present pressure distribution comparisons between experimental data and VAPE inviscid calculations as a function of angle of attack at the 19.3 percent semi-span. Figures 5.1-5 through 5.1-7, and 5.1-8 through 5.1-10 present similar comparisons for 55.5 and 83.1 percent semi-span , respectively. Figure 5.1-11 presents a comparison of the calculated and experimental lift curves and Figure 5.1-12 shows the comparison of pitching moments.

In Figure 5.1-13, the calculated and experimental span loadings are shown. On this graph, in addition to the basic VAPE solution, there are two other calculations shown. The "open ended" VAPE run was calculated to see what the effect of a very small gap (i.e. actual airfoil trailing edge) would be on the VAPE solution. Reference 5.1-2 indicates that opening the trailing edge in this type of potential flow method can be detrimental. In this case, very little effect was seen. The other case shown is taken from reference 5.1-3. There is a discrepancy between the inviscid results of reference 5.1-3 and the VAPE calculations near the wing tip which has not been resolved. However, one would not expect inviscid and experimental results to disagree over 80 percent of the semi-span and then agree near the tip. This suggests that the calculation of reference 5.1-3 lacked resolution near the wing tip.

The results of the inviscid VAPE calculations are as expected and are in reasonable agreement with the results shown in reference 5.1-2. This configuration was then run through VAPE using the viscous option. These cases were run for 4 and 6 degrees at a Reynolds number of 4 million. Figures 5.1-14 through 5.1-19 show pressure distributions at various spanwise stations comparing inviscid, viscous and experimental levels. Figure 5.1-20 presents a comparison of inviscid, "viscous" and experimental data for the span loading distributions. The predicted results differ from the experimental data by the same amount as results obtained in reference 5.1-2 on the same configuration. Various techniques for calculating the "viscous" lift in Table 6 of reference 5.1-2 in terms of a total lift loss factor K_3, are defined by:

$$K_3 = \frac{C_{L\ \text{potential}} - C_{L\ \text{viscous}}}{C_{L\ \text{potential}}} \qquad (5.1\text{-}1)$$

The studies conducted in reference 5.1-2 indicate that a value of K_3 on the order of .02 is reasonable for this configuration. Values of K_3 calculated by VAPE, shown in Table I, agree very well with the results of reference 5.1-2.

While the "viscous" solution matches other computational techniques, there still exists a sizable difference between the "viscous" solution and the experimental values. These differences can be attributed to the panel density as shown in Figure 5.1-21 taken from reference 5.1-2. Figure 5.1-21 shows the calculated potential flow lift from two calculation methods, references 5.1-4 and 5.1-5, as a function of spanwise and chordwise panelling. Reference 5.1-4 is essentially the same potential flow code contained in VAPE. Using the slope obtained from Figure 5.1-21 for the 50 chordwise points case to extrapolate the values calculated by VAPE to an infinite number of span stations, we obtain:

1) $\alpha = 4^\circ$, $C_{L_{extrapolated}} = .197$

2) $\alpha = 6^\circ$, $C_{L_{extrapolated}} = .31$

Comparing these to the experimental values of C_L presented in Table 1 shows excellent agreement. The results presented in Figure 5.1-21 are essentially what one should expect from a low order panel code. Thus, based on this comparison, the "viscous" algorithm seems to be working as expected.

TABLE 1 $R_N = 4.X10^6$

ANGLE OF ATTACK	POTENTIAL LIFT	"VISCOUS" LIFT	K_3	EXPERIMENTAL LIFT VALUES
4°	.2305	.2239	.029	.20
6°	.3438	.3367	.021	.30

REFERENCES:

5.1-1 Kolbe, C.D. and Bultz, F.W.: "The Forces and Pressure Distribution at Subsonic Speeds on a Plane Wing Having 45° of Sweepback, an Aspect Ratio of 3, and a Taper Ratio of 0.5", NACA RM A51931, Oct. 1951.

5.1-2 Kjelgaard, S.L. and Thomas, J.L.: "Comparison of Three-Dimensional Panel Methods with Strip Boundary Layer Theory Simulations to Experiment, NASA TM-80088, July 1979.

5.1-3 Hess, J.L.: "A Fully Automatic Combined Potential Flow Boundary Layer Procedure for Calculating Viscous Effects on the Lifts and Pressure Distributions of Arbitrary Three-Dimensional Configurations", McDonnell Douglas Report No. MDC 57491, June 1977.

5.1-4 Hess, J.L.: "Calculation of Potential Flow About Arbitrary Three-Dimensional Lifting Bodies", McDonnell Douglas Report No. MDC J5679-01, Oct. 1972.

5.1-5 Ehlers, F.E., Epton, M.A., Johnson, F.T., Magnus, A.E. and Ruppert, P.E.: "An Improved Higher Order Panel Method for Linearized Supersonic Flow", AIAA Paper No. 78-15, 1978.

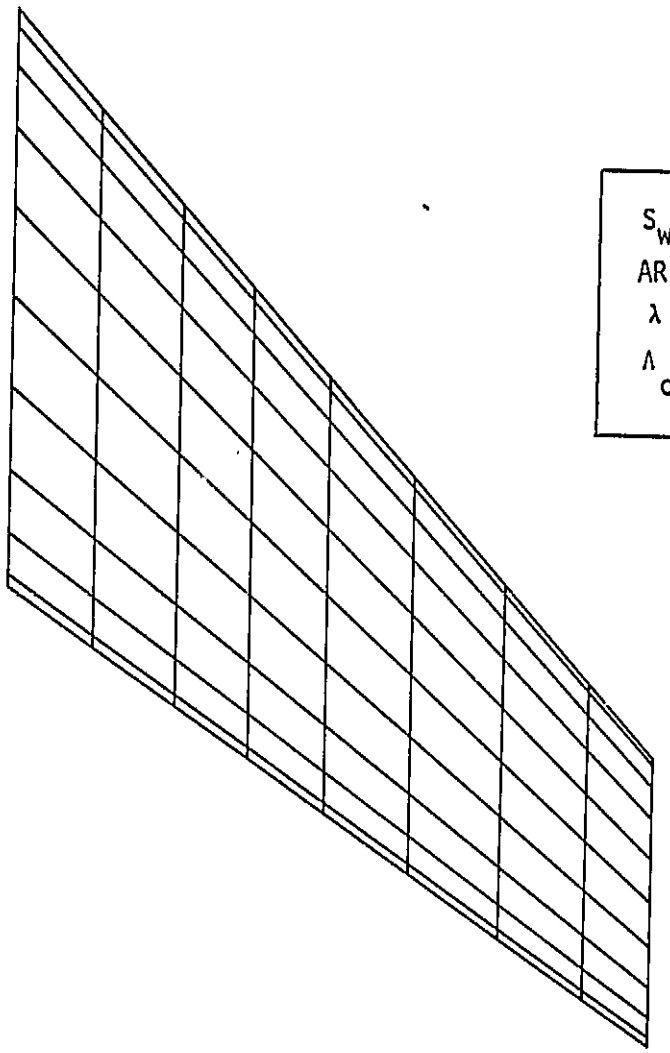

S_W	2903.9 IN^2
AR	3.0
λ	.5
$\Lambda_{c/4}$	45^o

FIGURE 5.1-1 TEST CASE FOR VISCOUS SOLUTION FROM NACA RM-A51G31

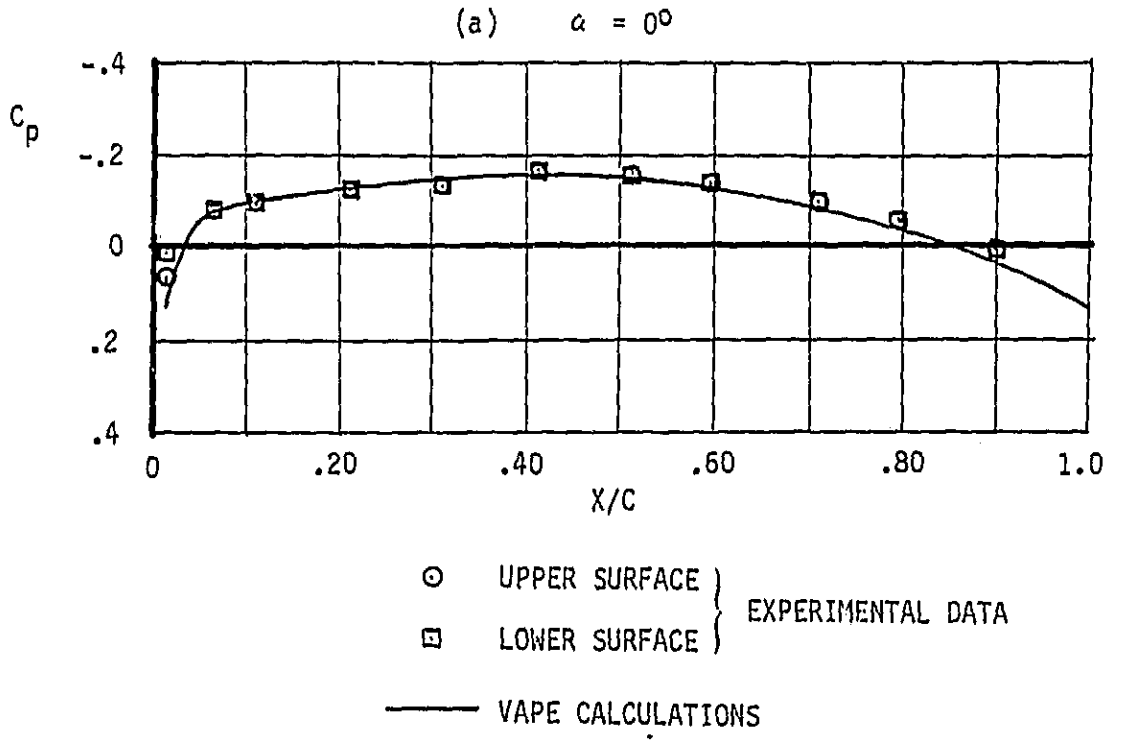

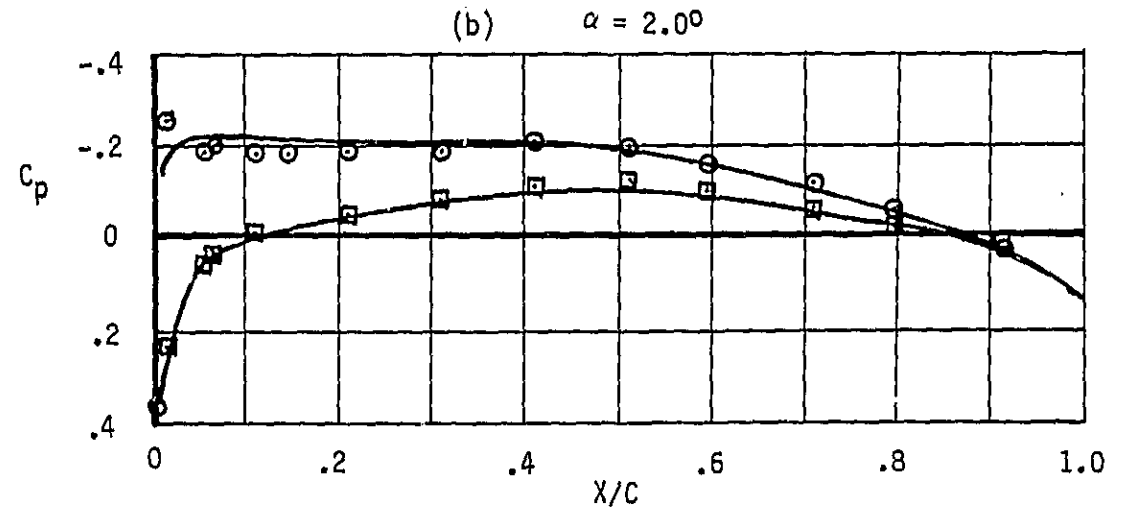

FIGURE 5.1-2 COMPARISON OF VAPE CALCULATIONS TO EXPERIMENTAL DATA FOR THE NACA RM-A51G31 WING AT 19.3 PERCENT SEMISPAN

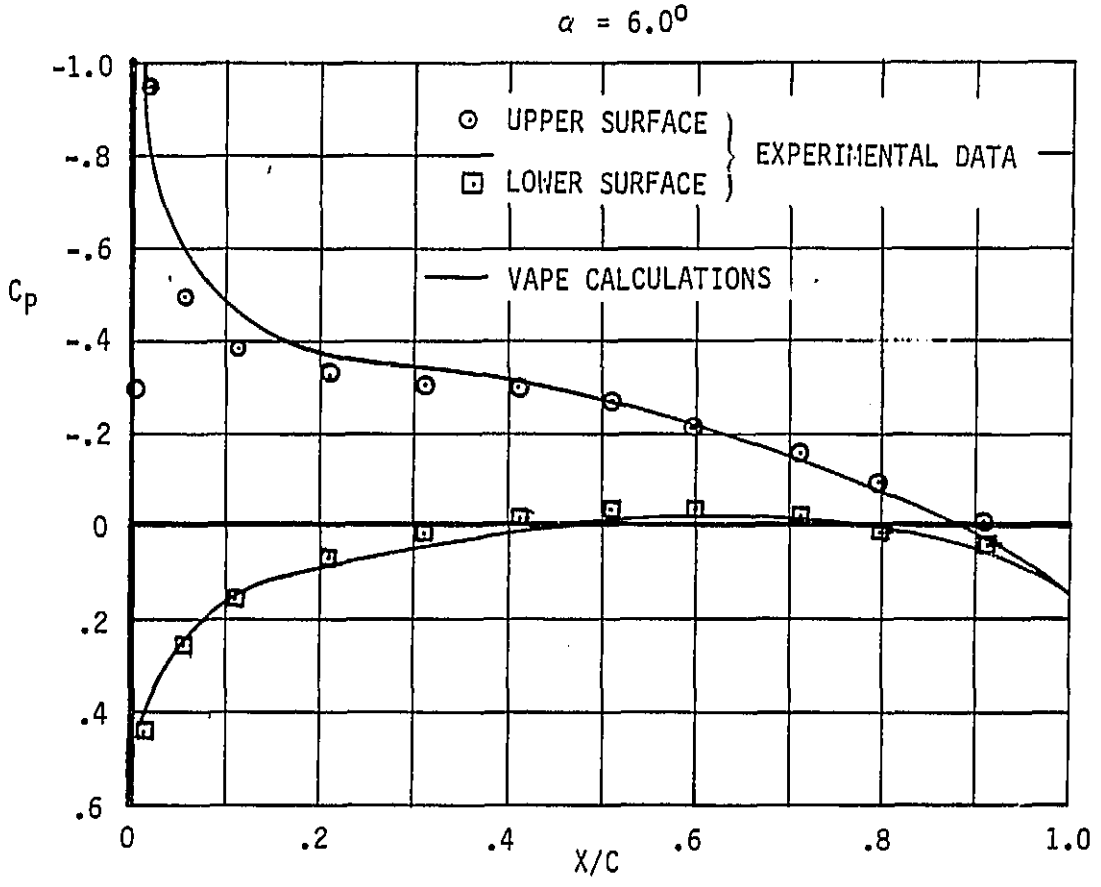

FIGURE 5.1-3 COMPARISON OF VAPE PREDICTIONS TO EXPERIMENTAL DATA FOR THE NACA RM-A51G31 WING AT 19.3 PERCENT SEMISPAN

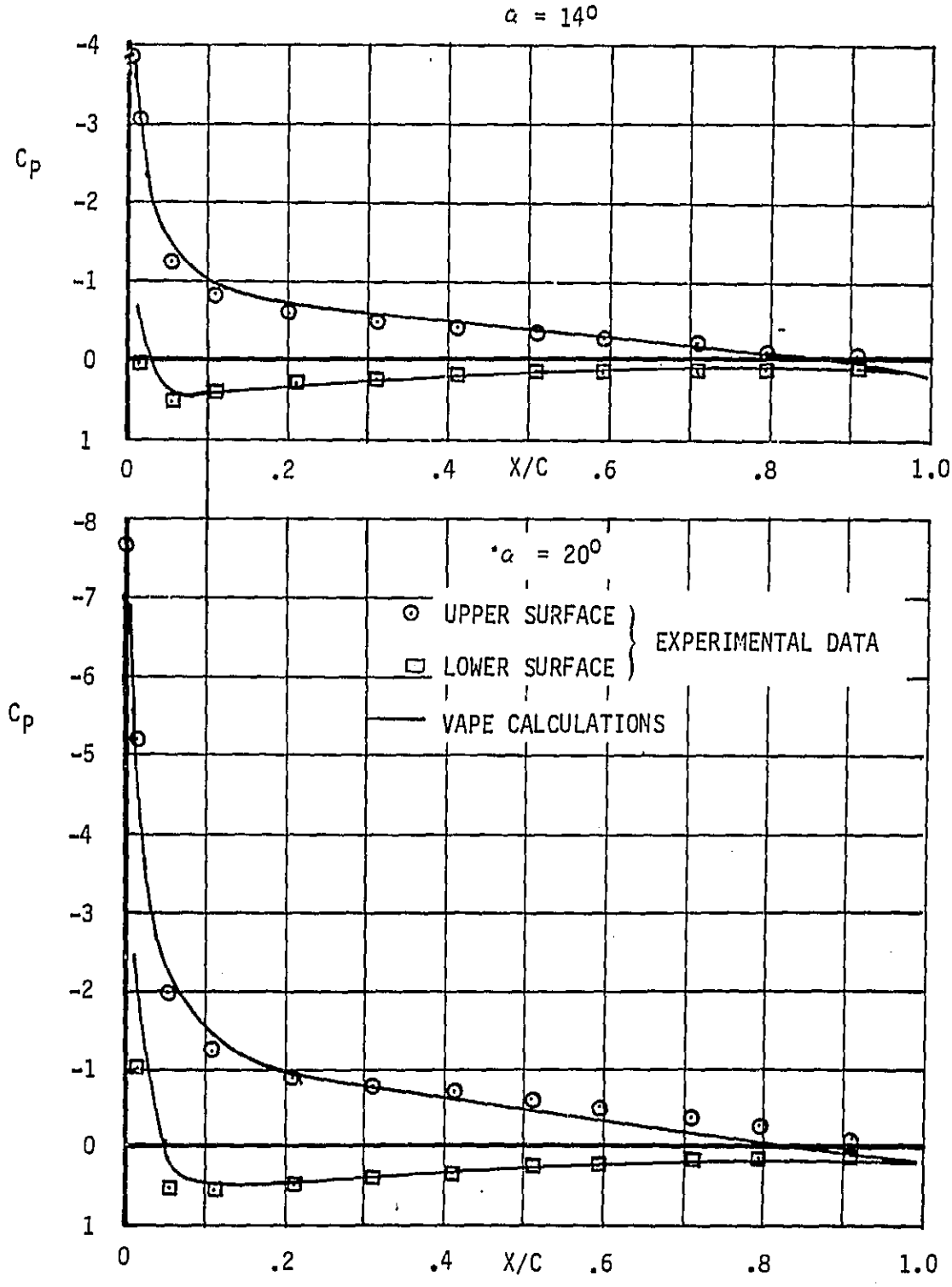

FIGURE 5.1-4 COMPARISON OF VAPE PREDICTIONS TO EXPERIMENTAL DATA FOR THE NACA RM-A51G31 WING AT 19.3 PERCENT SEMISPAN

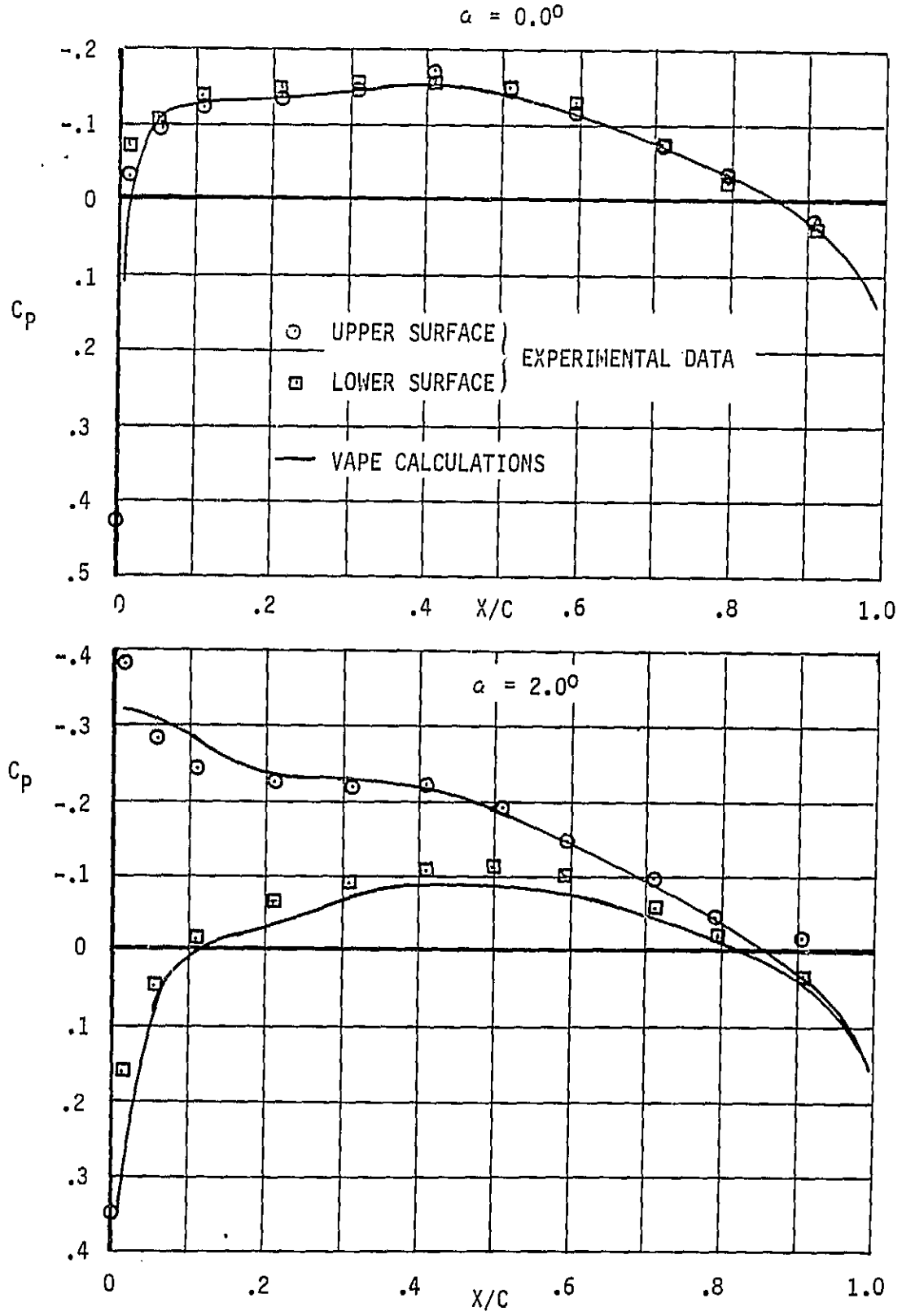

FIGURE 5.1-5 COMPARISON OF VAPE PREDICTION TO EXPERIMENTAL DATA FOR THE NACA RM-A51G31 WING AT 55.5 PERCENT SEMISPAN

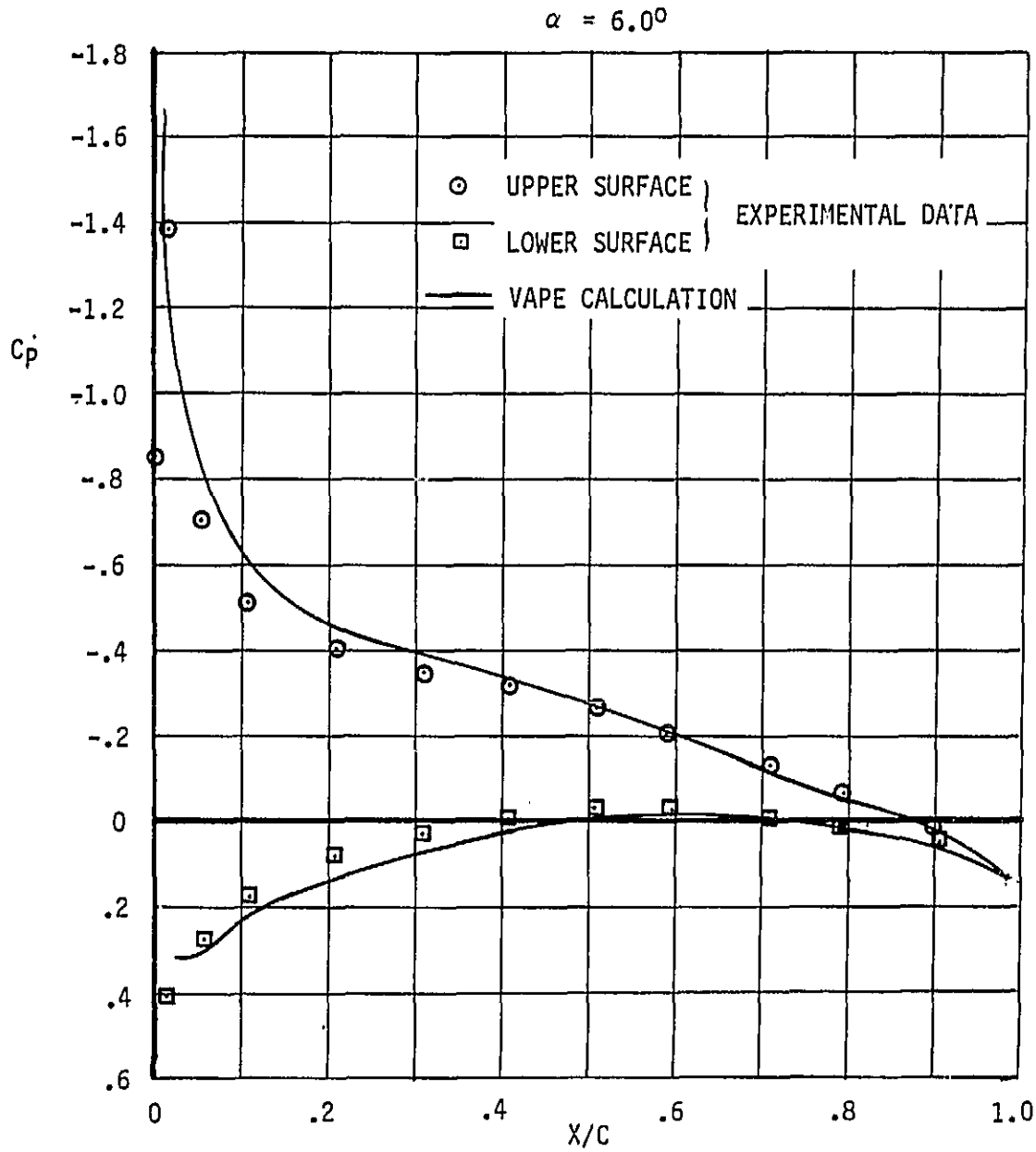

FIGURE 5.1-6 COMPARISON OF VAPE PREDICTION TO EXPERIMENTAL DATA FOR THE NACA RM-A51G31 WING AT 55.5 PERCENT SEMISPAN

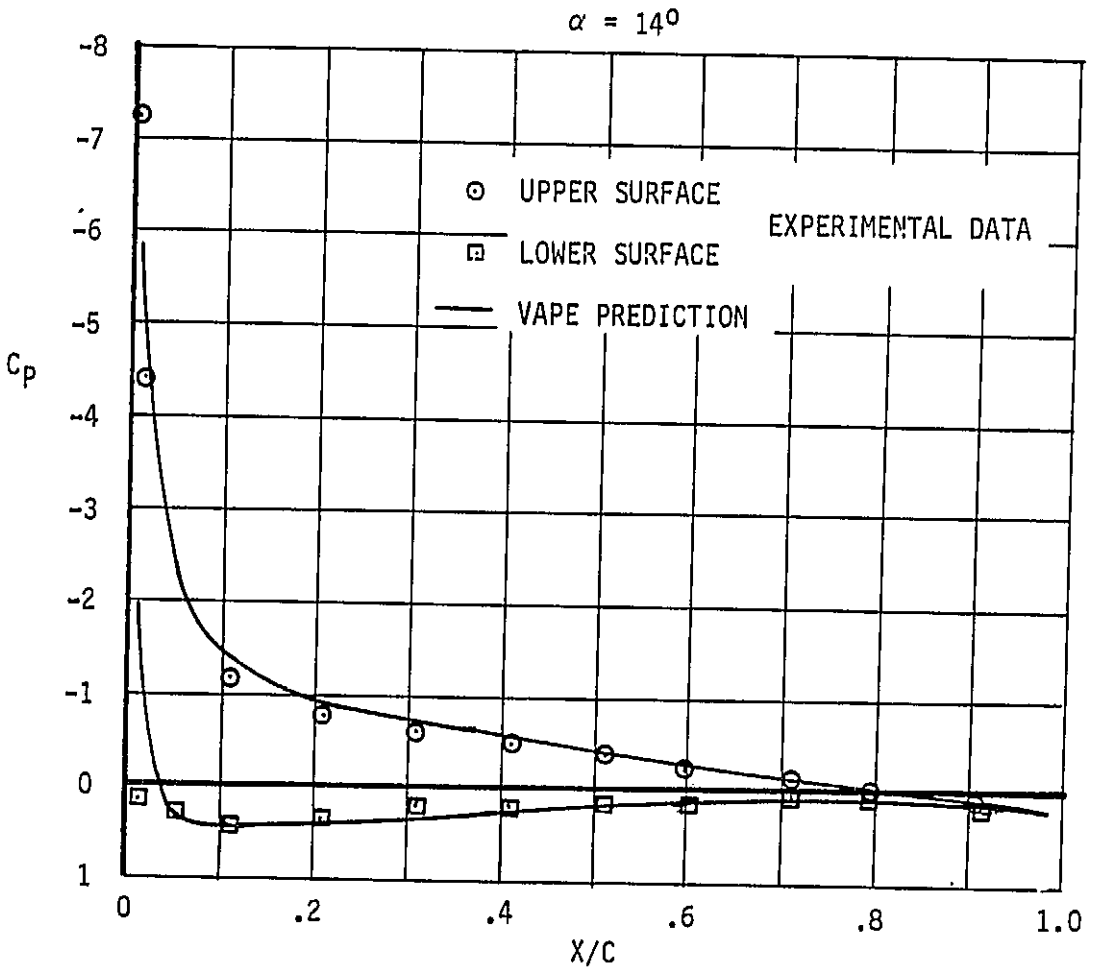

FIGURE 5.1-7 COMPARISON OF VAPE PREDICTIONS TO EXPERIMENTAL DATA FOR THE NACA RM-A51G31 WING AT 55.5 PERCENT SEMISPAN

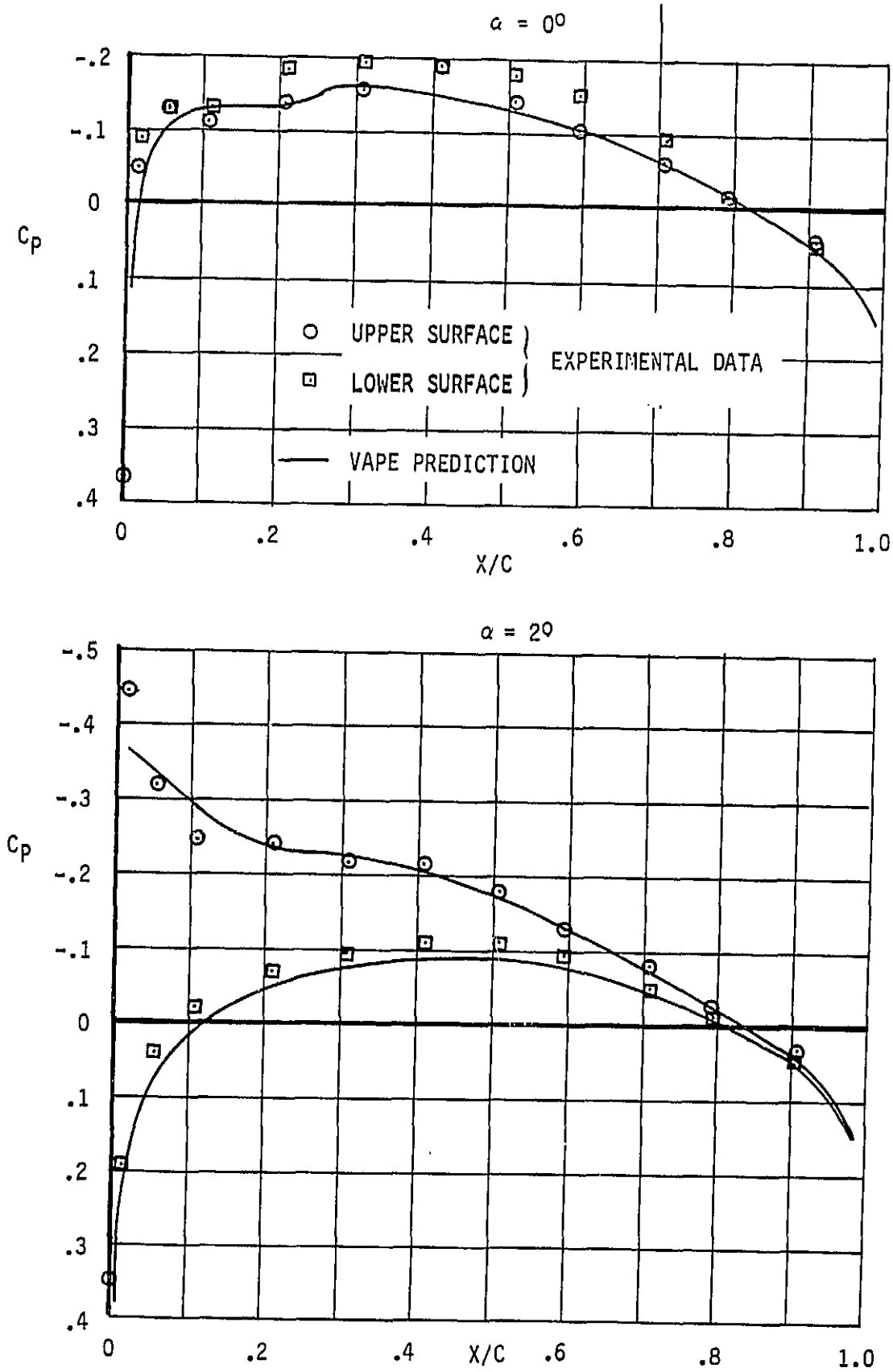

FIGURE 5.1-8 COMPARISON OF VAPE PREDICTIONS TO EXPERIMENTAL DATA FOR THE NACA RM-A51G31 WING AT 83.1 PERCENT SEMISPAN

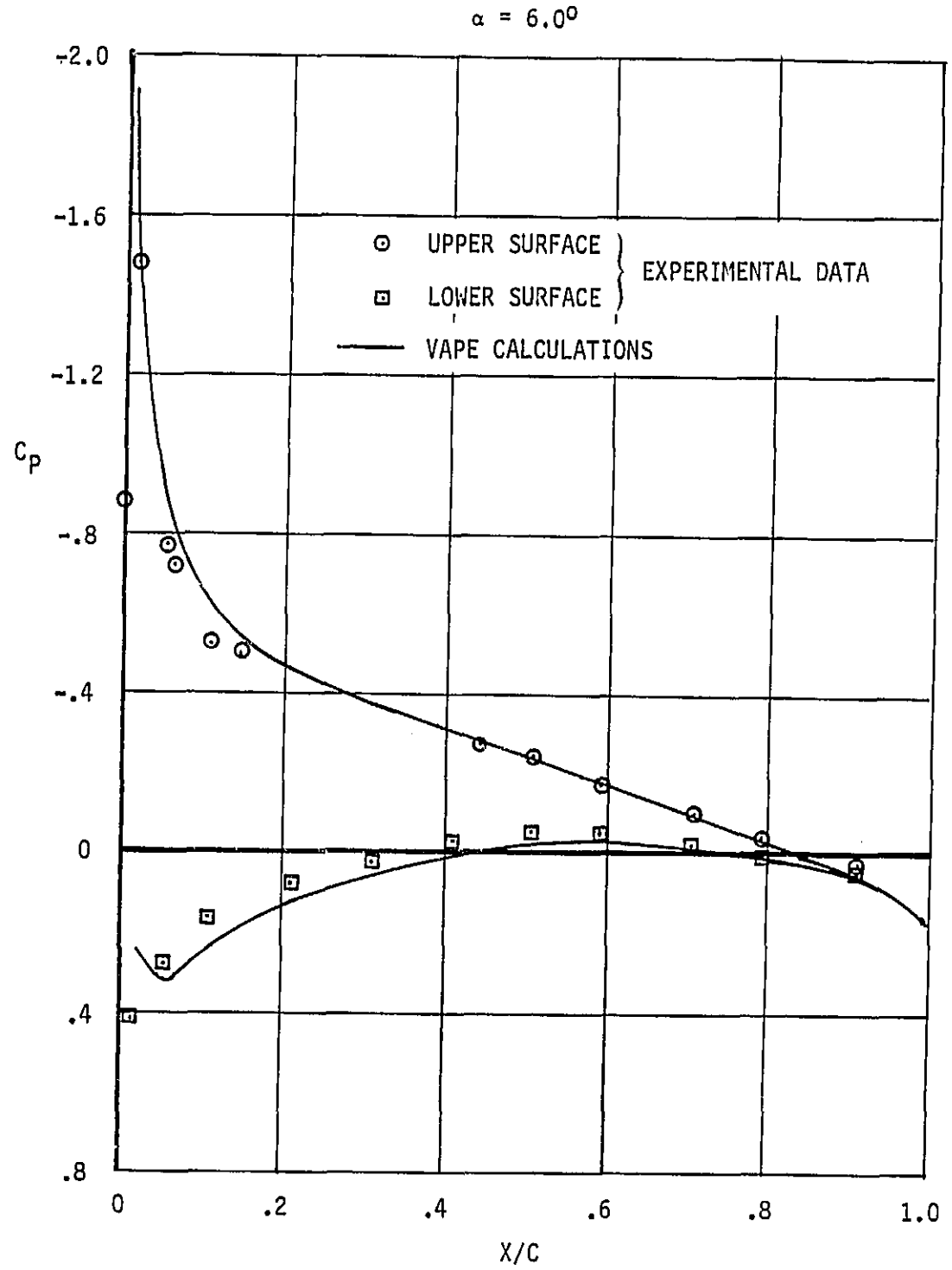

FIGURE 5.1-9 COMPARISON OF VAPE PREDICTIONS TO EXPERIMENTAL DATA FOR THE NACA RM-A51G31 WING AT 83.1 PERCENT SEMISPAN

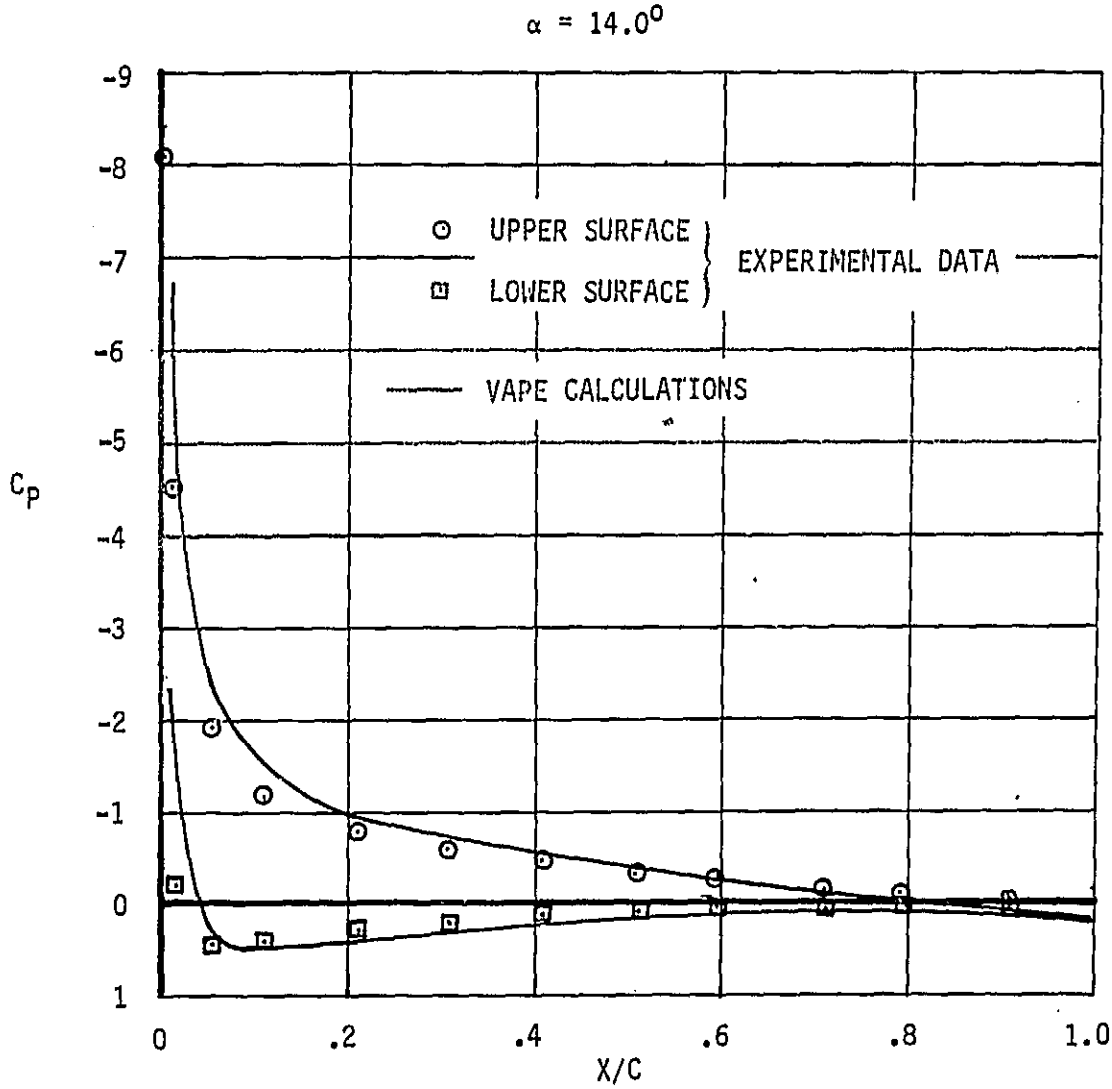

FIGURE 5.1-10 COMPARISON OF VAPE PREDICTIONS TO EXPERIMENTAL DATA FOR THE NACA RM-A51G31 WING AT 83.1 PERCENT SEMISPAN

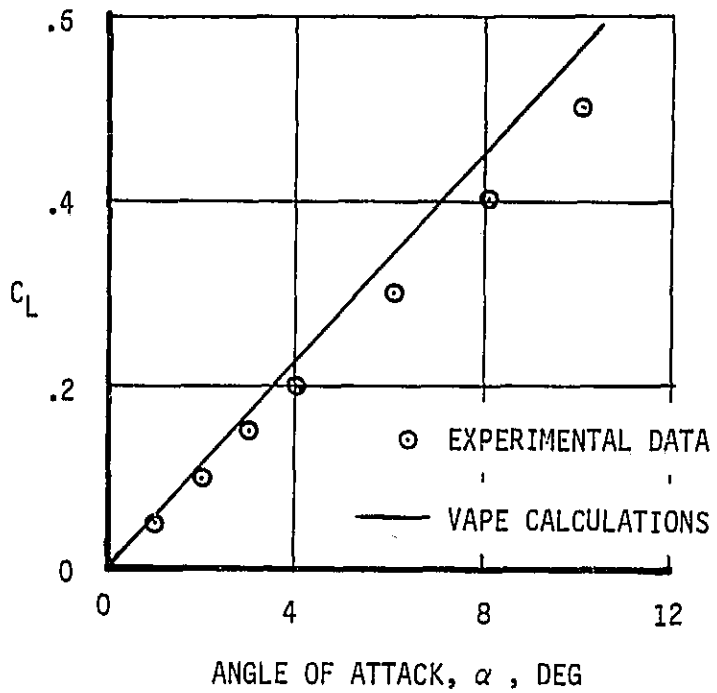

FIGURE 5.1-11 COMPARISON OF VAPE CALCULATED LIFT COEFFICIENT TO EXPERIMENTAL DATA FOR NACA RM-A51G31

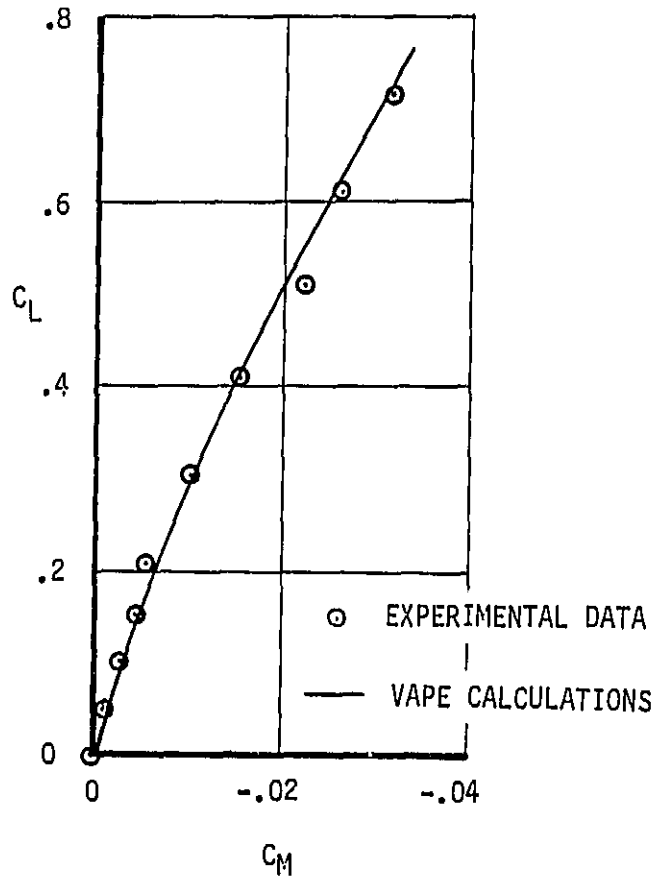

FIGURE 5.1-12 COMPARISON OF VAPE CALCULATED MOMENT COEFFICIENTS TO EXPERIMENTAL DATA FOR NACA RM-A51G31 WING

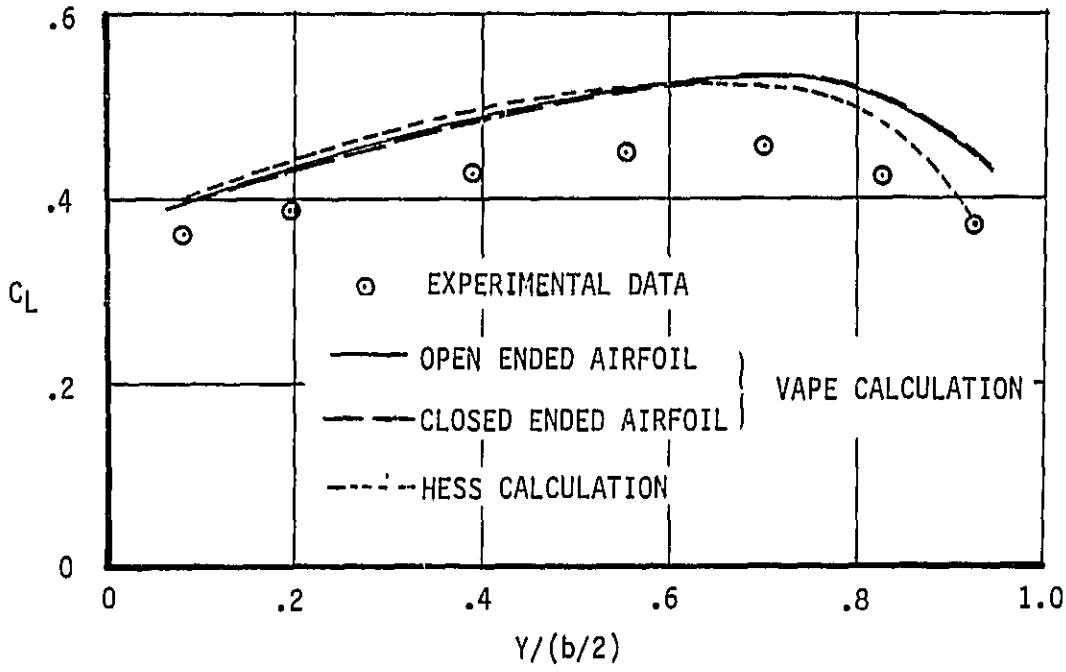

FIGURE 5.1-13 COMPARISON OF VAPE CALCULATIONS AND EXPERIMENTAL SPANWISE DISTRIBUTIONS OF SECTION LIFT COEFFICIENT FOR A NACA RM-A51G31 WING AT 8.2° ANGLE OF ATTACK

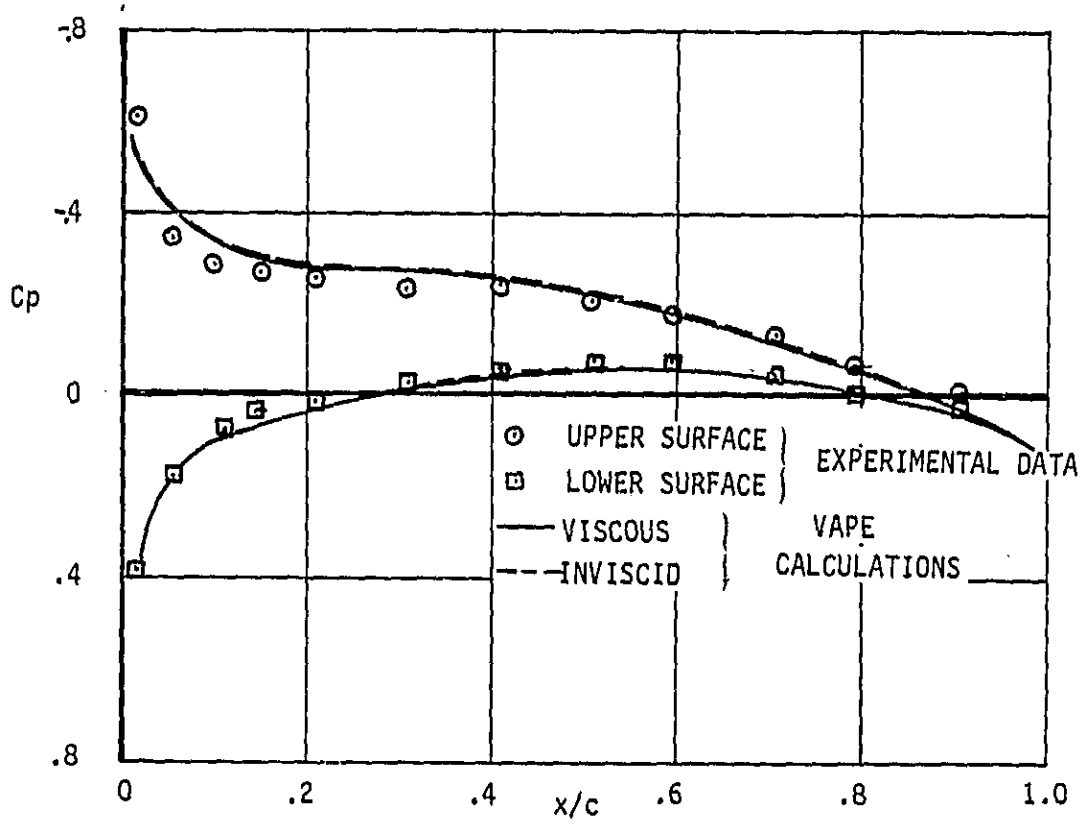

FIGURE 5.1-14 COMPARISON OF VAPE CALCULATIONS WITH AND WITHOUT VISCOUS EFFECTS TO EXPERIMENTAL DATA FOR WING OF NACA RM-A51G31, $\alpha = 4^{o}$, $\eta = .195$

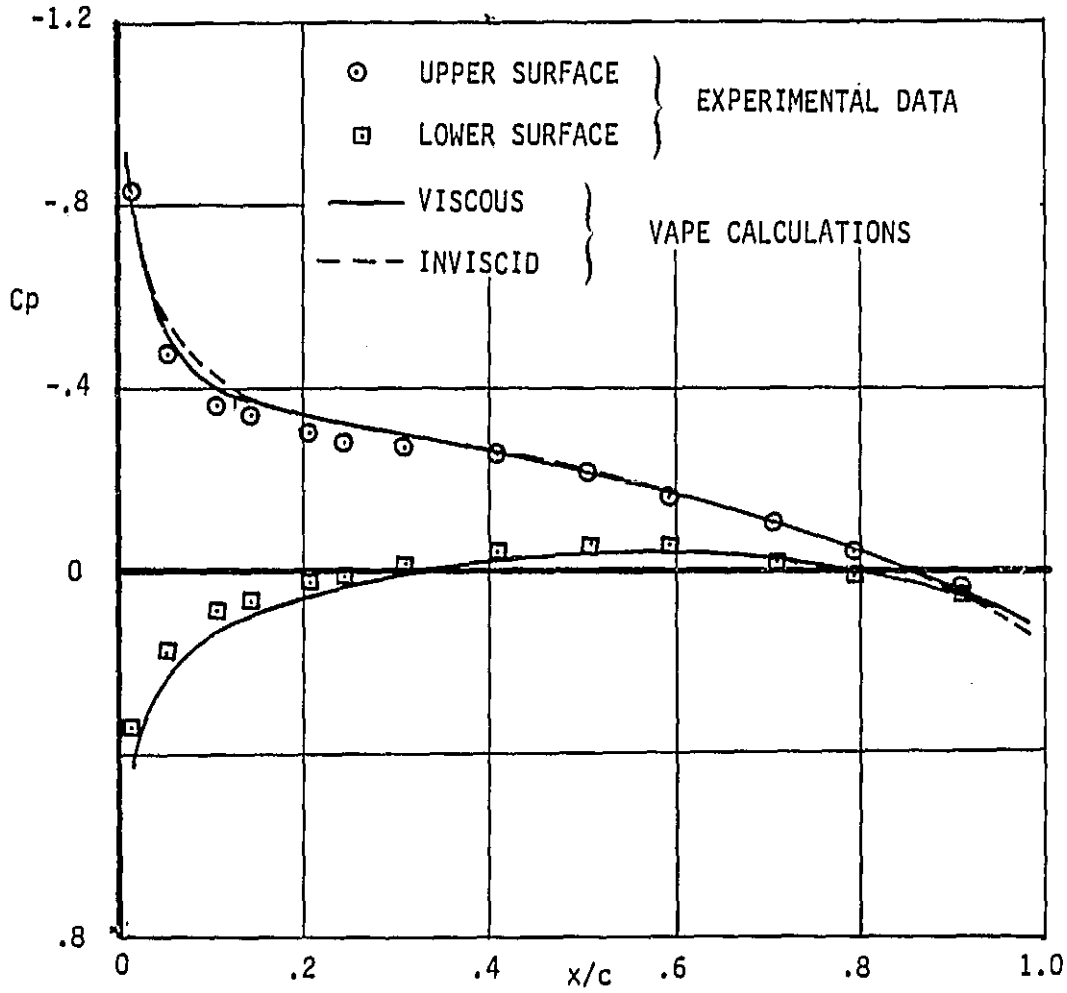

FIGURE 5.1-15 COMPARISON OF VAPE CALCULATIONS WITH AND WITHOUT VISCOUS EFFECTS TO EXPERIMENTAL DATA FOR WING OF NACA RM-A51G31, $\alpha = 4^{o}$ $\eta = .555$

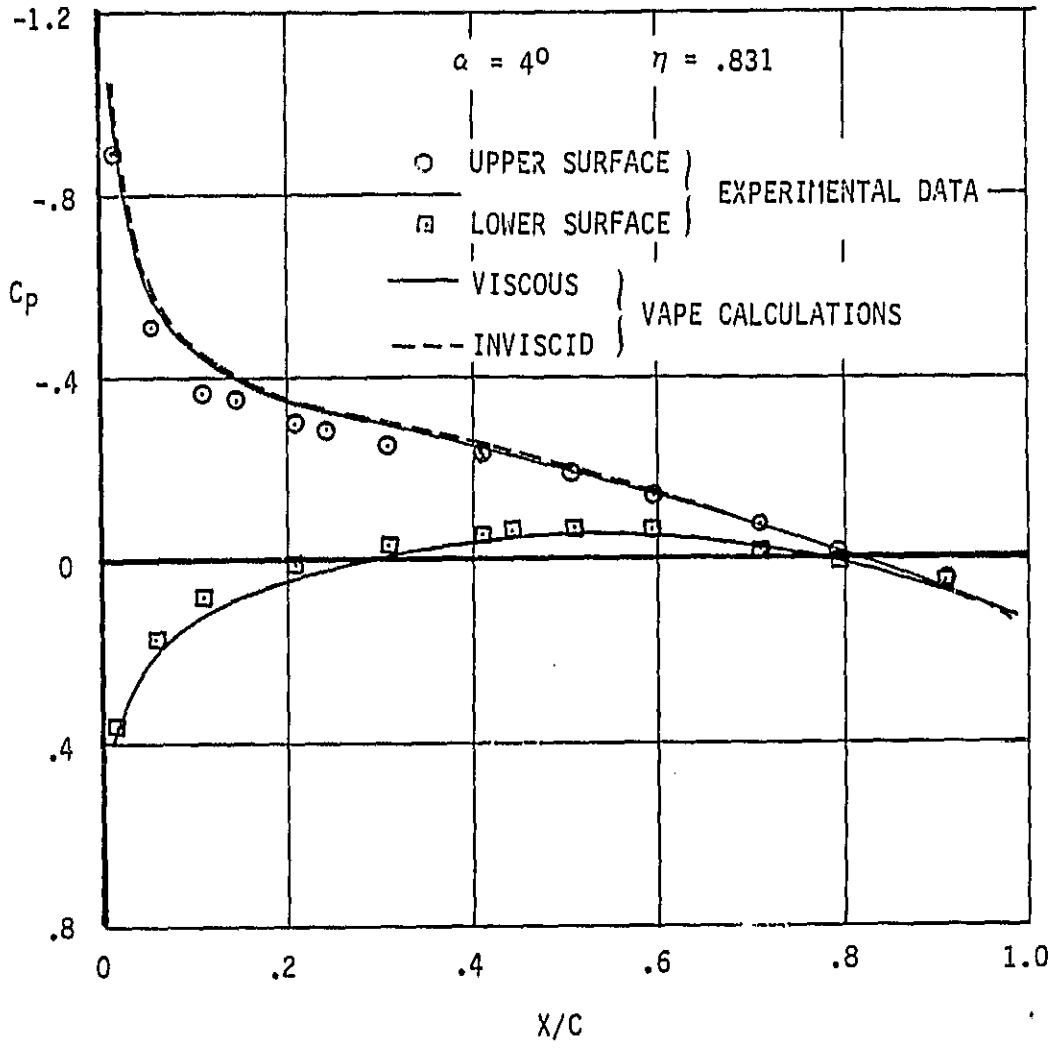

FIGURE 5.1-16 COMPARISON OF VAPE CALCULATIONS WITH AND WITHOUT VISCOUS EFFECTS TO EXPERIMENTAL DATA FOR WING OF NACA RM-A51G31

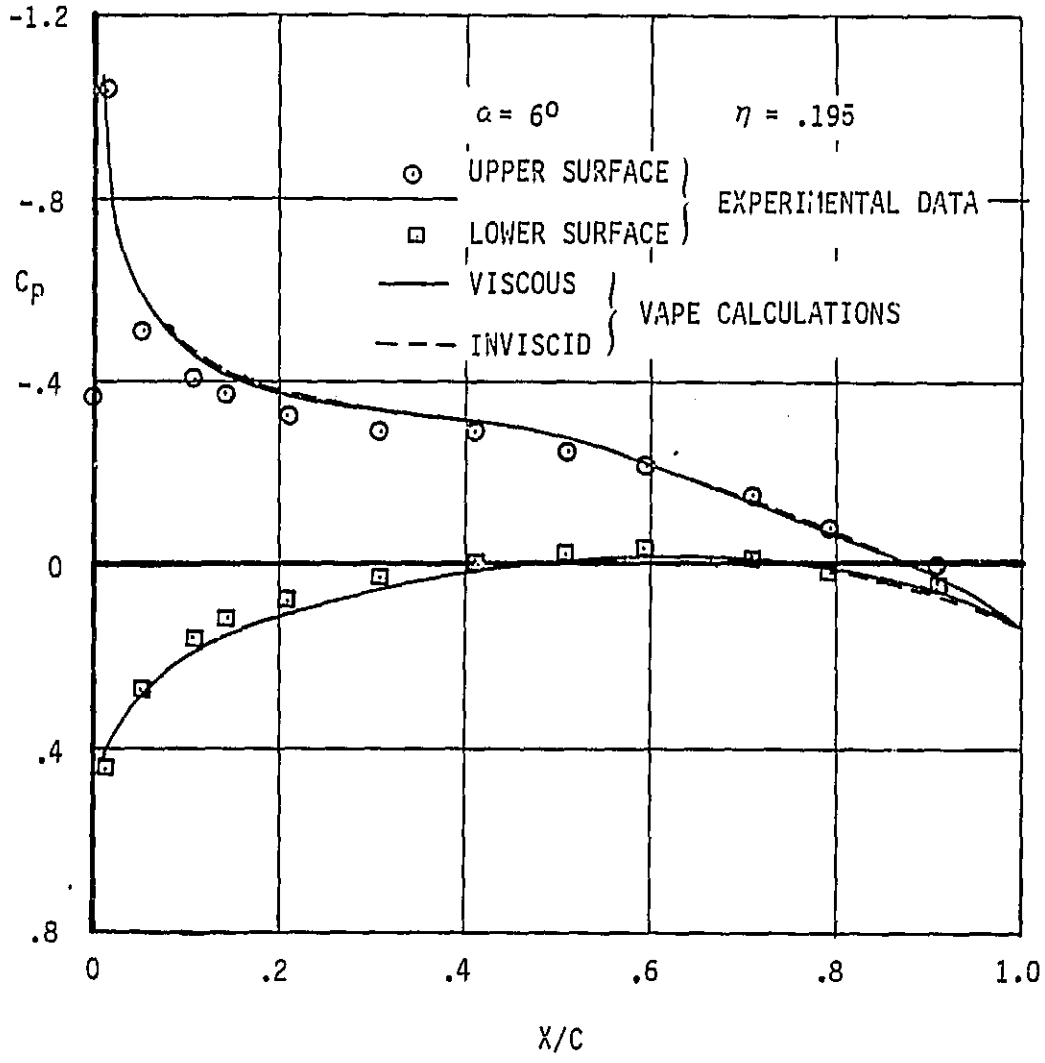

FIGURE 5.1-17 COMPARISON OF VAPE CALCULATIONS WITH AND WITHOUT VISCOUS EFFECTS TO EXPERIMENTAL DATA FOR WING OF NACA RM-A51G31

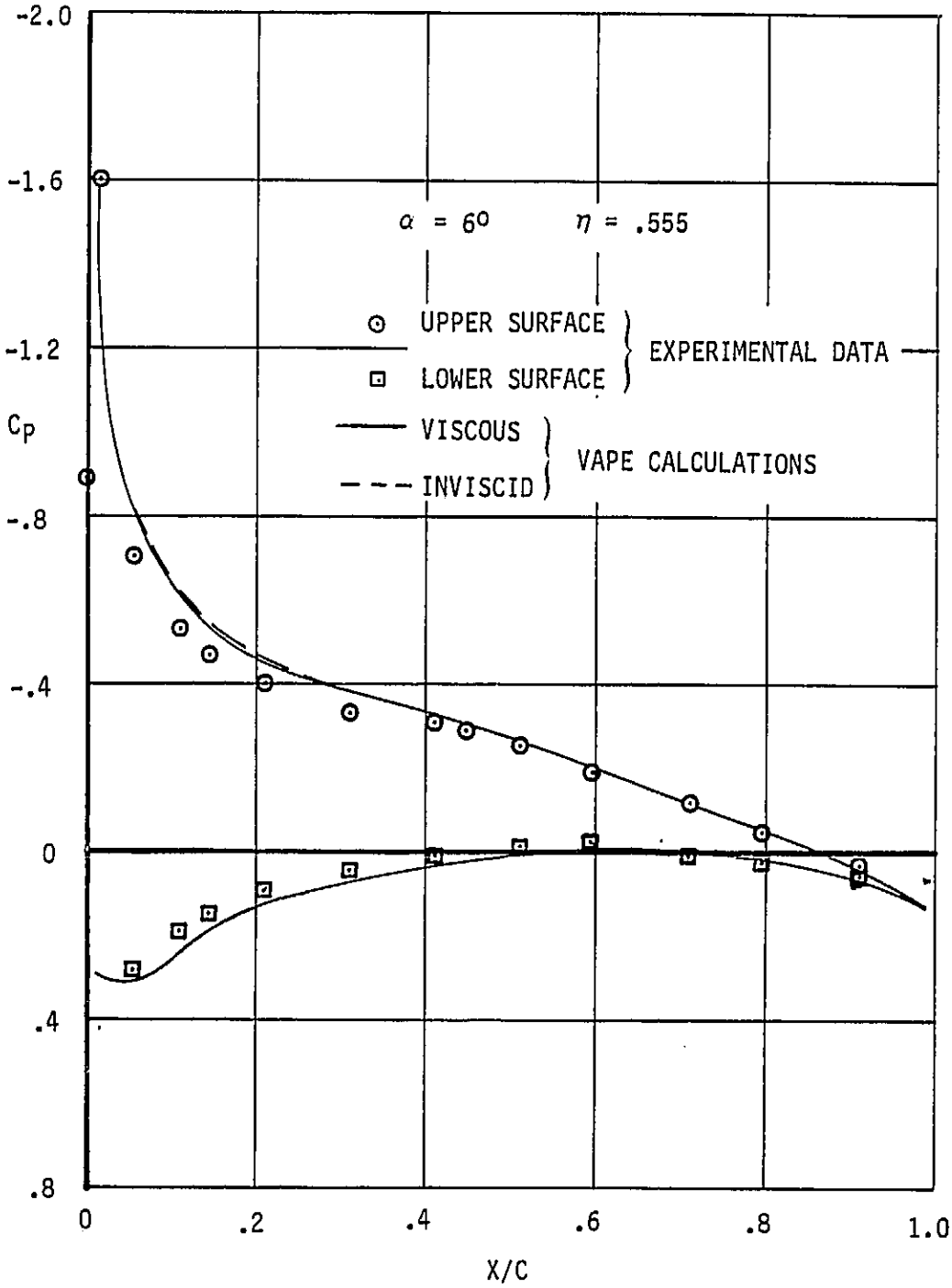

FIGURE 5.1-18 COMPARISON OF VAPE CALCULATIONS WITH AND WITHOUT VISCOUS EFFECTS TO EXPERIMENTAL DATA FOR WING OF NACA RM-A51G31

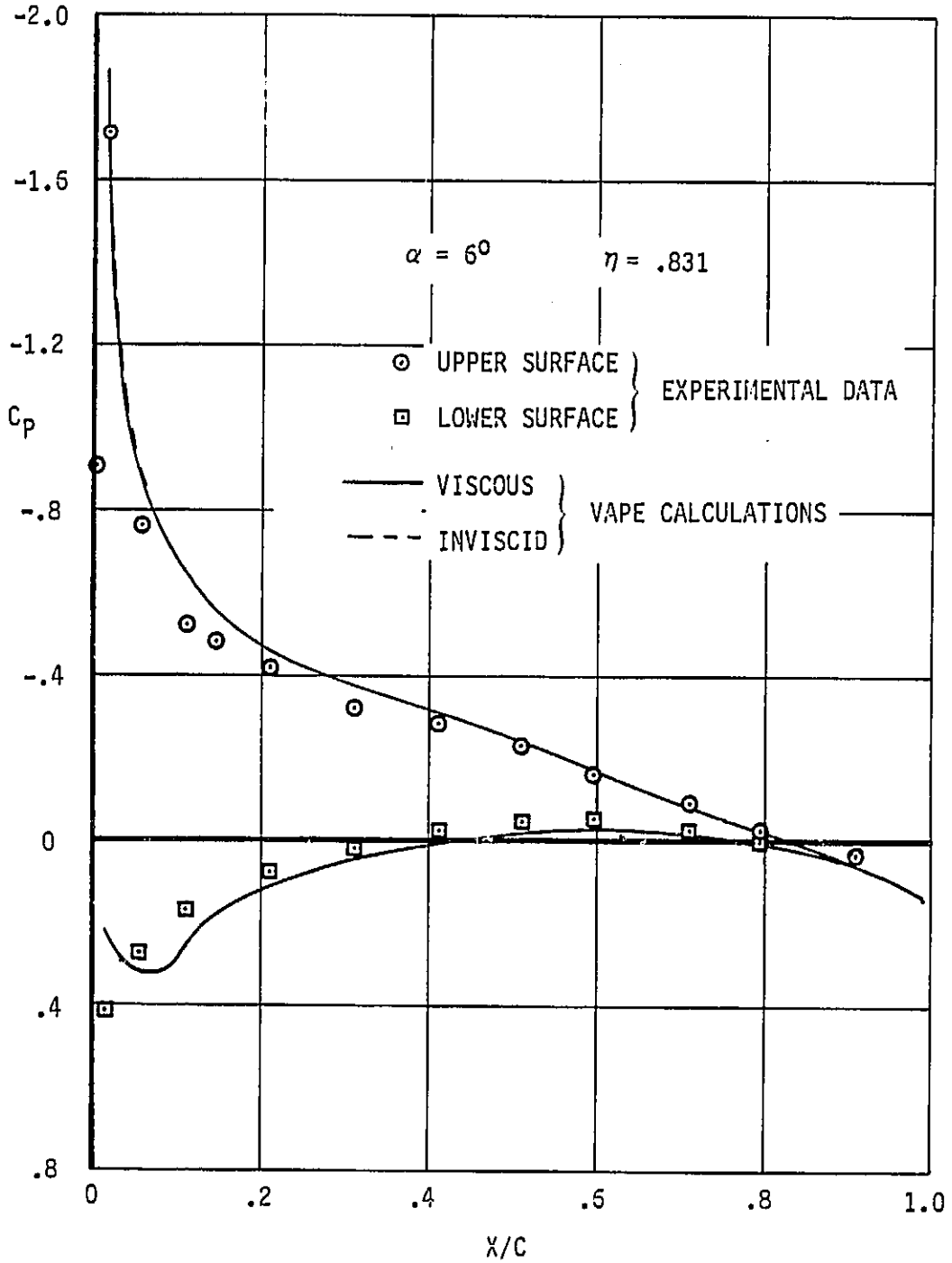

FIGURE 5.1-19 COMPARISON OF VAPE CALCULATIONS WITH AND WITHOUT VISCOUS EFFECTS TO EXPERIMENTAL DATA FOR NACA RM-A51G31

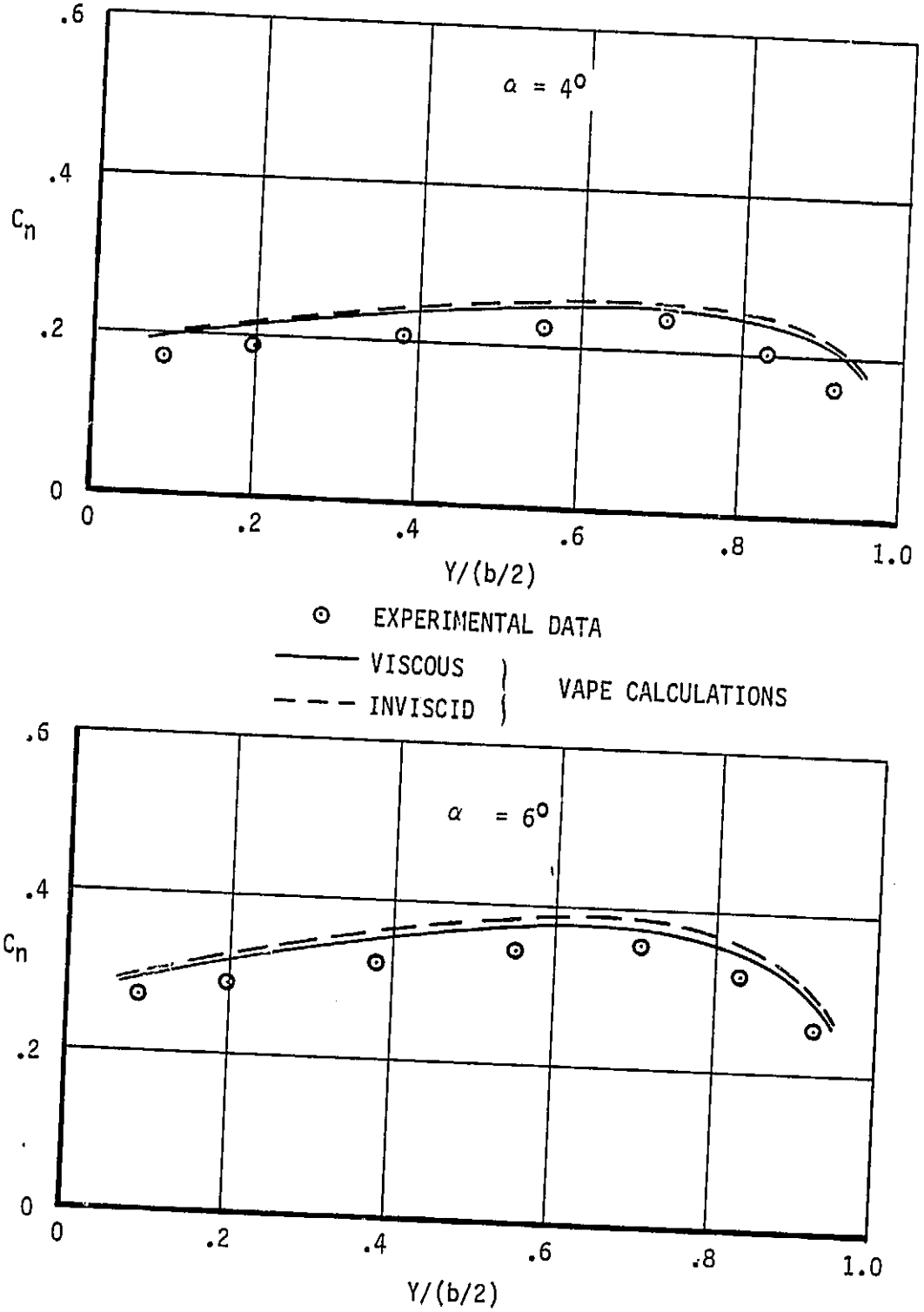

FIGURE 5.1-20 COMPARISON OF VAPE CALCULATIONS WITH AND WITHOUT VISCOUS EFFECTS TO EXPERIMENTAL DATA FOR SPAN LOAD DISTRIBUTION ON WING OF NACA RM-A51G31

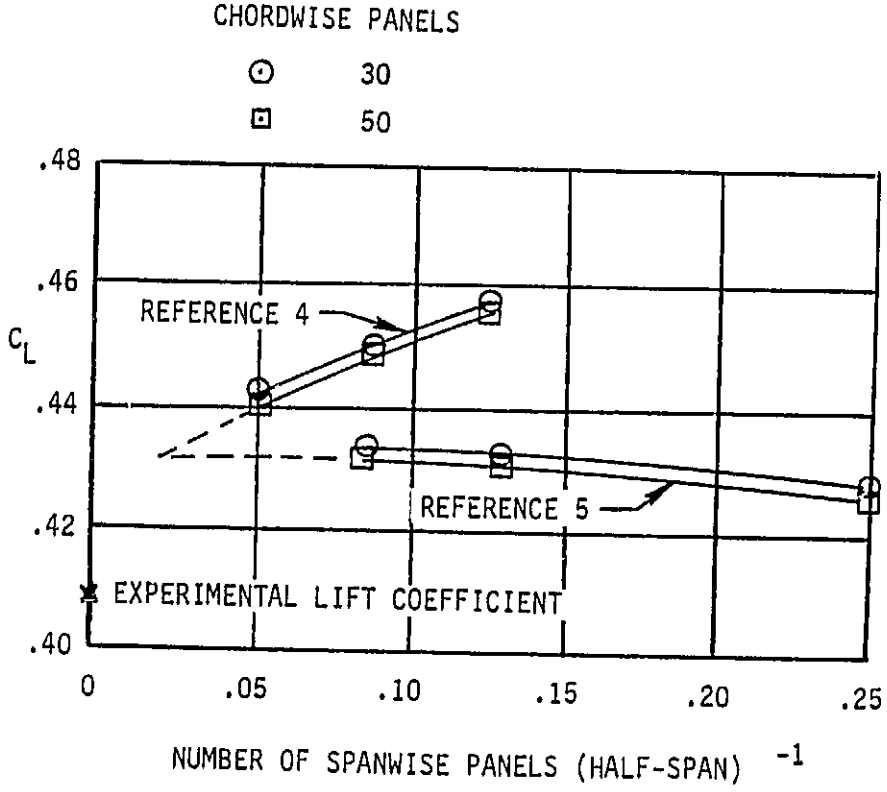

FIGURE 5.1-21 POTENTIAL FLOW RESULTS AS A FUNCTION OF PANEL DENSIITY

5.2 VISCOUS VERIFICATION - CASE 2

The configuration of reference 5.2-1 has been used as the second verification run for the VAPE viscous calculation. This configuration, as shown in Figure 5.2-1, is a simple aspect ratio 5.9 rectangular wing planform.

This configuration was also selected to determine the sensitivity of the method to spanwise paneling. Two inviscidly cases were analyzed: (1) a uniform spanwise paneling, and (2) a variable spanwise paneling. The latter case was completely arbitrary. Figures 5.2-2 and 5.2-3 present comparisons of the calculation and analytical results for the local normal force as a function of spanwise location. The two cases showed essentially the same results, except that due to the more detailed spacing near the tip, the non-uniform distribution was slightly better. Figures 5.2-4 and 5.2-5 present comparisons between calculated and experimental values of normal force and pitching moment versus angle of attack. Again, the agreement between inviscid and experiment is very good. Figure 5.2-6 presents comparisons between VAPE inviscid pressures and experiment at one spanwise station ($\eta = .2$).

This configuration was then run through VAPE with the viscous effects included. The results are presented in Figures 5.2-7 through 5.2-9. Figure 5.2-7 presents normal force versus angle of attack comparisons showing very good agreement between viscous calculations and experimental data. Figure 5.2-8 shows similar comparisons for pitching moment, again indicating excellent agreement. Figure 5.2-9 presents comparisons of experimental and calculated results for span loading. In this case, the agreement with experiment is good for both the inviscid and viscous calculations. The predictions presented were done using the free transition option which allows the program to choose the transition point.

The data generated by VAPE on this configuration was examined to determine how well the algorithms to predict transition from laminar to turbulent flow and to predict turbulent flow separation, worked. The transition from laminar to turbulent flow can be predicted as discussed in Section 4.2 in one of two ways. A transition location according to an empirical predictive technique or laminar separation with subsequent flow reattachment can be predicted by VAPE. For the case analyzed, there are no experimental values available for the transition point location. Therefore, the results of the VAPE calculations for this case can only be judged qualitatively. The calculations indicate that at the low angles of attack (less than 8 degrees) transition is predicted by the empirical technique, whereas at the higher angles (8 degrees and above), transition is determined by laminar separation with subsequent flow reattachment. These results seem reasonable based on past experiences with similar wing planforms and section shapes. The prediction techniques are fairly standard and have been used for two-dimensional calculations very successfully for several years. Therefore, they are expected to be fairly reasonable for planforms which are not highly swept and have a reasonable aspect ratio. The results should be used carefully if the configurations deviate from the above, and if necessary, the transition point should be specified in the input.

The turbulent separation locations predicted by VAPE on this configuration were also studied. The experimental data pressure distributions did not show any obvious flow separation at the angles of attack analyzed ($\alpha \leq 16^\circ$). That is, there was no area of constant pressure at the trailing edge which can be indicative of trailing edge separation. It was noticed, however, that the trailing edge pressures did decrease as the angle of attack increased. Since this is also an indication of trailing edge separation, it

was decided to look closely at the experimental trailing edge values. Figures 5.2-10 through 5.2-14 present the experimental trailing edge pressures as a function of span and angle of attack. As can be seen, for most spanwise sections, the pressures remain constant at some pressure greater than .1 at low angles and then begin to decrease at the higher angles. The exact location of separation cannot be determined from these charts, but it can be assumed that the presence of turbulent trailing edge separation is indicated by the decreasing pressures. The VAPE calculations show that turbulent separation occurs for almost all of the spanwise sections for all angles of attack above 12 degrees. This agrees very well with the qualitative analysis of the pressures in Figures 5.2-10 through 5.2-14 in that, by 12 degrees, all of the data show trailing edge pressures considerably less than the low angle of attack values. The above discussion indicates that the turbulent separation technique is doing a reasonable job for this three-dimensional case and should do a good job on most similar configurations (low sweep, high aspect ratio). If the configuration has a low aspect ratio or high sweep, then spanwise flow becomes much more important and the turbulent separation prediction should be used with caution.

The results of this study confirm the findings in Section 5.1 that the viscous algorithm does a good job of predicting the viscous effects on lifting surfaces where the flow is essentially all attached.

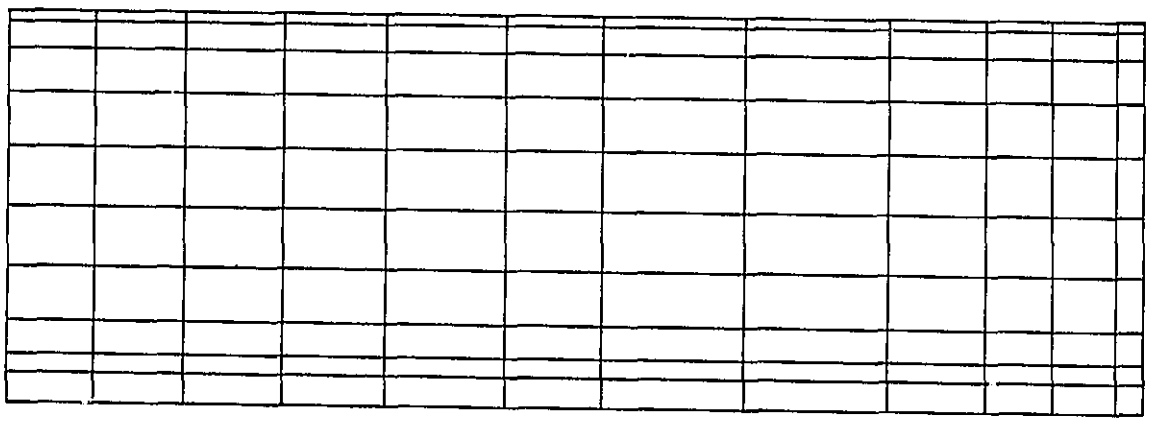

FIGURE 5.2-1 TEST CASE FOR VISCOUS SOLUTION FROM NASA TND 8307
$\Lambda = 0^{o}$, AR = 5.9

REFERENCES:

5.2-1 Yip, L.P. and Shubert, S.L.: "Pressure Distribution on a 1- by 3-Meter Semi-Span Wing at Sweep Angles from 0° to 40° in Subsonic Flow", NASA Tnd-8307, Dec. 1976.

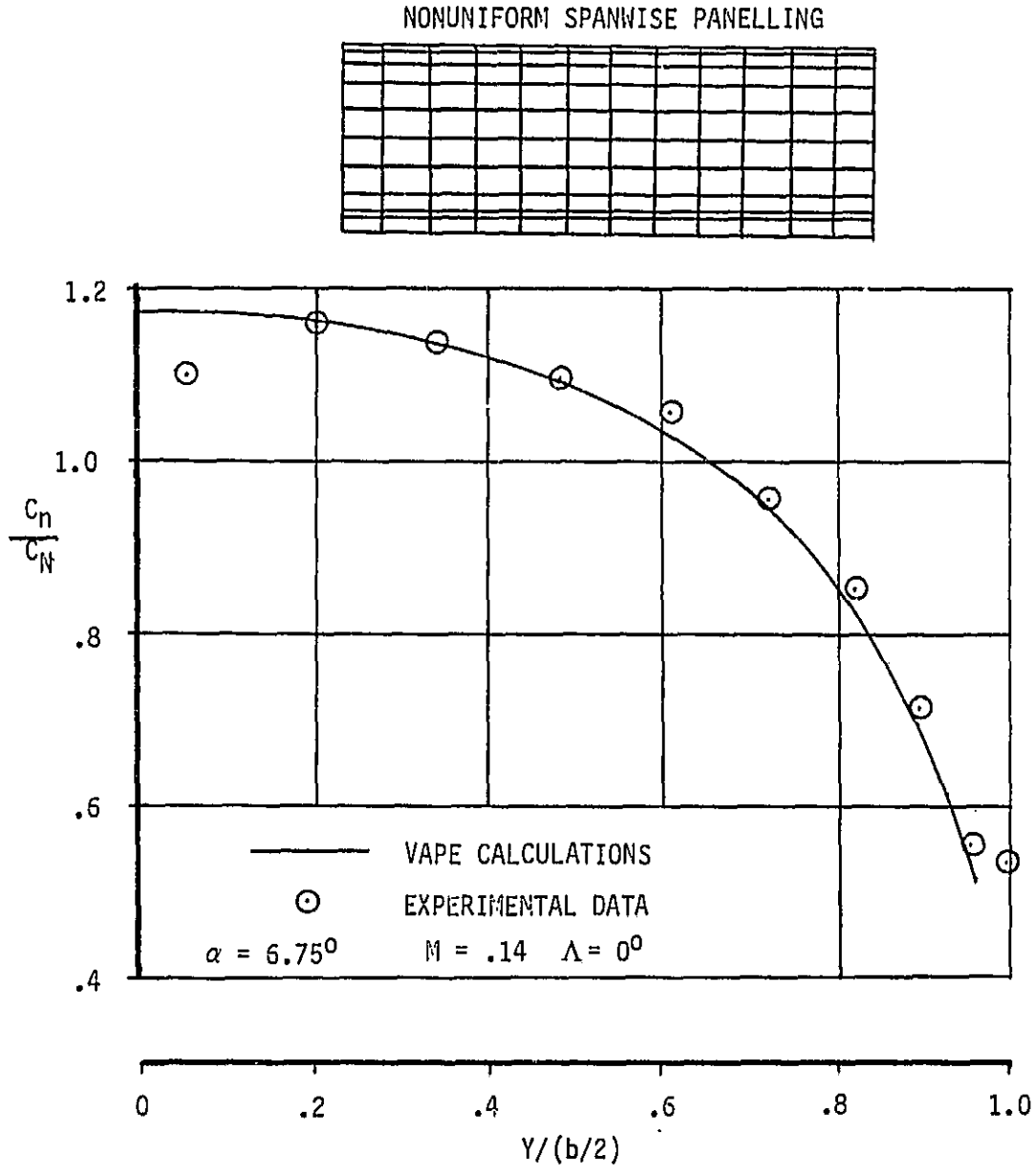

FIGURE 5.2-2 COMPARISON OF VAPE CALCULATED SPAN LOAD DISTRIBUTION TO EXPERIMENTAL DATA FOR WING OF NACA TND 8307

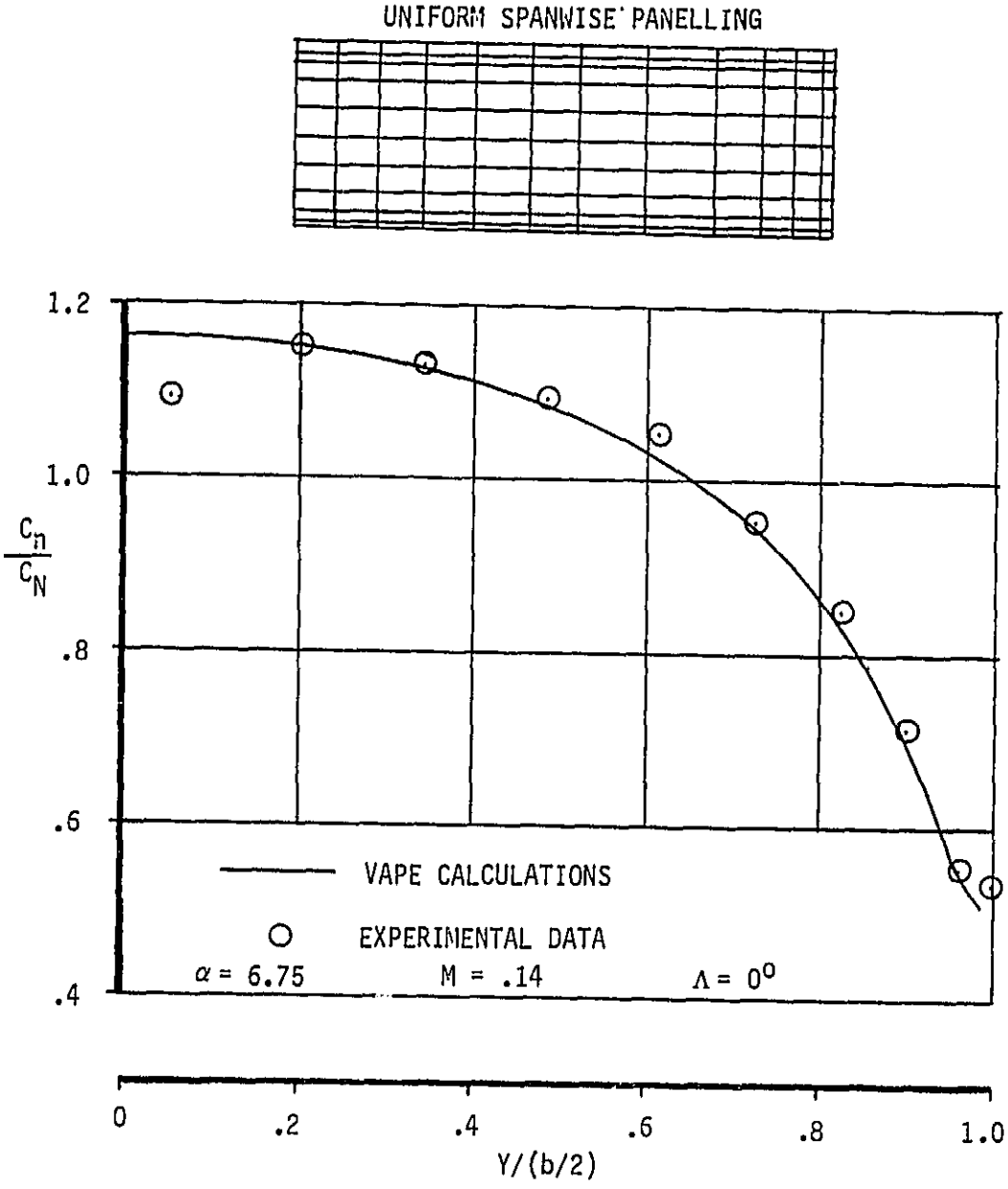

FIGURE 5.2-3 COMPARISON OF VAPE CALCULATED SPAN LOAD DISTRIBUTIONS TO EXPERIMENTAL DATA FOR WING OF NACA TND 8307

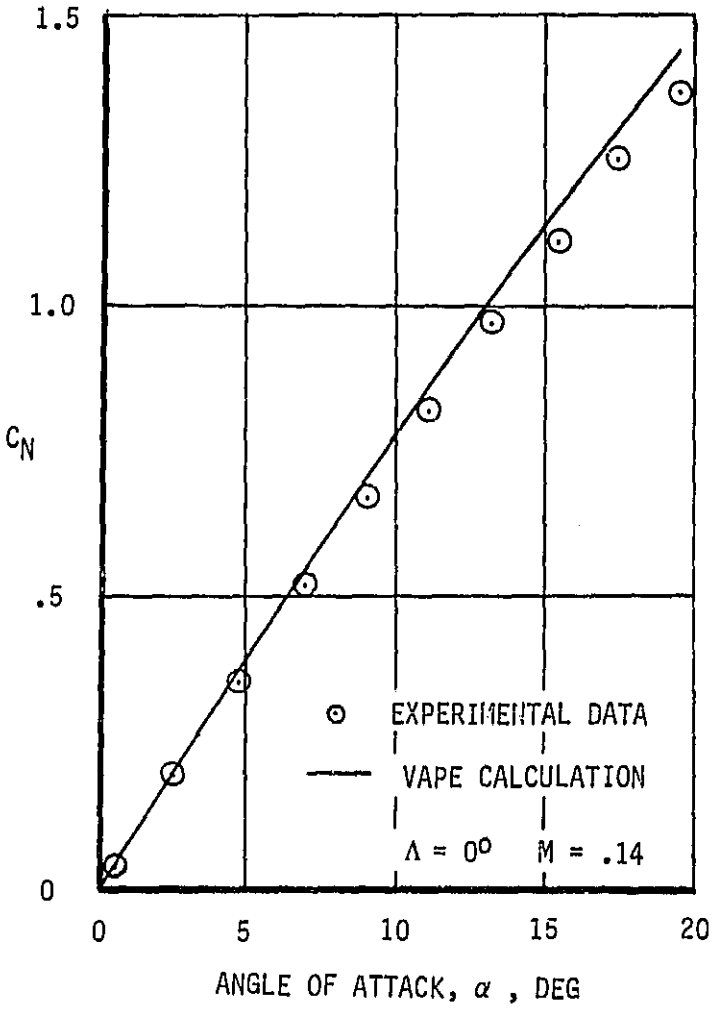

FIGURE 5.2-4 COMPARISON OF VAPE CALCULATED TOTAL NORMAL FORCE TO EXPERIMENTAL DATA FOR WING OF NACA TND 8307

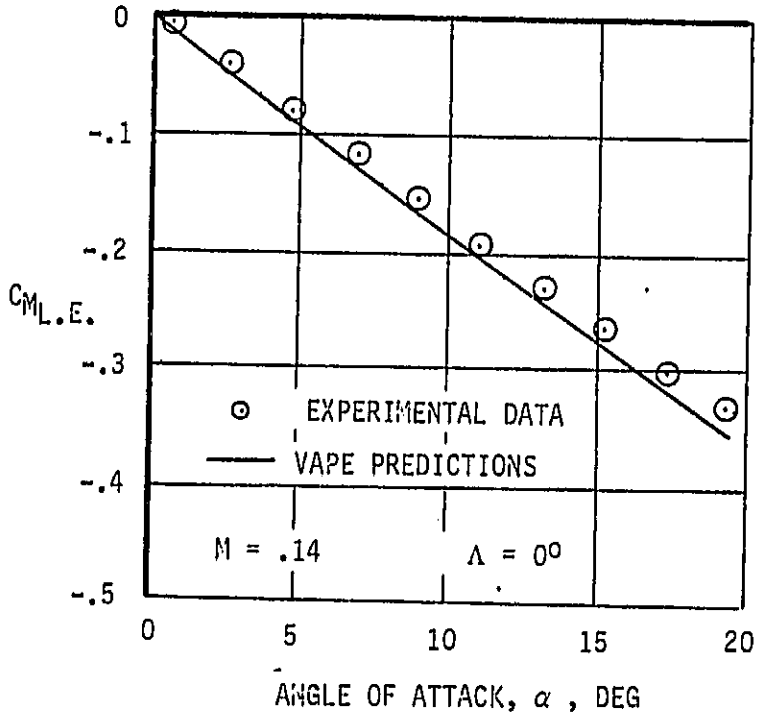

FIGURE 5.2-5 COMPARISON OF VAPE CALCULATED PITCHING MOMENT COEFFICIENTS TO EXPERIMENTAL DATA FOR WING OF NACA TND 8307

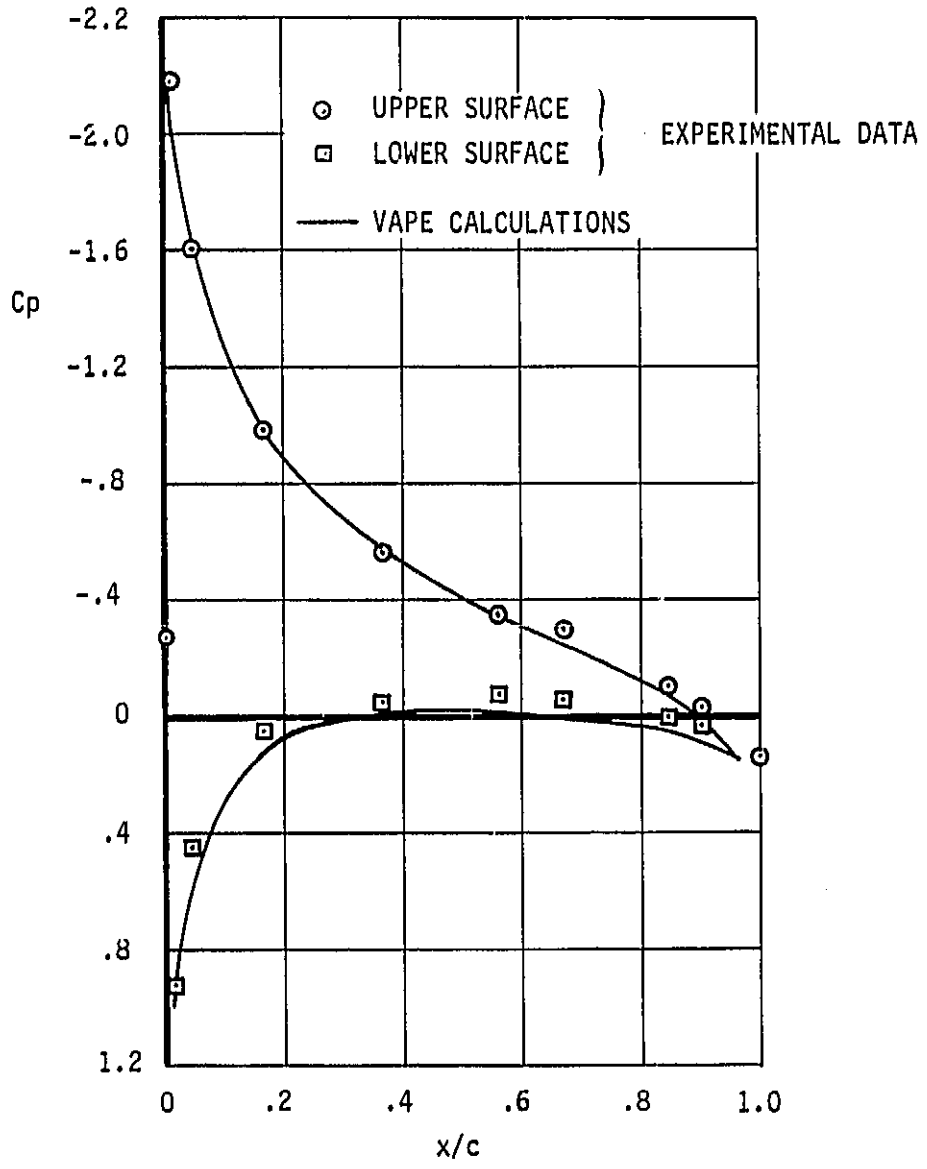

FIGURE 5.2-6 PRESSURE COEFFICIENT DISTRIBUTION FOR A NASA TND 8307 WING, $\alpha = 6.75^{o}$, $\eta = .20$

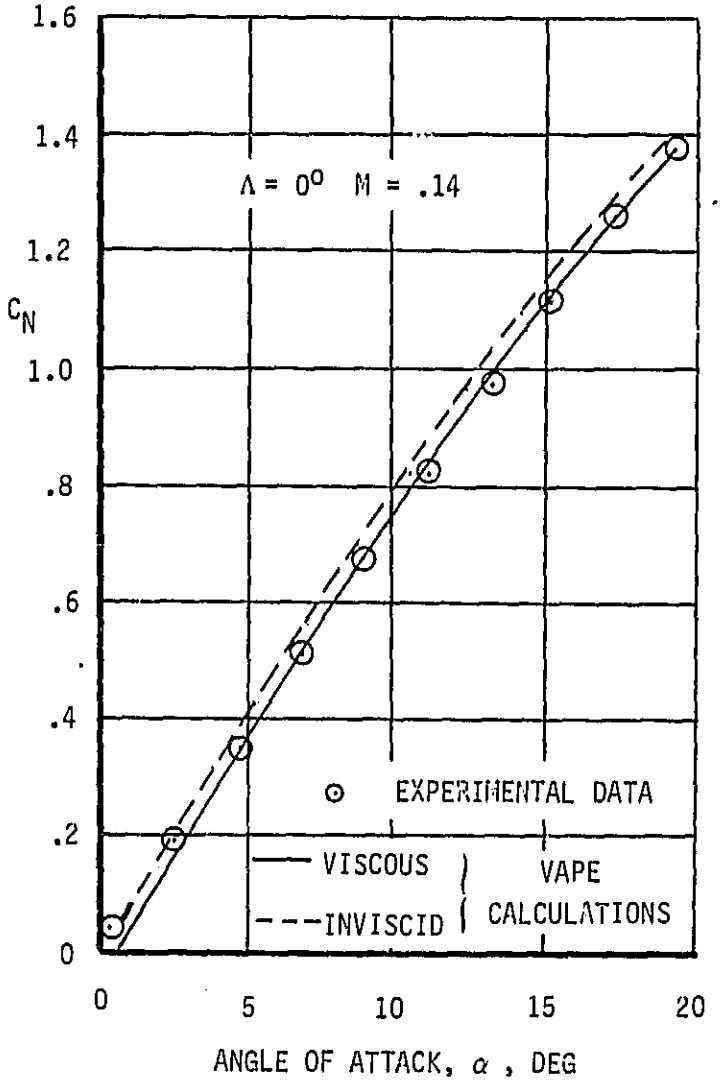

FIGURE 5.2-7 COMPARISON OF VAPE CALCULATED NORMAL FORCE WITH AND WITHOUT VISCOUS EFFECTS FOR WING OF NACA TND 8307

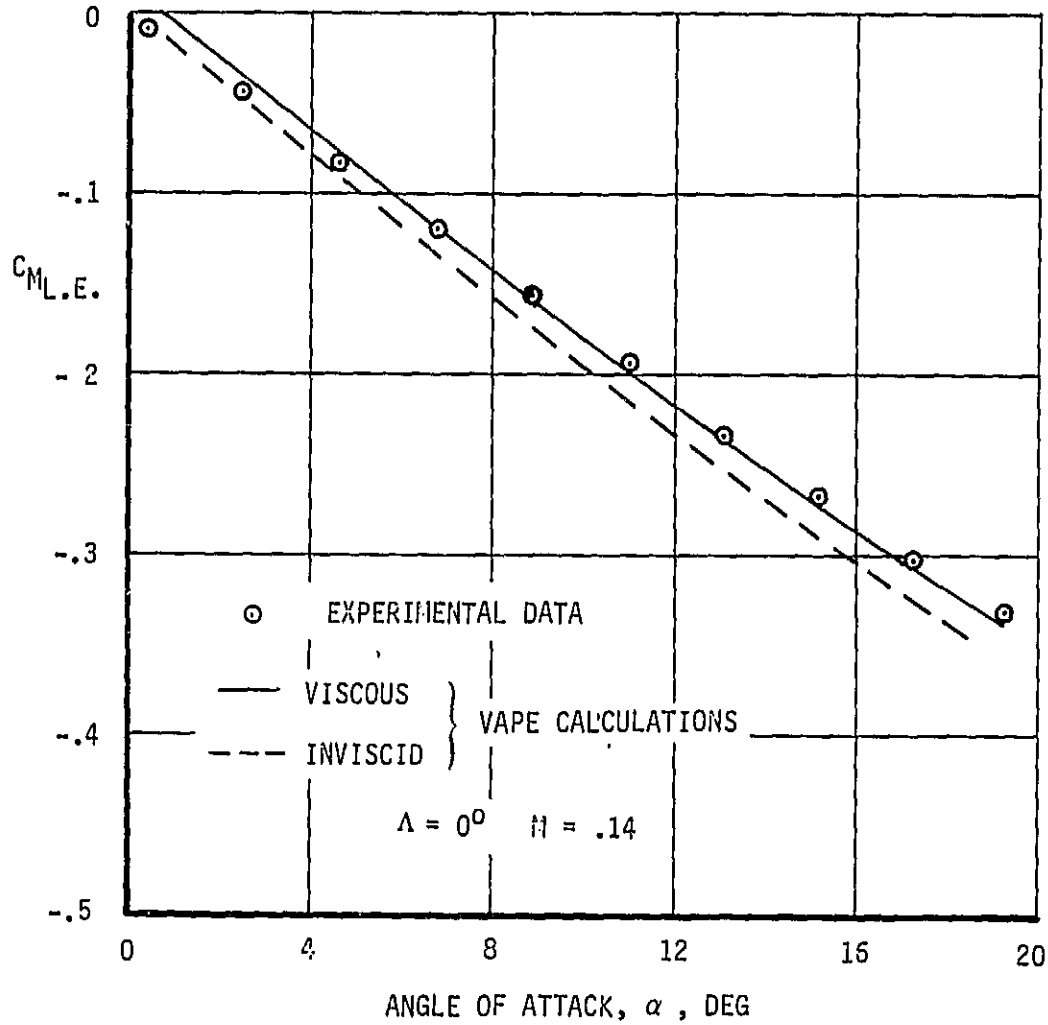

FIGURE 5.2-8 COMPARISON OF VAPE CALCULATED PITCHING MOMENT COEFFICIENTS WITH AND WITHOUT VISCOUS EFFECTS FOR WING OF NACA TND 8307

ORIGINAL PAGE IS
OF POOR QUALITY

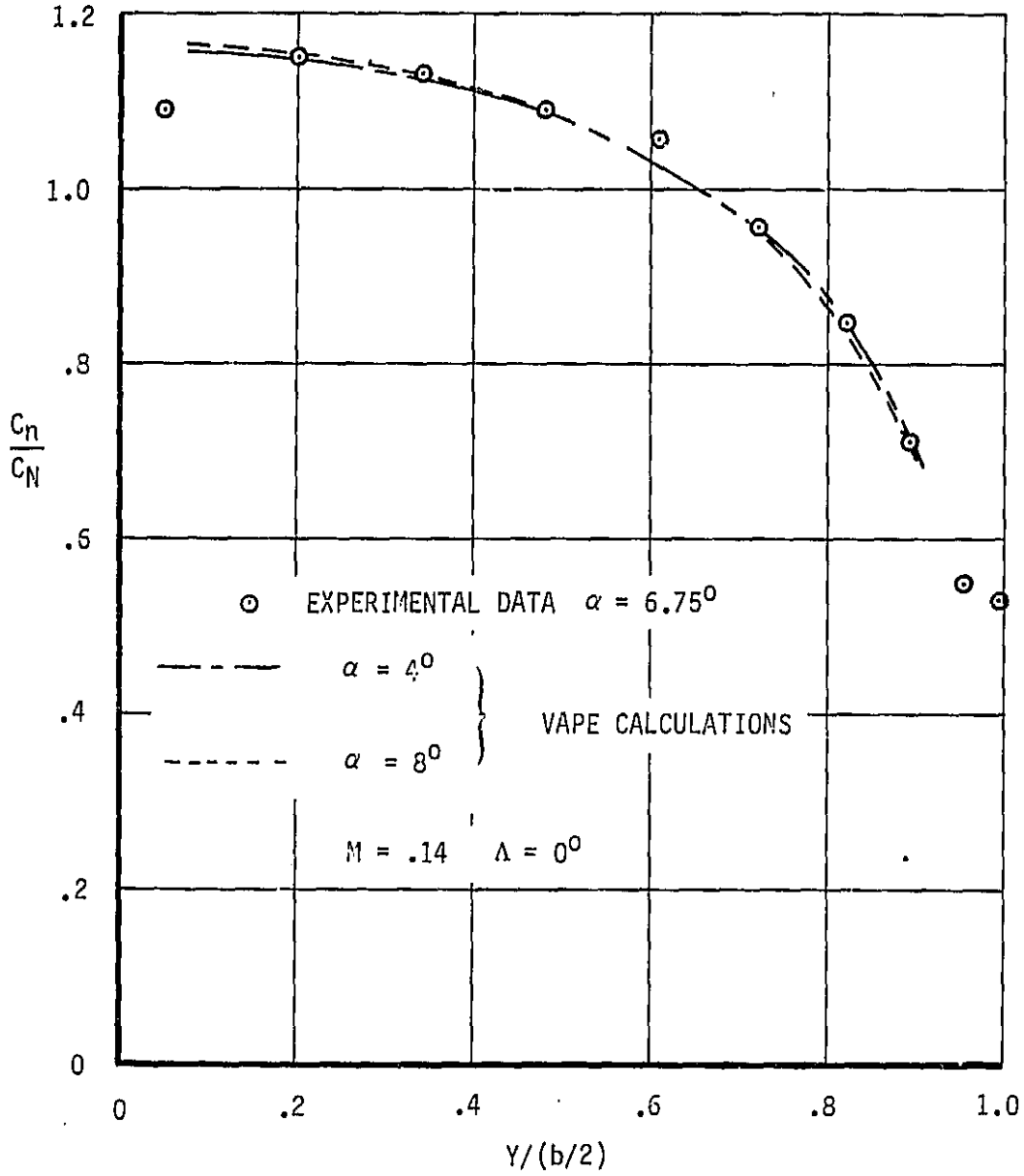

FIGURE 5.2-9 COMPARISON OF VAPE CALCULATED SPAN LOADING TO EXPERIMENTAL DATA FOR WING OF NACA TND 8307

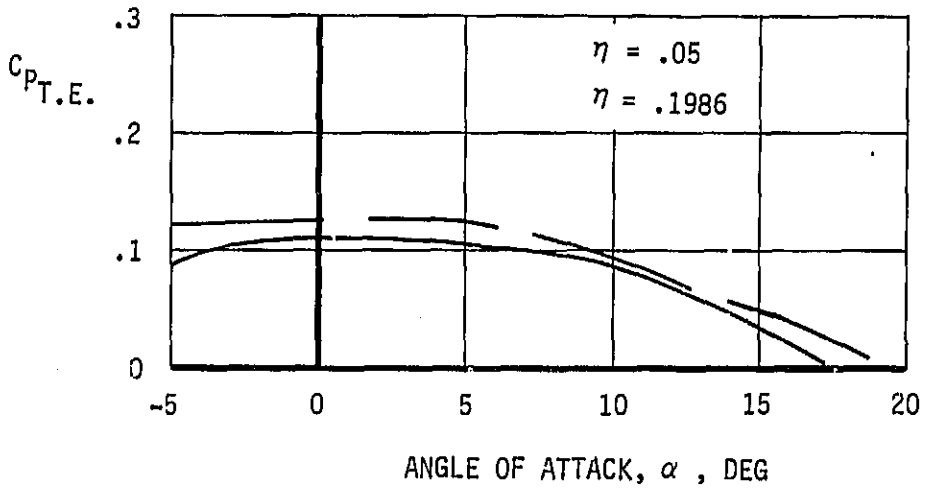

FIGURE 5.2-10 TRAILING EDGE PRESSURE VARIATION WITH ANGLE OF ATTACK

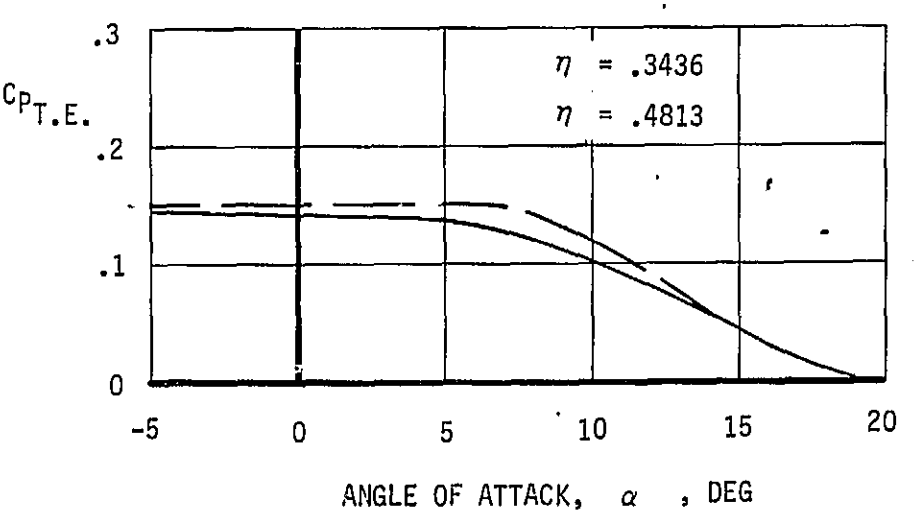

FIGURE 5.2-11 TRAILING EDGE PRESSURE VARIATION WITH ANGLE OF ATTACK

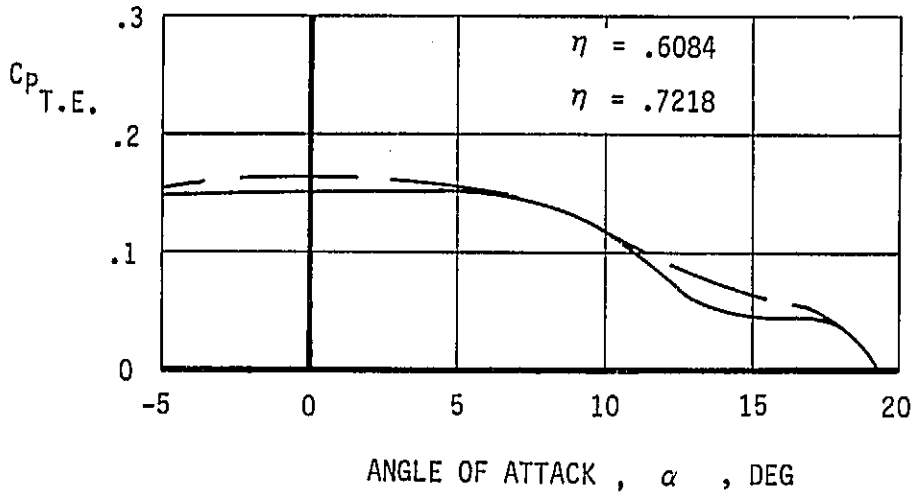

FIGURE 5.2-12 TRAILING EDGE PRESSURE VARIATION WITH ANGLE OF ATTACK

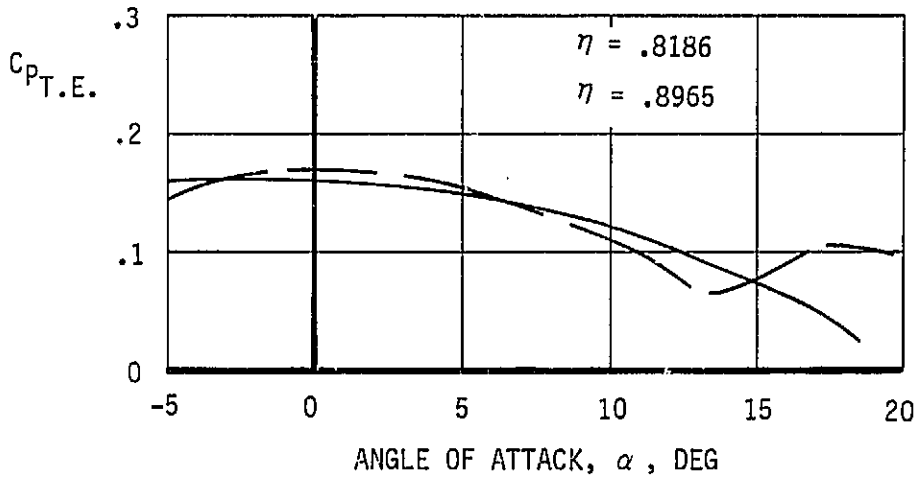

FIGURE 5.2-13 TRAILING EDGE PRESSURE VARIATION WITH ANGLE OF ATTACK

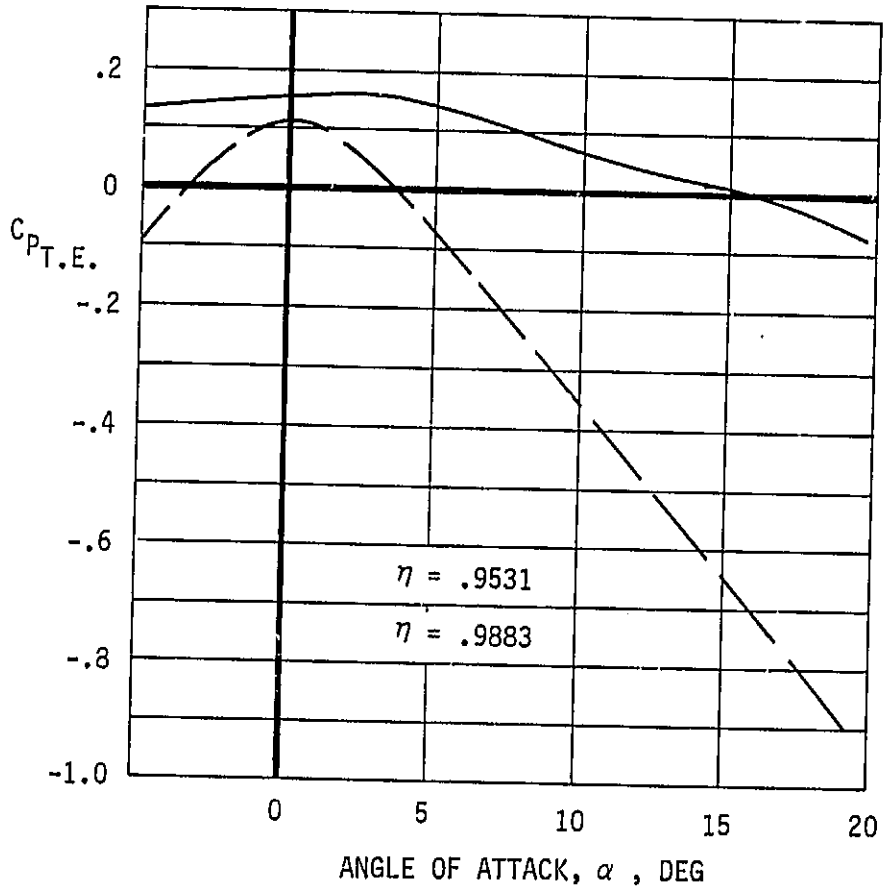

FIGURE 5.2-14 TRAILING EDGE PRESSURE VARIATION WITH ANGLE OF ATTACK

6.0 STOL MODEL

The STOL region of flight is defined as the region where the aircraft is taking off or landing and very close to the ground at a reasonable forward speed. The lift jets are deflected such that they impinge the ground forming wall jets, which are not being reflected back to the aircraft. The wall jets increase entrainment and thus increase the "suck-down" effect of the jets on the aircraft. A technique to predict this effort has been developed and incorporated into the Weston jet model contained in the VAPE program as discussed in Section 3.4.

This model was not evaluated under the previous NADC contract effort. Therefore, one objective of this contract was to evaluate the STOL model against experimental data for a full airplane configuration. The configuration of Reference 6.0-2 was chosen since it offered data for several jet nozzle shapes at various heights above the ground.

REFERENCES:

6.0-1 Beatty, T.D. and Kress, S.S.: "Prediction Methodology for Propulsive Induced Forces and Moments of V/STOL Aircraft in Transition/STOL Flight", Naval Air Development Center Report, NADC-77119-30, July 1979.

6.0-2 Vogler, R.D.: "Ground Effects on Single-and Multiple Jet VTOL Models at Transition Speeds Over Stationary and Moving Ground Planes," NASA TN D-3213, Jan. 1966.

6.1 VERIFICATION OF STOL MODEL

The STOL model of reference 6.1-1 (see Figure 6.1-1) has been analyzed by using the inviscid part of VAPE for two different heights above the ground. This model consists of a square fuselage fitted with a simple nose shape, a tapered wing and a simulated canopy. The wing has an aspect ratio of 2.8, a leading edge sweep of 40 degrees and a taper ratio of .40. The single round jet has a diameter of 3.5 inches. The first analysis was for a very large height simulating no ground effect. The results for this test case are presented in Figures 6.1-2 through 6.1-5 in terms of a lift divided by thrust, (L/T). The results calculated for the configuration are in relatively good agreement in terms of trends as a function of angle of attack and jet velocity ratio. Several items about the VAPE model were investigated to see if the agreement between the experiment and prediction could be improved. First, a wing thickness of 1 percent T/C was chosen arbitrarily to simulate the flat plate wing on the wind tunnel model. The Hess potential flow program, as shown earlier, is sensitive to panel density. The program is also sensitive to the ratio of wing thickness relative to the panel length. For example, on a wing with a T/C of 1 percent, the panel lengths should be no greater than 0.5 percent chord. This results in a very large number of panels and extremely expensive computer runs. Rather than increase the panel number in the above case to meet this criteria, another approach was used to produce improved results with less panels. That is, arbitrarily increase the wing T/C so that the ratio of panel length to T/C is improved. This will affect the results in terms of total magnitude by a small amount, but should not affect the induced loads. Therefore, a thicker 5 percent T/C wing was run and the results are presented in Figure 6.1-5. The slope of the L/T curve of the thicker wing is in better agreement with experiment, but is still too low.

This was the first test case run with a jet on the centerline and a plane of symmetry imposed. Therefore, two runs were made, one with the same basic geometry but with the jet area reduced to 1/2 of the original. The results for this case are shown in Figure 6.1-3. A second case consisting of the complete model (i.e. no planes of symmetry) was run with the correct jet area. The results obtained were identical to that obtained with the correct jet area on the model with the plane of symmetry imposed. Therefore, it has been established that if the jet is on the centerline and a plane of symmetry is used in VAPE, the total area of the jet must be used.

A case was also run with the model positioned at a height of seven diameters above the ground. The L/T calculated for this case was only slightly different than the no-ground effect case. Figure 6.1-6 shows this configuration with the ground plane added. Note that the ground plane is rotated with respect to the model. In order for the aircraft at angle of attack to have the proper relationship to the ground plane, one of the two must be rotated. In this case, it was decided to rotate the ground plane by the negative of the angle of attack rather than rotate the more complicated aircraft model. Figure 6.1-7 shows VAPE calculations compared to experimental data for the lift to thrust ratio as a function of configuration height above the ground for an R value of 10. This figure shows that the VAPE calculations at zero degrees angle of attack agrees very well (within 5 percent) with experimental data for the entire h/d range. Figure 6.1-8 presents a comparison of the calculated L/T data and the experimental data as a function of angle of attack for an h/d of 1.0 and an R value of 10. This figure presents experimental data for both a moving and still ground plane which shows approximately a 14 percent difference between the two techniques. The

calculated values lie between these two curves. At this h/d, the moving ground plane data should be the more accurate. These two curves show that the STOL method does a very good job of predicting ground effect on the total configuration, even at very low heights.

The experimental data used in this comparison is slightly in error due to the lack of thrust calibration. The fact that L/T is 1.0, out-of-ground effect, when the angle of attack and dynamic pressure are zero, indicates that there are propulsive induced effects that are not being accounted for properly. An estimate was made to determine the magnitude of the hovering induced effects in the out-of-ground condition. The method of reference 6.1-2 was used and a value slightly less than 1 percent was calculated. This is a small value, but does indicate a probable source of differences in the above comparisons.

REFERENCES:

6.1-1 Vogler, R.D.: "Ground Effects on Single- and Multiple-Jet VTOL Models at Transition Speeds Over Stationary and Moving Ground Planes", NASA TND-3213, Jan. 1966.

6.1-2 Gentry, Carl L. and Margason, R.J.: "Jet-Induced Lift Losses on VTOL Configuration Hovering In and Out of Ground Effect," NASA TN D-3166, 1966.

FIGURE 6.1-1 STOL CONFIGURATION
ref. NASA TND-3213

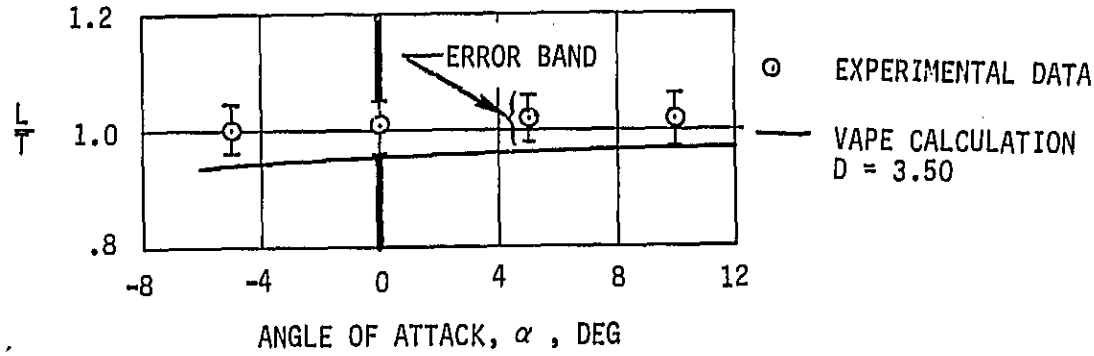

FIGURE 6.1-2 COMPARISON OF VAPE PREDICTIONS TO EXPERIMENTAL DATA FOR STOL MODEL OUT OF GROUND EFFECT, R = 20

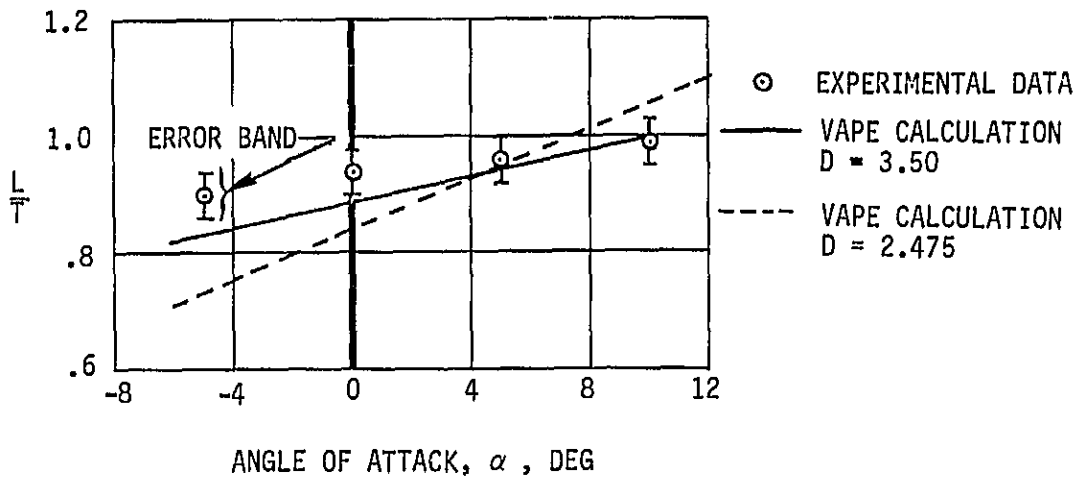

FIGURE 6.1-3 COMPARISON OF VAPE PREDICTIONS TO EXPERIMENTAL DATA FOR STOL MODEL OUT OF GROUND EFFECT, R = 10

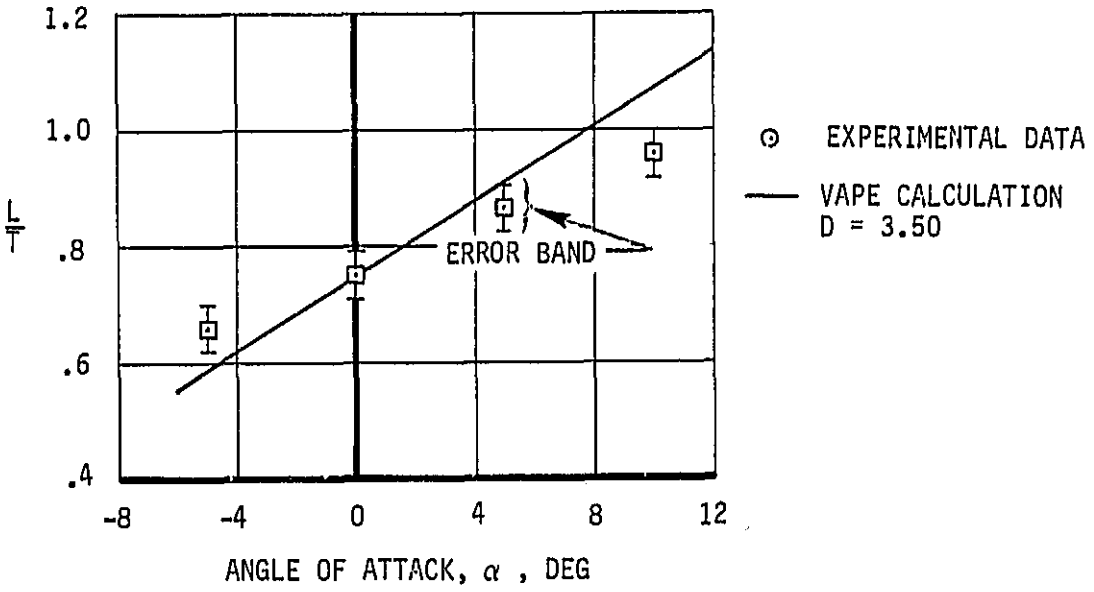

FIGURE 6.1-4 COMPARISON OF VAPE PREDICTIONS TO EXPERIMENTAL DATA FOR STOL MODEL OUT OF GROUND EFFECT, R = 5.88

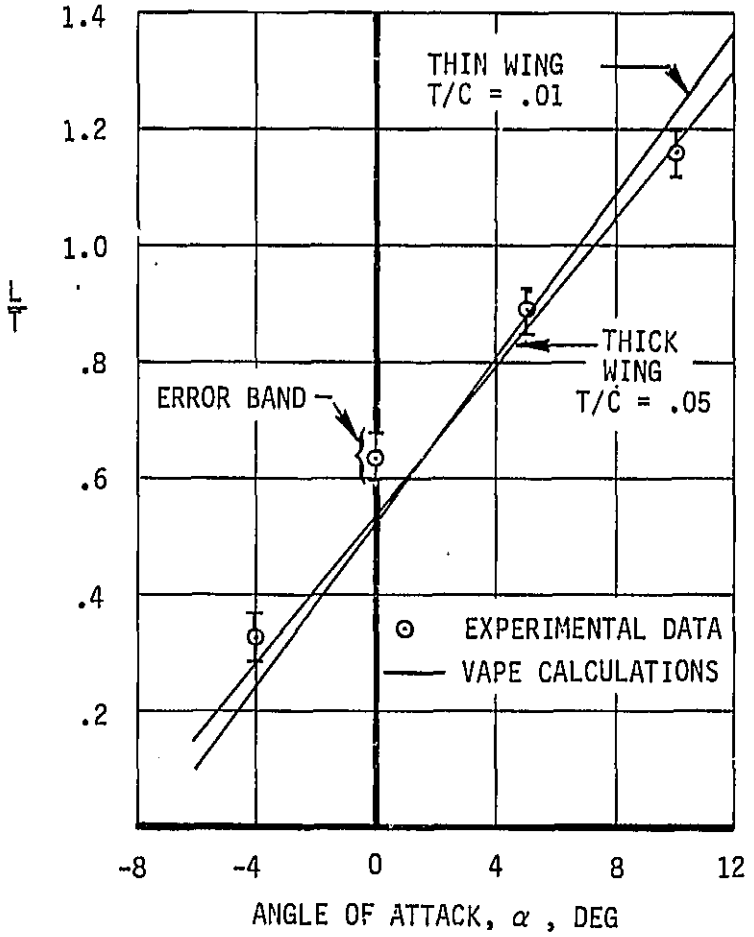

FIGURE 6.1-5 COMPARISON OF VAPE PREDICTIONS TO EXPERIMENTAL DATA FOR STOL MODEL OUT OF GROUND EFFECT, R = 4

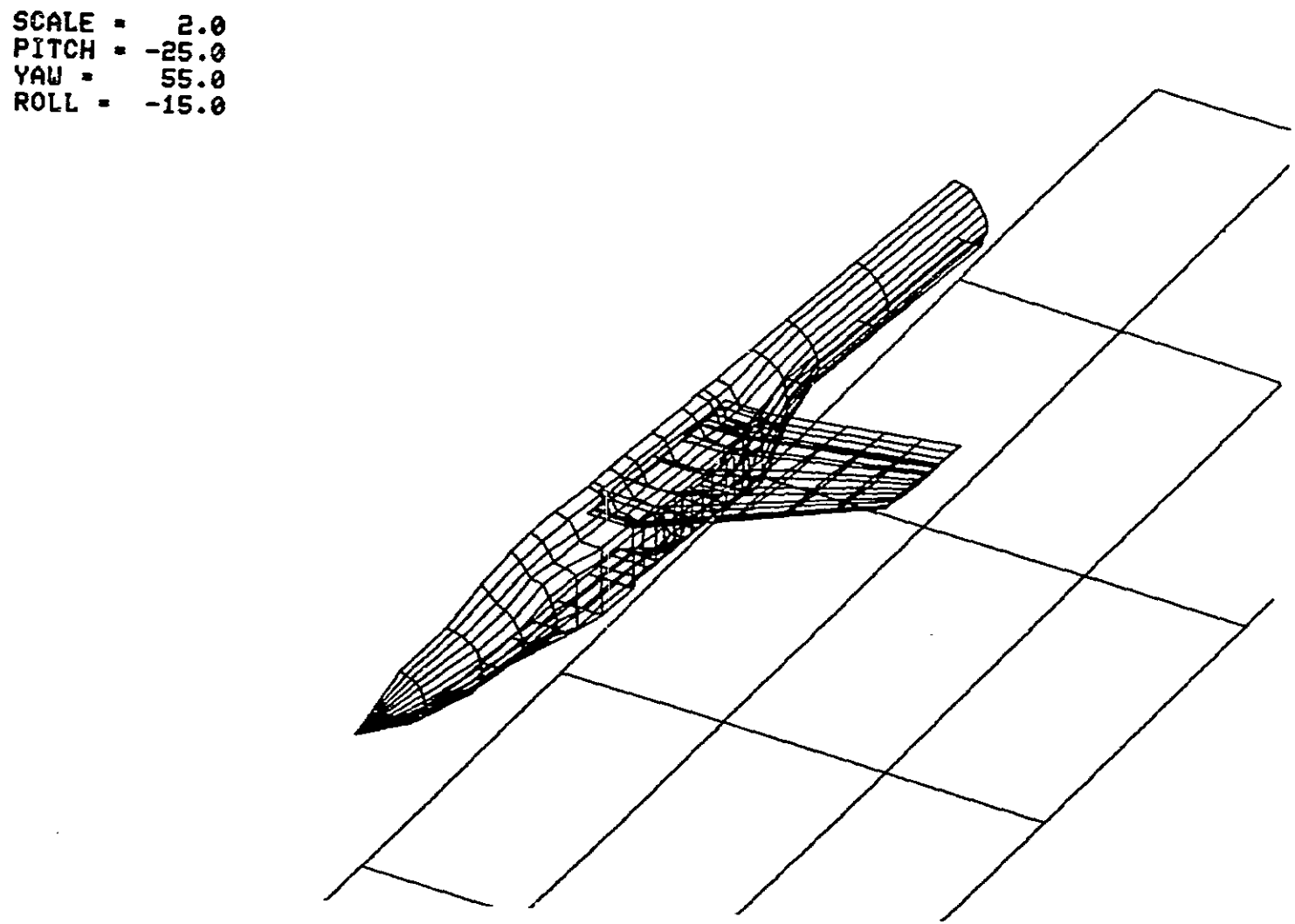

FIGURE 6.1-6a STOL MODEL IN THE PRESENCE OF A GROUND PLANE

FIGURE 6.1-6b STOL MODEL IN THE PRESENCE OF A GROUND PLANE

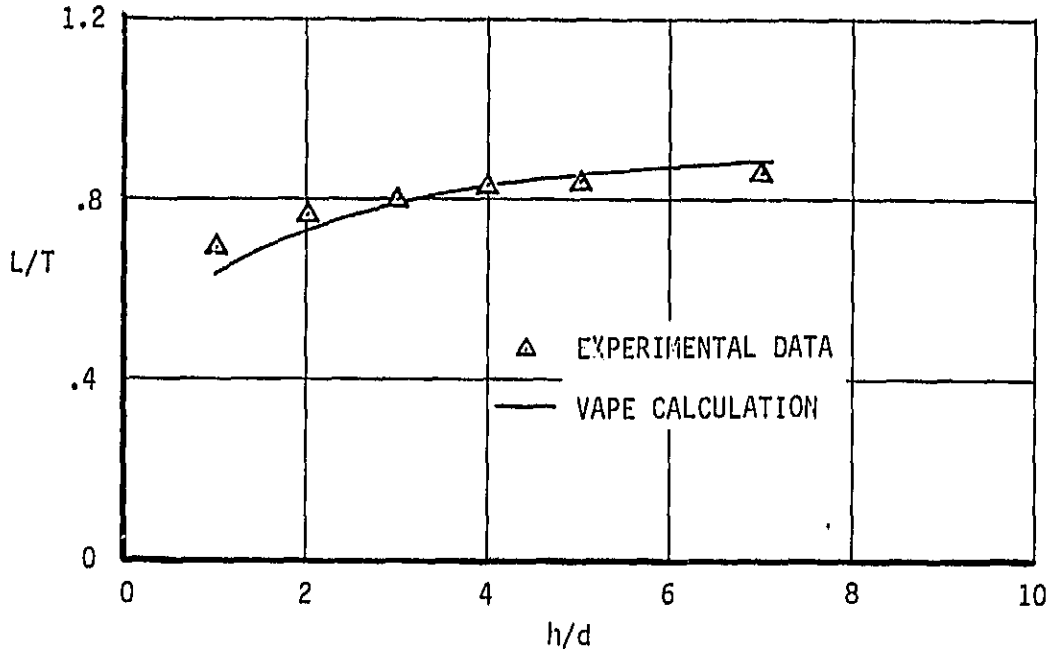

FIGURE 6.1-7 COMPARISON OF VAPE CALCULATED LIFT/THRUST RATIOS TO EXPERIMENTAL DATA FOR VARIOUS HEIGHTS ABOVE THE GROUND PLANE. α = 0 DEG, R = 10

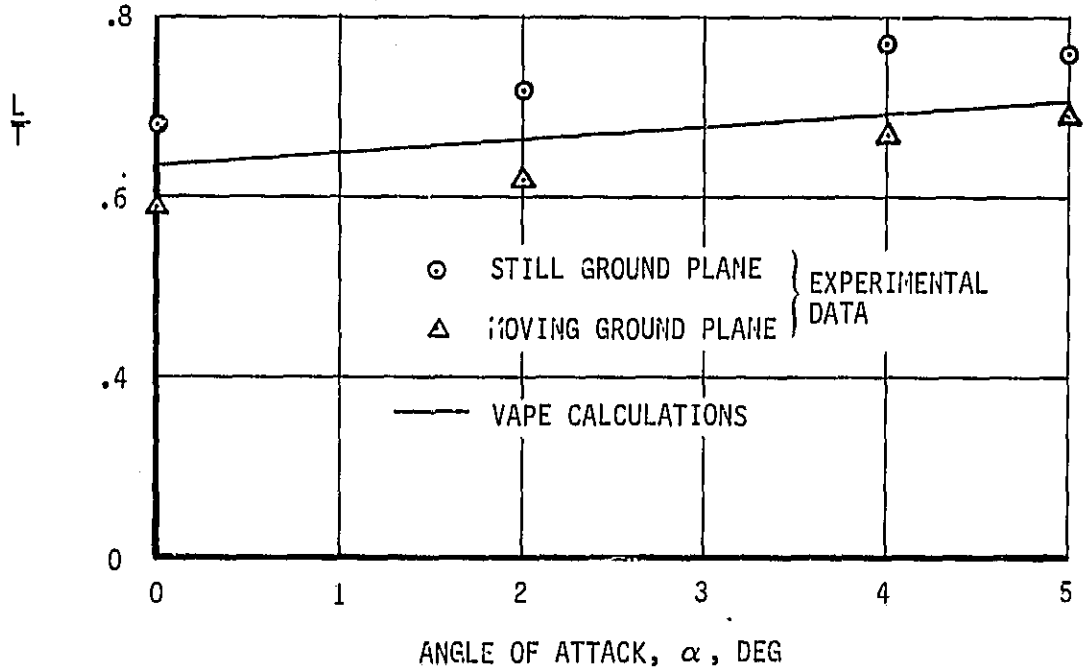

FIGURE 6.1-8 COMPARISON OF VAPE CALCULATED LIFT/THRUST RATIOS TO EXPERIMENTAL DATA FOR h/D = 1.0 R = 10

7.0 VAPE APPLICABILITY TO VATOL CONFIGURATIONS

When vertical attitude takeoff and landing (VATOL) aircraft transition from vertical attitude to conventional horizontal flight, they must pass through a region where exhaust jets are at considerable angles with respect to the flight path. Therefore, in this region, the flow models contained in the VAPE system may be applicable. The applicability of VAPE to VATOL configurations will depend on the flight path and the limitations of the jet models contained in VAPE.

The jets on VATOL aircraft are normally mounted at the rear of the configuration. This location should produce propulsive induced effects which are of a much lower order of magnitude than conventional V/STOL configurations. However, there may be an effect, even though small, which could adversely affect the vehicle control.

Therefore, a study was performed to determine if VAPE could be used to predict the propulsive induced effects on VATOL configurations throughout part of their flight profile. The study concentrated on a representative configuration, reference 7.0-1, for which there was a set of good experimental data.

This configuration was run inviscidly through the VAPE code. The initial run was for a model where the actual base area was paneled (Figure 7-1a), as well as the jet exhaust. A more conventional paneling, where the afterbody is continued aft, was also executed (Figure 7-1b). The results of this study point out several problem areas in the analysis of any powered aircraft configurations:

(1) Large amounts of separated flow at angles-of-attack of the fuselage reference line greater than 10 degrees;

(2) The effect of canard vorticies and wake and separated wing vorticies on the wing lift; and

(3) The relationship of aircraft angle-of-attack relative to jet crossflow direction.

Figures 7-2 through 7-5 show the effect of the above first two items on the normal force of the various vehicle components. Figure 7-2 presents several comparisons between predicted and experimental results for the VATOL configuration. First, the two VAPE calculations using a cutoff afterbody and an extended afterbody are shown. The cutoff afterbody is an attempt at modeling the actual aft end of the fuselage. This results in a 90 degree external corner (between the afterbody and the base) which produces large flow accelerations in VAPE. In real life, the flow will separate from the surface at this corner and proceed aft, producing a configuration similar to the extended afterbody case. Comparisons of calculated and experimental pressure distributions on the fuselage boattail show that the extended afterbody does a better job of simulating the aft end (see Figure 7-3). Therefore, the extended afterbody case was used as a power-off baseline.

The two experimental curves presented in Figure 7-2 show the difference between a power-off configuration and a power-on configuration. These two curves differ, but not by large amounts.

These comparisons are relatively good up to 5 degrees angle of attack. Above 5 degrees, the experimental normal force becomes nonlinear due to a considerable vortex lift increment. Figure 7-2 presents the normal force

comparison between theory and experiment on the canard surface. The comparison here is good throughout the entire angle of attack range. Figure 7-3 presents a similar comparison for the wing surface. In this case, the wing normal force is always less than the experimental values. Again, at small angles the results are only slightly low, but above 5 to 10 degrees, the discrepancy increases. Therefore, above 10 degrees, the normal force calculations are not in agreement except for the canard. The reasons for these differences were listed above. The comparisons of calculated and experimental pressure distributions provide evidence of both separated and vortex flow effects. Figure 7-6 shows the calculated and experimental pressure distributions at approximately 60 percent semispan for an angle of attack of approximately 10 degrees. The experimental data shows a much lower loading indicative of flow separation. The VAPE results are potential flow with no separation effects and thus show a much higher loading. Figure 7-7 shows a similar comparison at 35 percent semispan for approximately a 10 degree angle of attack. Here the results look very good, indicating that the inboard wing section is not separated, and experiences little, if any, vortex flow effect. However, as the angle of attack is increased, the vortex effects become dominant as shown in Figure 7-8. This figure indicates a much higher loading was measured at 30 degrees angle of attack than predicted.

The above discussion indicates that the VAPE calculations must be done at low angles of attack if accurate values of the aerodynamic coefficients are desired. This leads to a conflict with a problem area mentioned above. Since the jets are aligned with the fuselage centerline, the crossflow applied to the jets is due entirely to angle of attack. Coupled with the low angle of attack requirement dictated by the first two items above, the jet crossflow angle is small (i.e. less than 15 degrees). However, the VAPE method is currently assumed applicable only to configurations with jet deflections greater than approximately 30 degrees. So, with the above contradictions, how is VAPE applied to a VATOL configuration? Two alternatives are suggested: (1) apply VAPE to jet deflection angles of 30 degrees of less; and (2) perform the calculations at high values of angle of attack with and without jets operating, and use the increment between these solutions as the jet effect and then apply this jet effect to conventional predictions for aerodynamic chracteristics without jets.

The experimental data on the configuration of Figure 7-16 with a now circular fuselage for the required runs from reference 7.0-1 was plotted and compared to the predicted values. Figures 7-9 through 7-14 present experimental/calculated data comparisons at three differenct fuselage stations for an angle of attack of approximately 20 degrees for the powered and unpowered cases. The last station, 219.3, is the last predicted station on the fuselage (the end of the body is at approximately station 220). These comparisons show a general agreement, especially in terms of incremental power effects.

The results obtained above indicate some concerns in the use of VAPE to predict power effects on VATOL configurations. The inability of the current jet methods to operate in areas with small crossflow angles over the jets (low angles of attack for VATOL) limits the method to high angle of attack. Unfortunately, at the higher angles of attack, separation begins to appear on the configuration which is also outside the range of VAPE's potential flow codes. VAPE is currently applicable only in a relatively small angle of attack range. In this range, the local shape of the exhaust plume and the body boundary layer produce effects as large, if not larger, than the entrainment effects. Therefore, for VAPE to be applicable to VATOL configurations, two areas must be pursued in the future. First, a method for

the low jet deflection region must be incorporated into VAPE. This method must extend the jet method from 30 degrees down to 0 degrees. In addition, the shape of the jet must be modeled carefully to insure reasonable plume effects. Secondly, viscous effects must be added to the body to account for the boundary layer effects on the afterbody at the jet exit. Both of these tasks can and should be done as future efforts since they are beyond the scope of the contract.

REFERENCES:

7.0-1 Minter, E.A. and Yates, R.W.: "Wind Tunnel Test of a .4 Scale Fighter Model at High Angles of Attack - Analysis of Pressure Data", NASA CR-166198, July 1981.

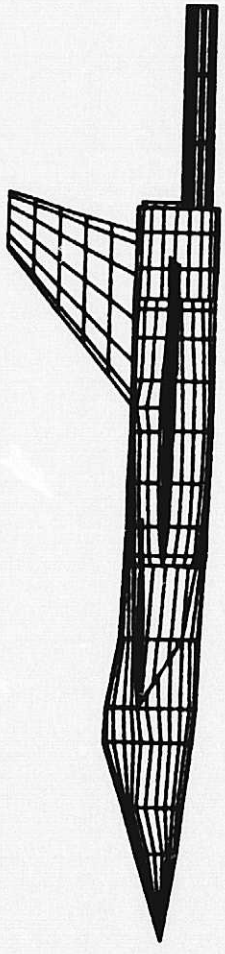

FIGURE 7-1a VOUGHT VATOL CONFIGURATION MODEL

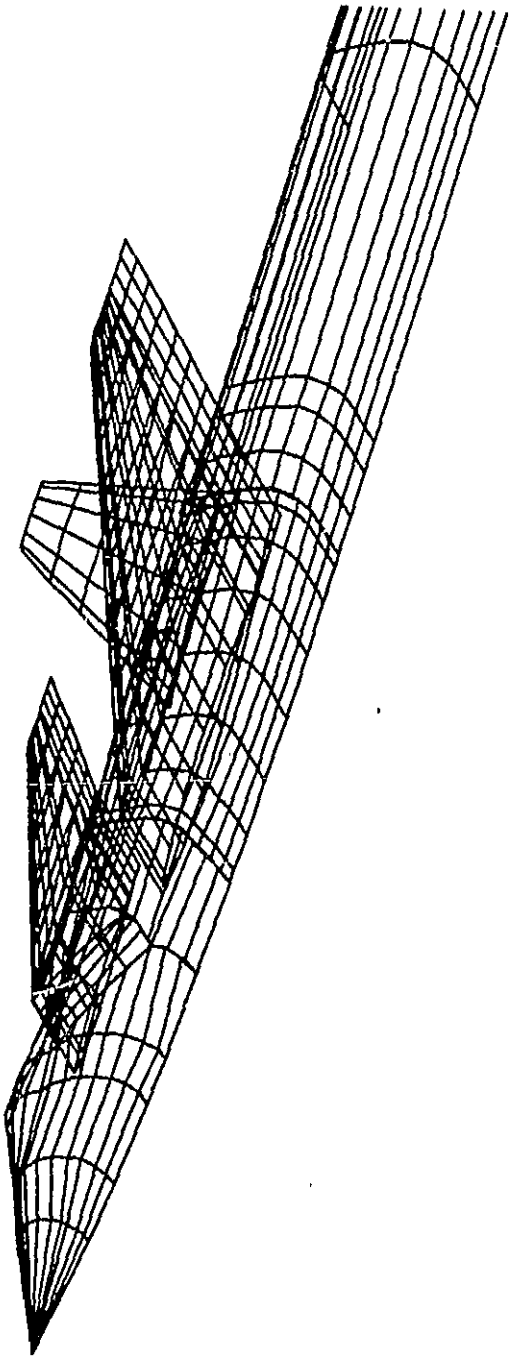

FIGURE 7-1b VOUGHT VATOL CONFIGURATION MODEL

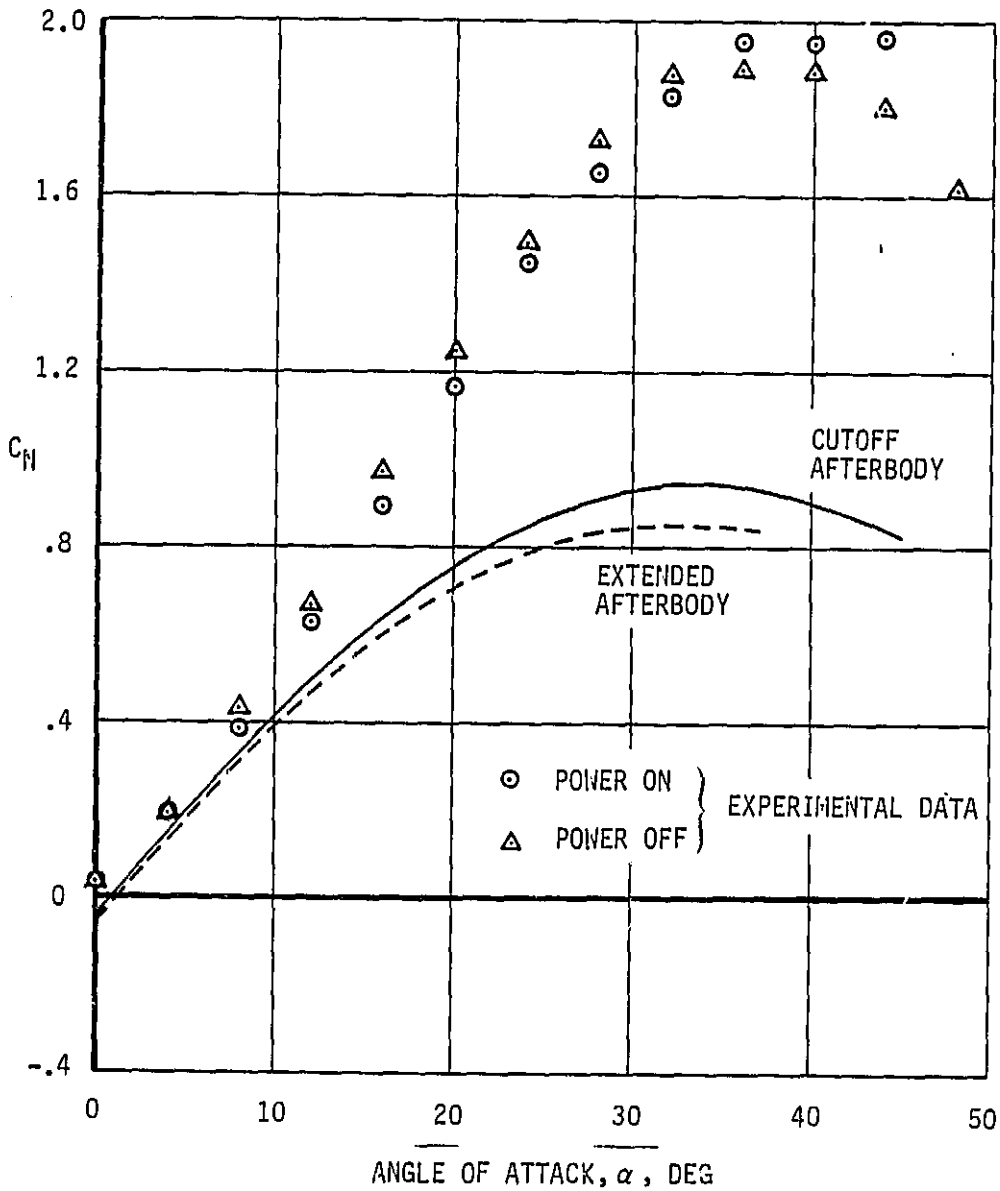

FIGURE 7-2 COMPARISON OF VAPE CALCULATIONS OF C_N TO EXPERIMENTAL DATA FOR THE VOUGHT VATOL MODEL

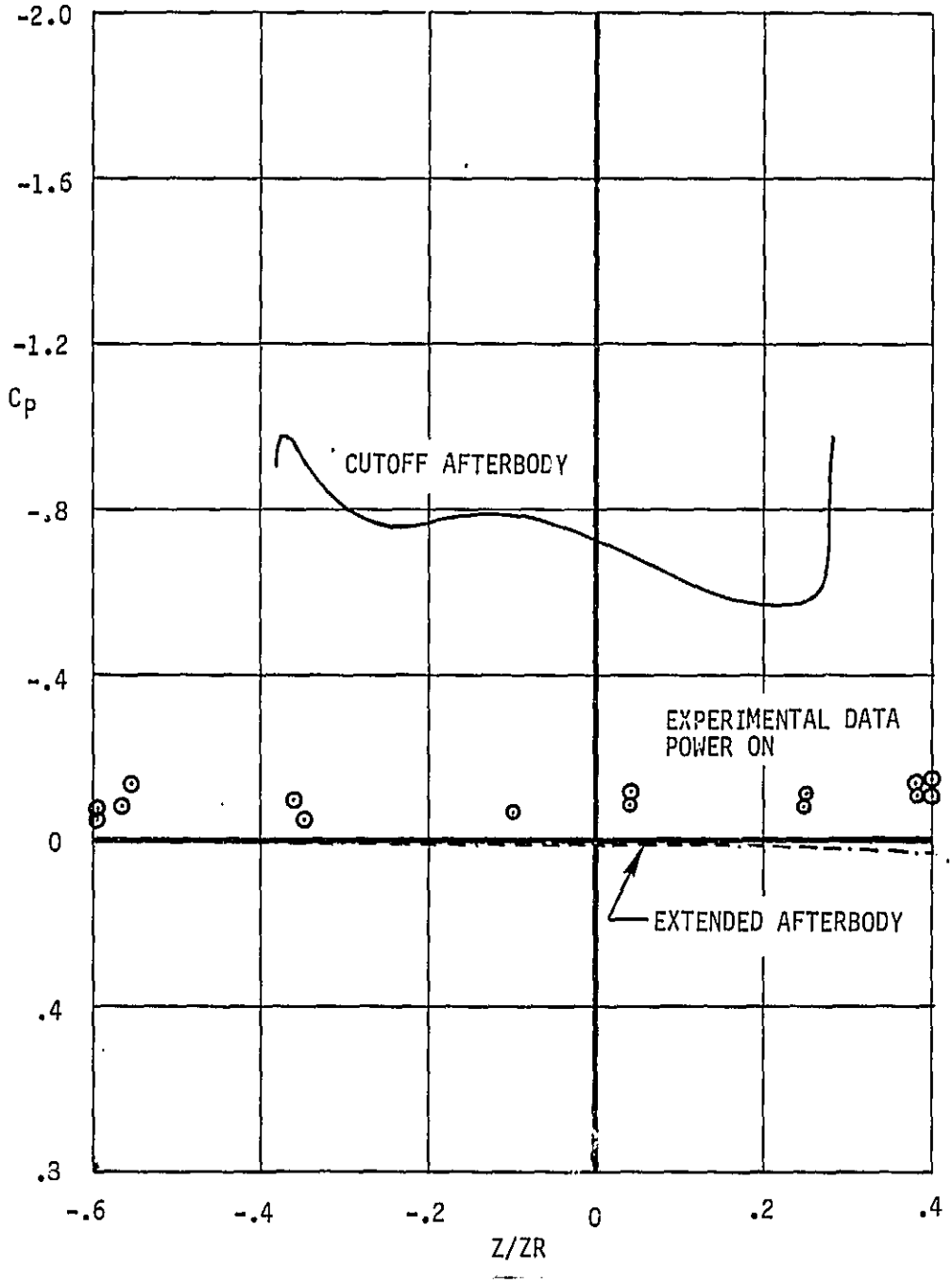

FIGURE 7-3 COMPARISON OF VAPE CALCULATED BOATTAIL PRESSURES TO EXPERIMENTAL DATA FOR VOUGHT VATOL MODEL

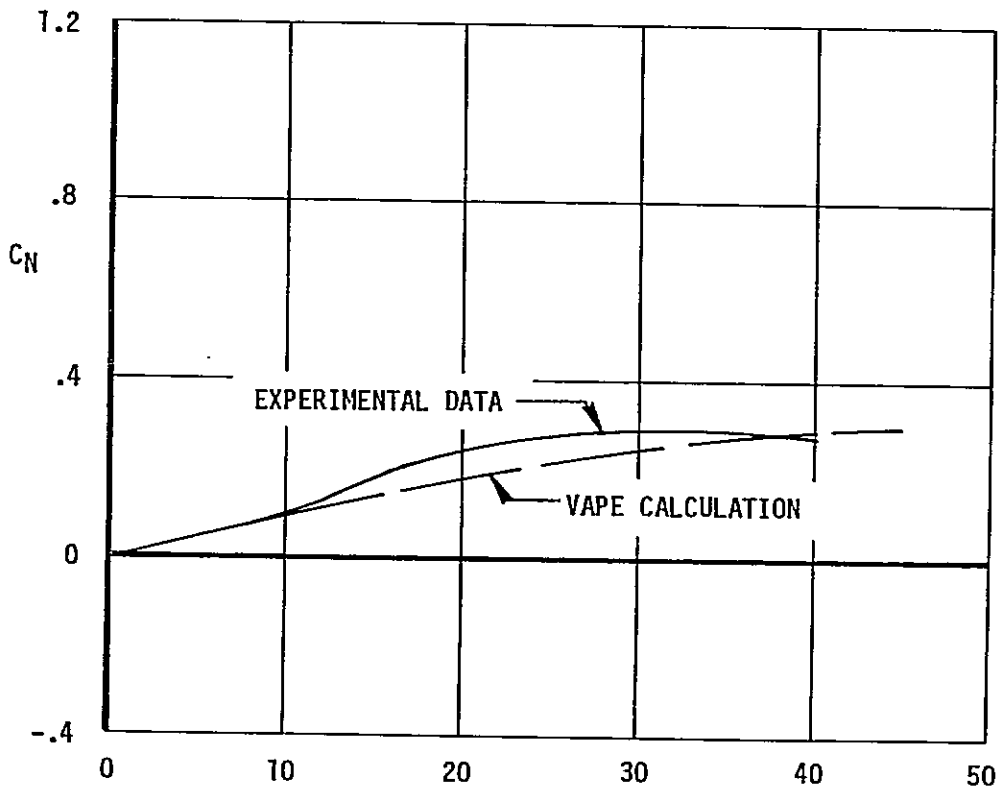

FIGURE 7-4 COMPARISON OF VAPE CALCULATED NORMAL FORCE TO EXPERIMENTAL DATA FOR THE CANARD OF THE VATOL MODEL

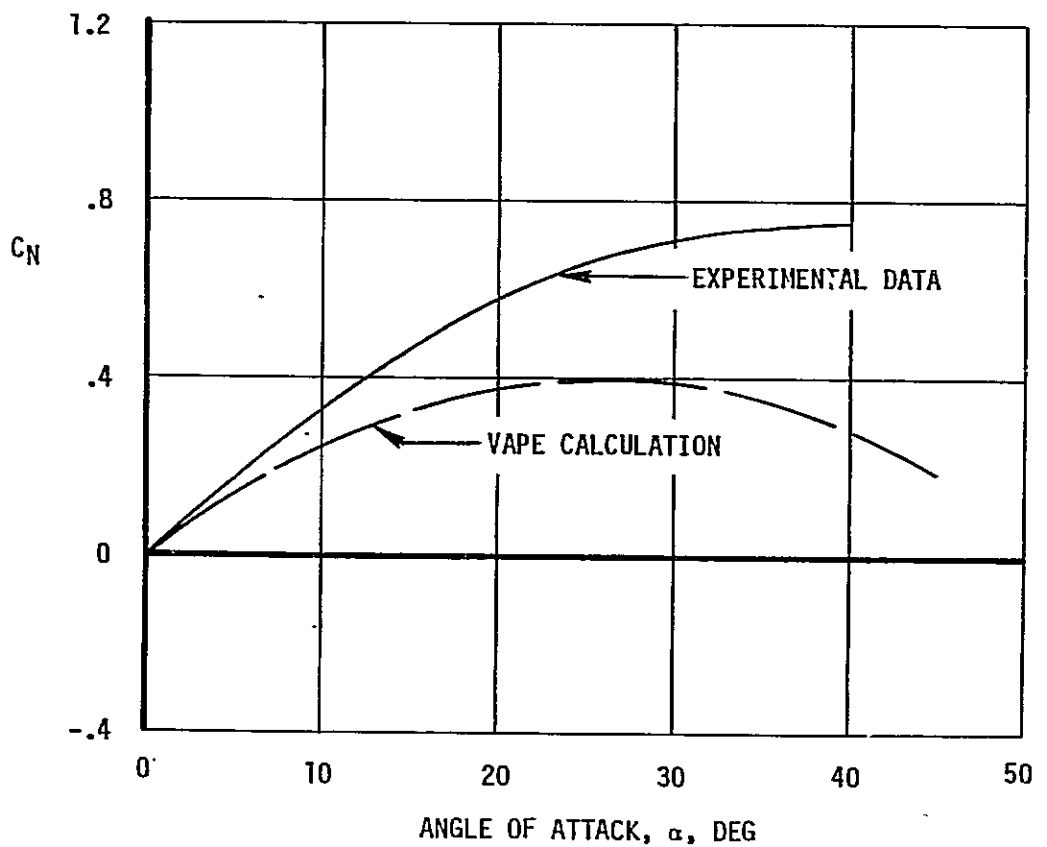

FIGURE 7-5 COMPARISON OF VAPE CALCULATED NORMAL FORCE TO EXPERIMENTAL DATA ON THE WING OF THE VATOL MODEL

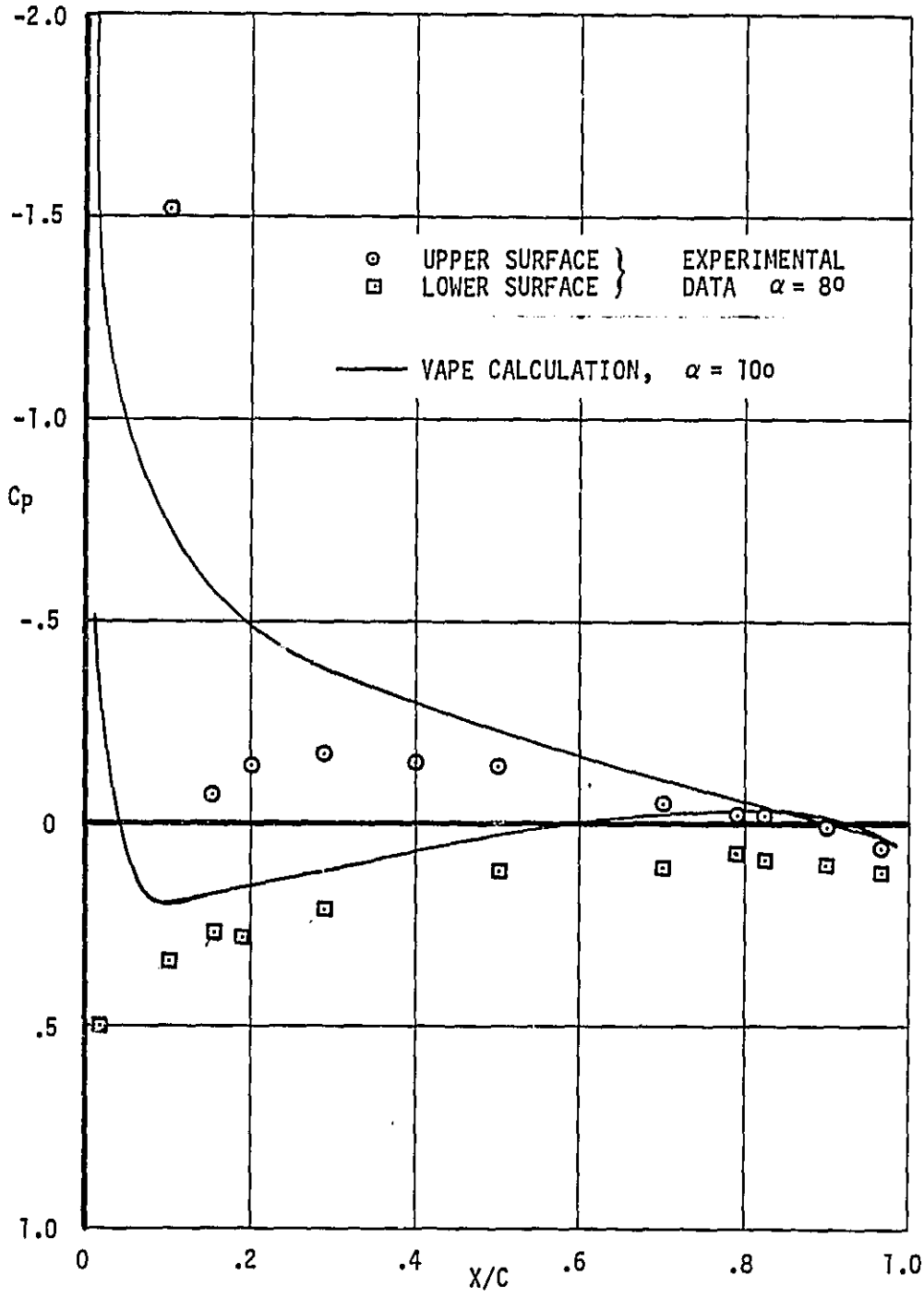

FIGURE 7-6 COMPARISON OF VAPE CALCULATED PRESSURE COEFFICIENTS TO EXPERIMENTAL DATA FOR THE VOUGHT VATOL MODEL WING AT η = .6

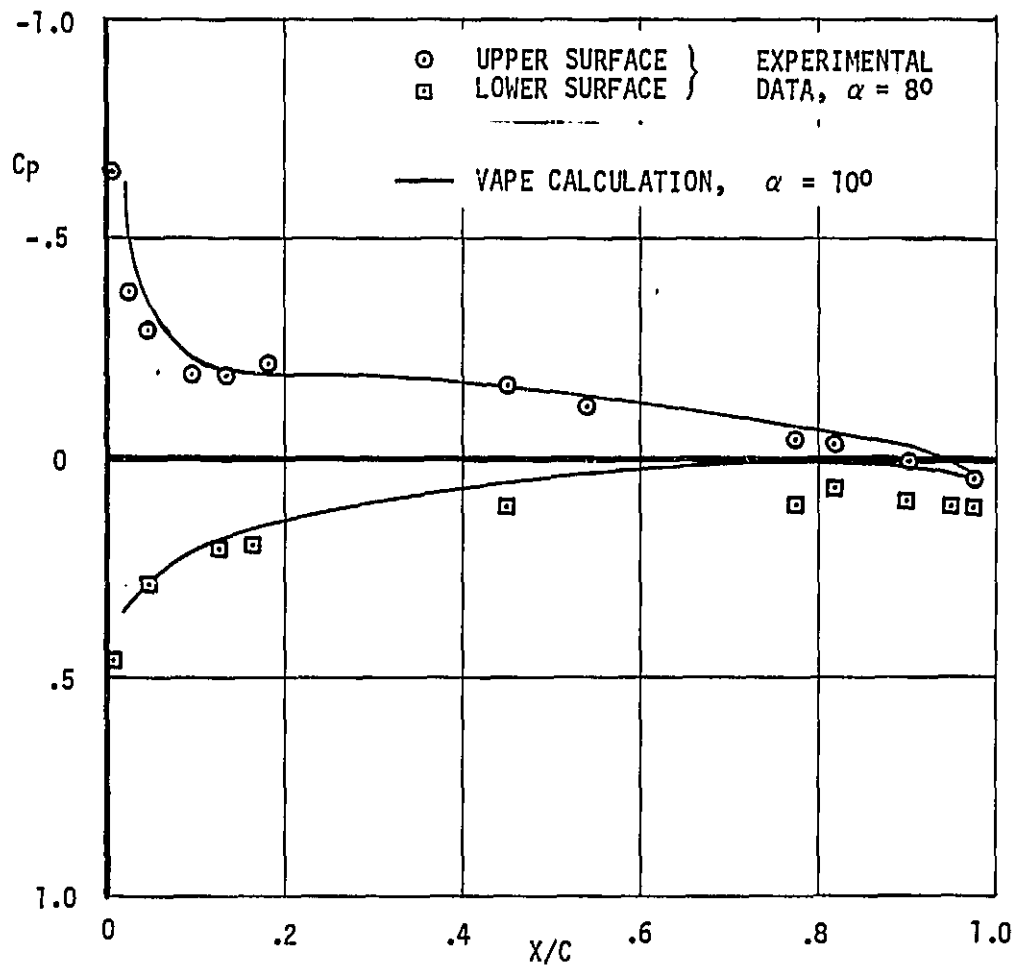

FIGURE 7-7 COMPARISON OF VAPE CALCULATED PRESSURE COEFFICIENTS TO EXPERIMENTAL DATA FOR THE VOUGHT VATOL MODEL WING AT η = .35

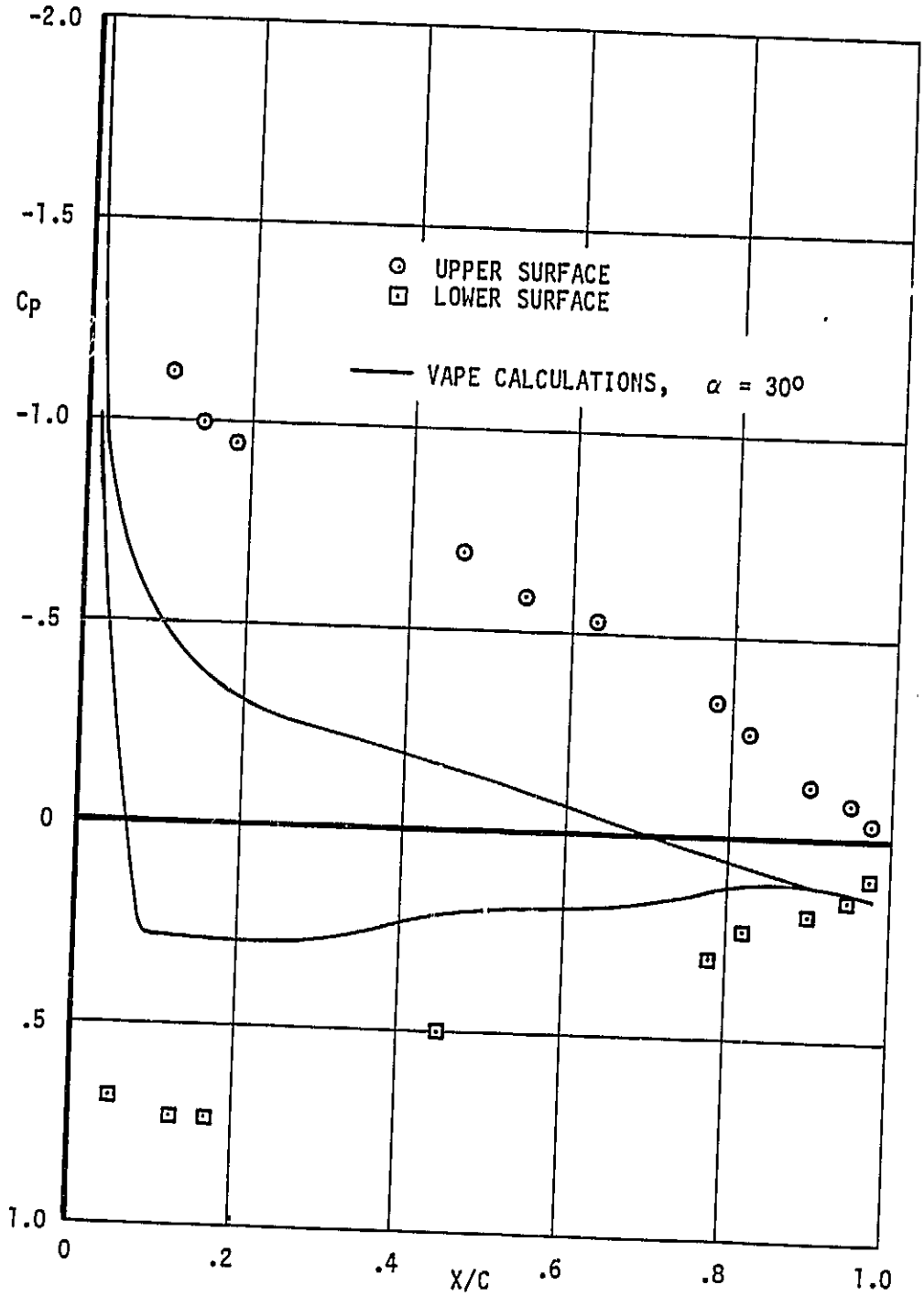

FIGURE 7-8 COMPARISONS OF VAPE CALCULATED PRESSURE COEFFICIENTS TO EXPERIMENTAL DATA FOR THE VOUGHT VATOL MODEL WING AT η = .35

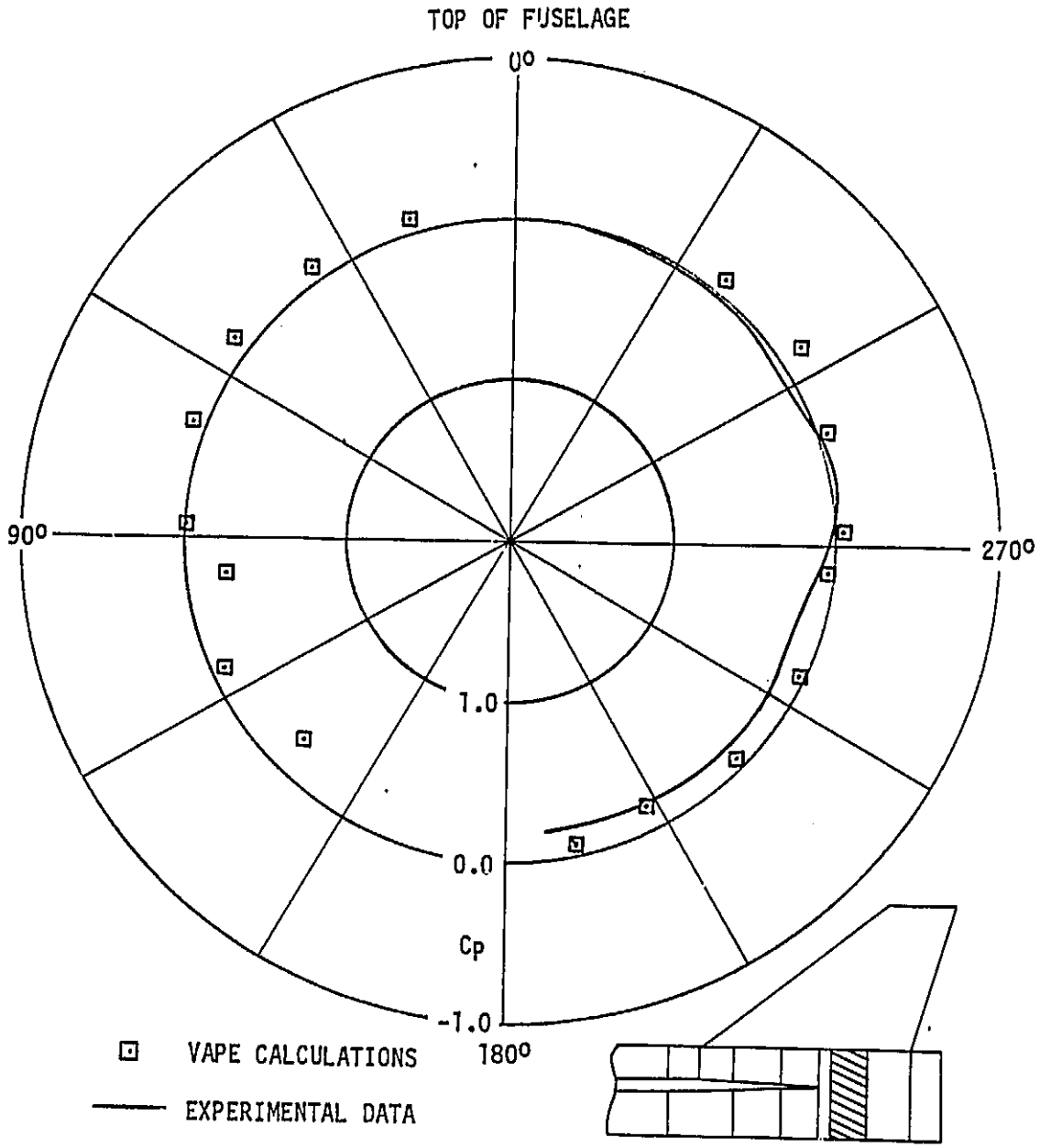

FIGURE 7-9 COMPARISON OF VAPE CALCULATED PRESSURE COEFFICIENTS TO EXPERIMENTAL DATA ON THE VATOL MODEL AFT FUSELAGE AT STATION 199.5, α = 20.4°, NO JETS OPERATING

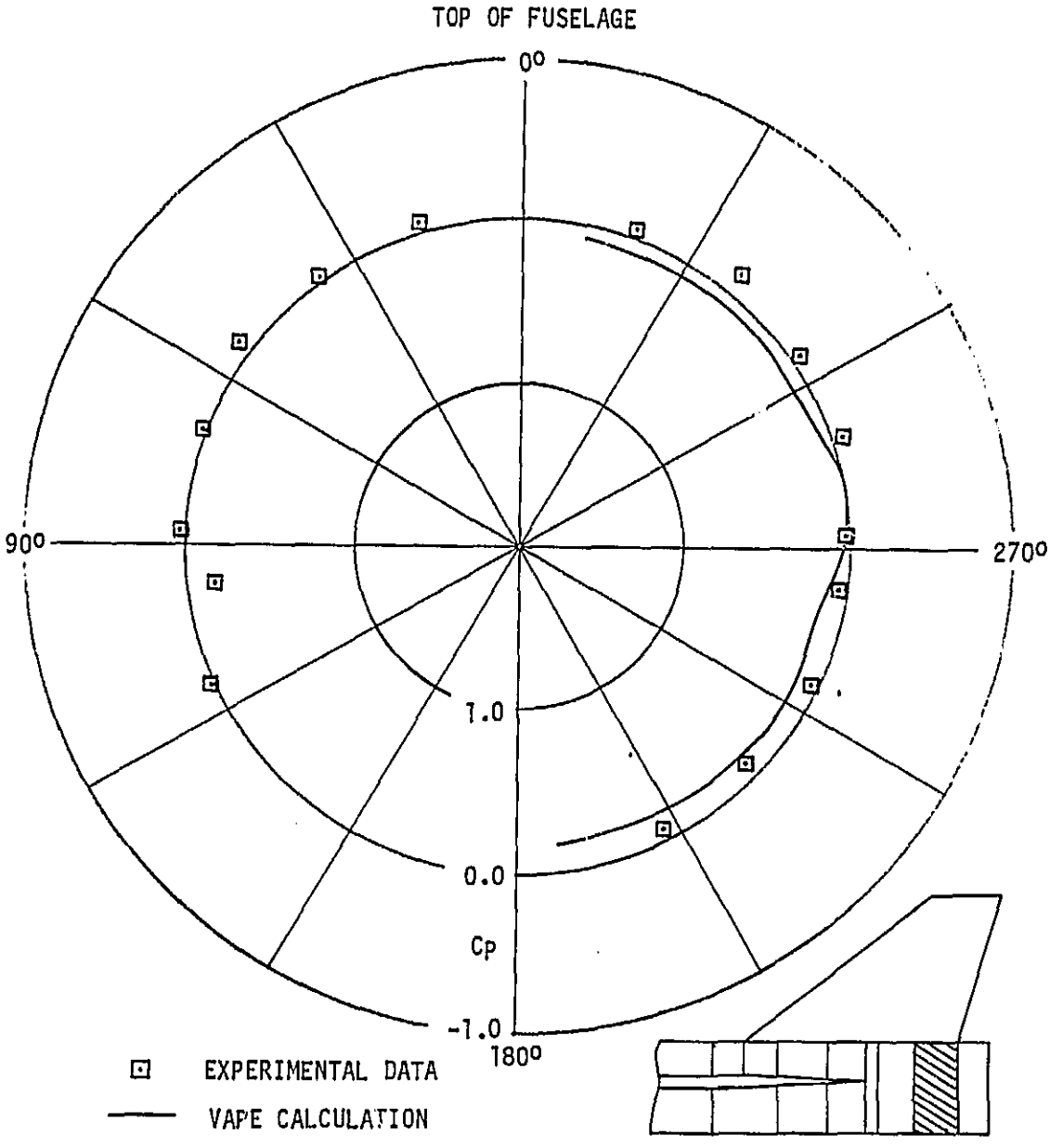

FIGURE 7-10 COMPARISON OF VAPE CALCULATED PRESSURE COEFFICIENTS TO EXPERIMENTAL DATA ON THE VATOL MODEL AFT FUSELAGE AT STATION 207.1, $\alpha = 20.4^{o}$, NO JETS OPERATING

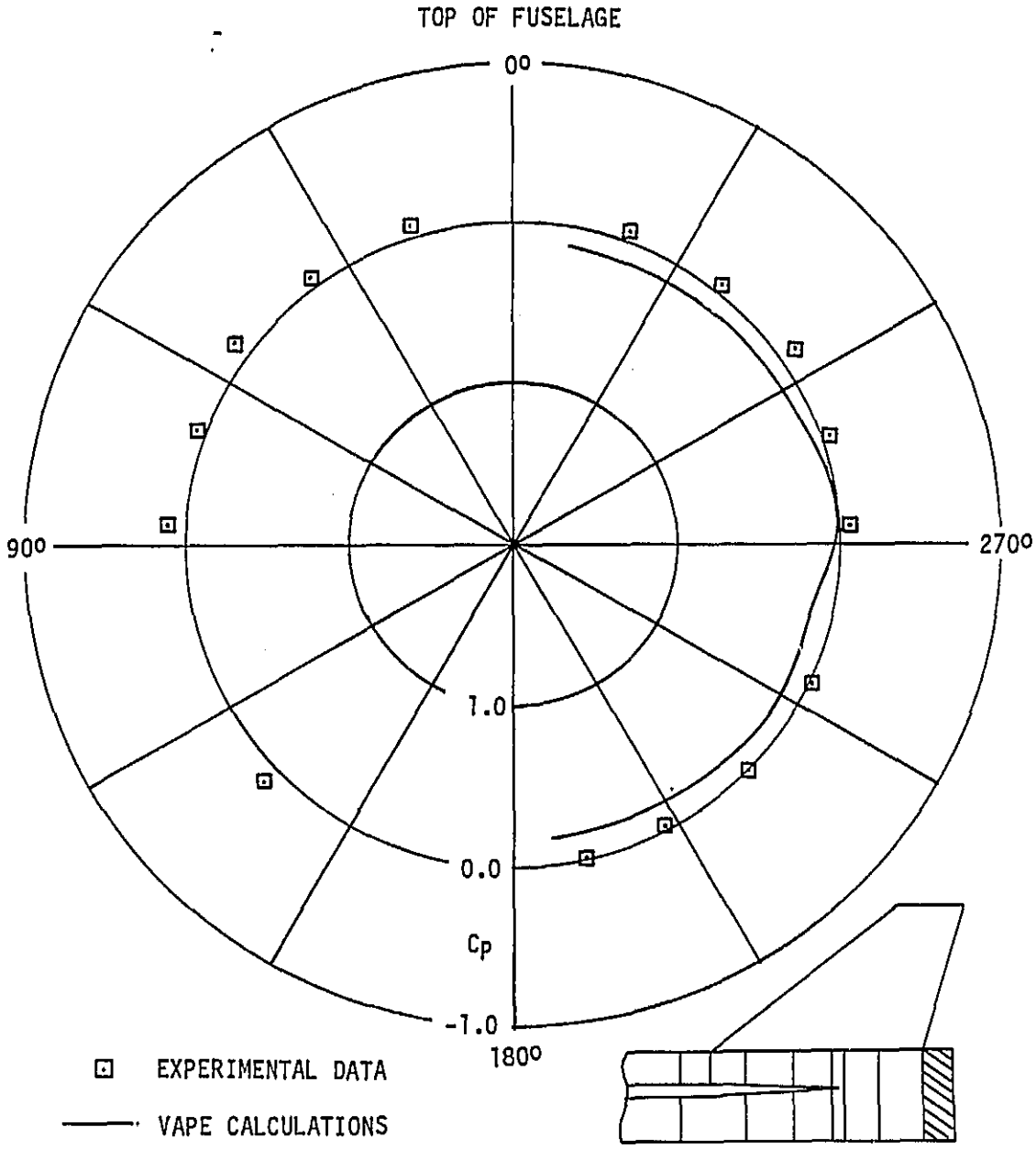

FIGURE 7-11 COMPARISON OF VAPE CALCULATED PRESSURE COEFFICIENTS TO EXPERIMENTAL DATA ON THE VATOL MODEL AFT FUSELAGE AT STATION 219.3, $\alpha = 20.4^{\circ}$, NO JETS OPERATING

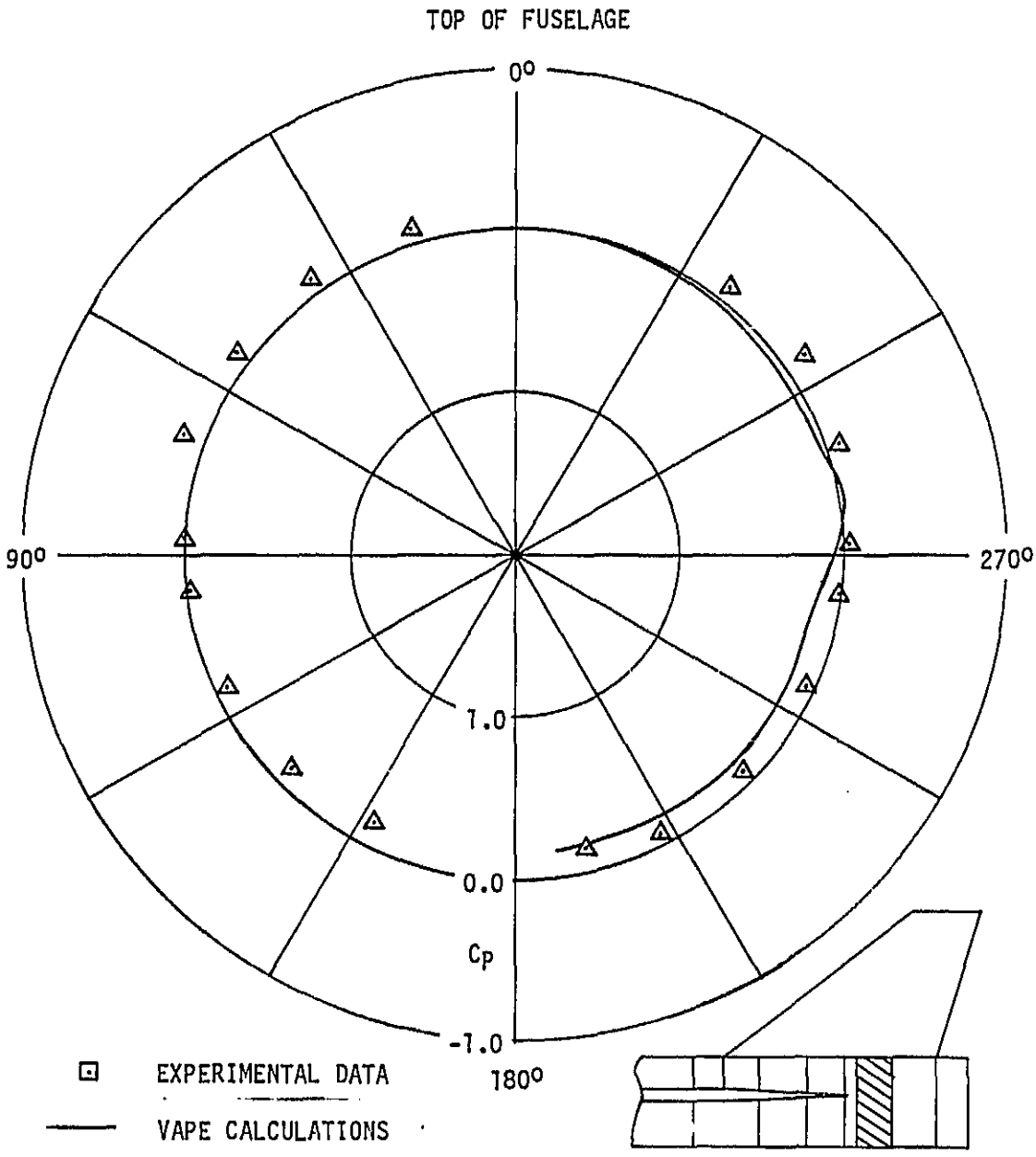

FIGURE 7-12 COMPARISON OF VAPE CALCULATED PRESSURE COEFFICIENTS TO EXPERIMENTAL DATA ON THE VATOL MODEL AFT FUSELAGE AT STATION 199.5, α = 20.4°, JETS OPERATING

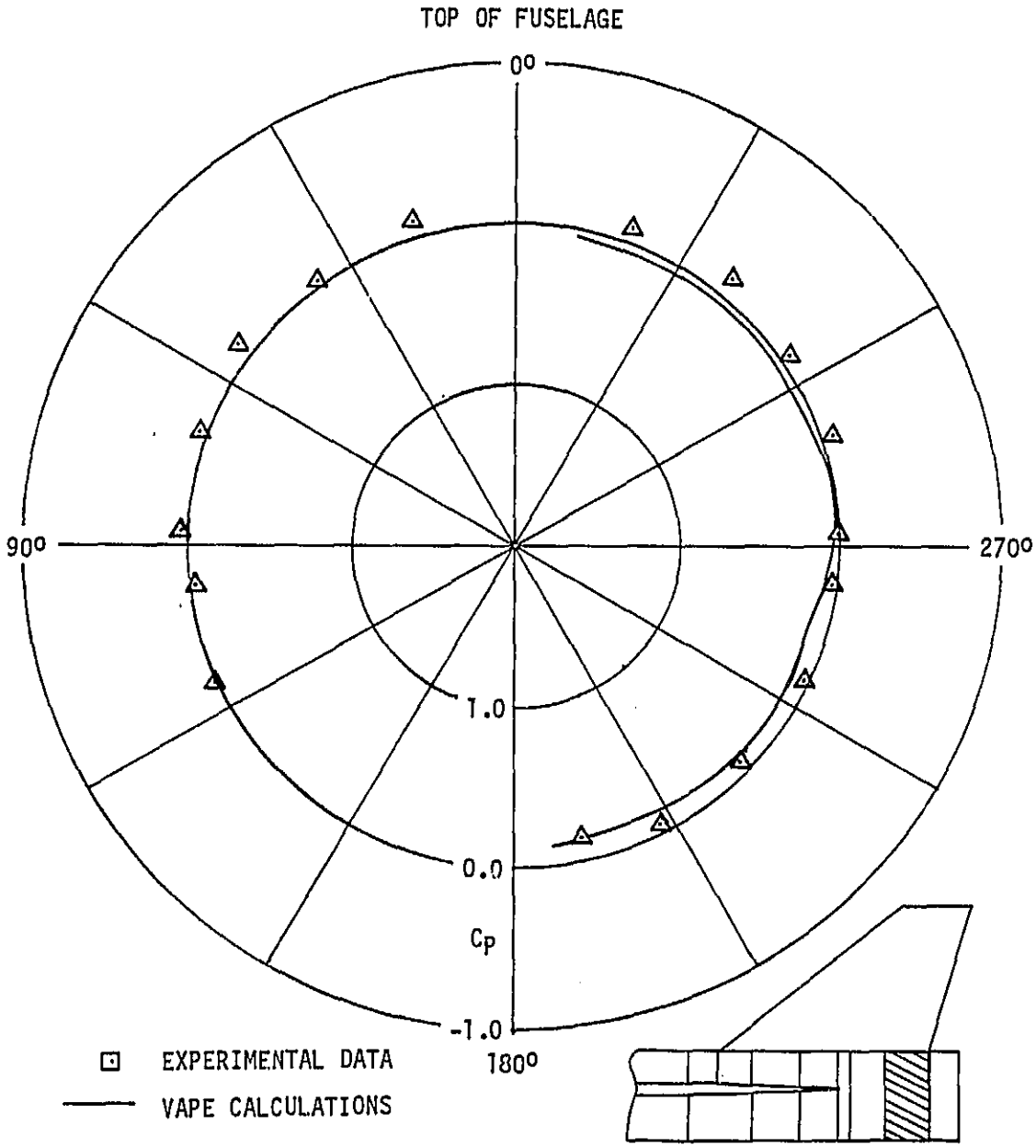

FIGURE 7-13 COMPARISON OF VAPE CALCULATED PRESSURE COEFFICIENTS TO EXPERIMENTAL DATA ON THE VATOL MODEL AFT FUSELAGE AT STATION 207.1, α = 20.4°, JETS OPERATING

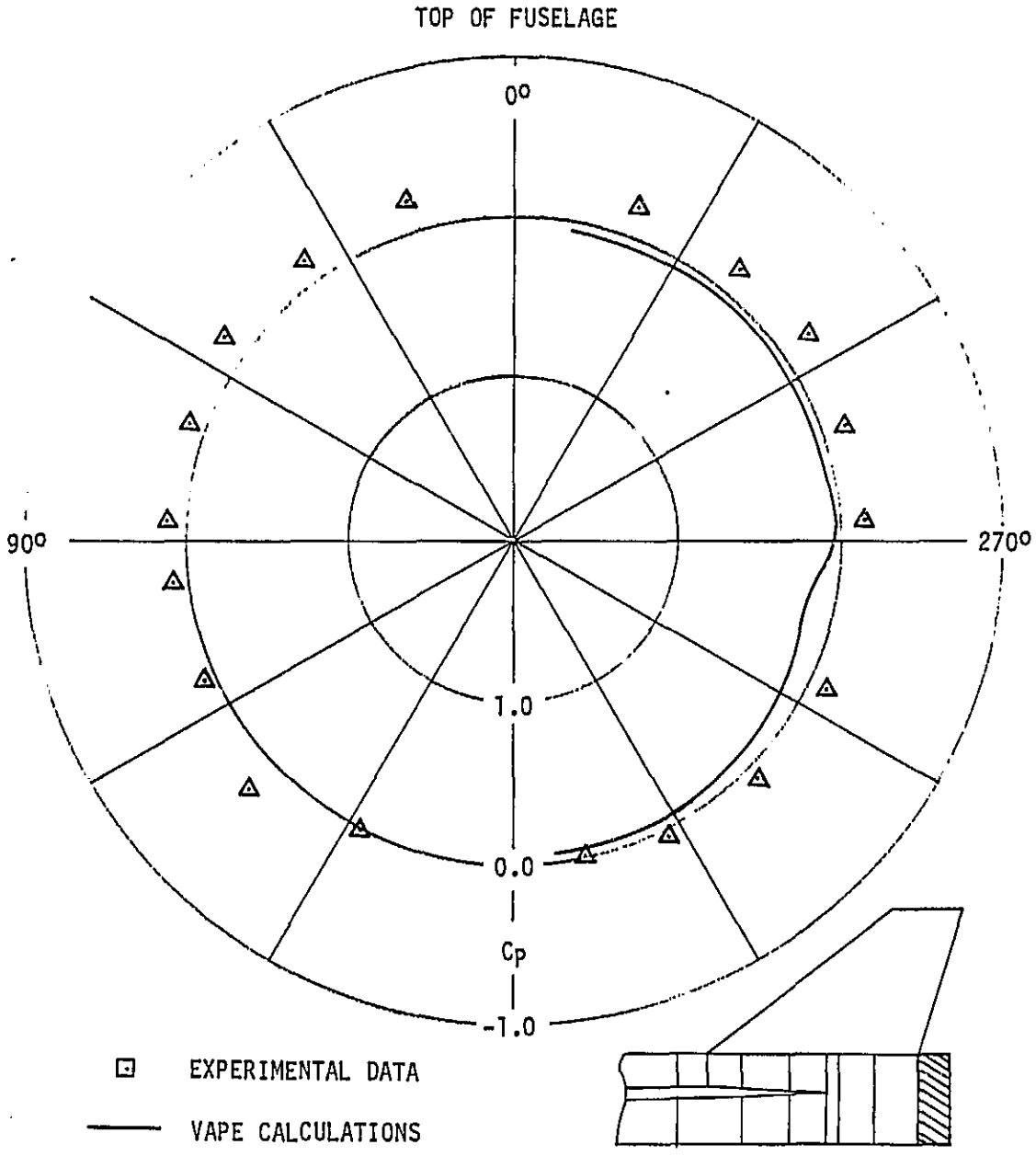

FIGURE 7-14 COMPARISON OF VAPE CALCULATED PRESSURE COEFFICIENTS TO EXPERIMENTAL DATA ON THE VATOL MODEL AFT FUSELAGE AT STATION 219.2, α = 20.4°, JETS OPERATING

8.0 SUBSTANTIATION OF VAPE RECTANGULAR JET MODEL

The rectangular jet code was evaluated using a configuration of reference 8.0-1 shown in Figure 8-1 and described in section 6.1. This configuration has an aspect ratio 9.8 rectangular jet orientated in a streamwise direction on the fuselage centerline. Four jet velocity ratios R were analyzed for a jet deflection angle of 90 degrees and the results are presented in terms of lift to thrust (L/T) ratios in Figures 8-2 through 8-5. Figure 8-2 presents a comparison showing very good agreement between experimental data and VAPE calculations for an R of 20. Similar results are shown in Figure 8-3 for R = 10, however, the calculated results are slightly higher than the experimental values. The last two figures for R = 6 and 4 show the same comparisons with the calculated values always higher than the experimental values. As can be seen, there is less agreement in terms of absolute levels as the value of R decreases.

A possible explanation of this discrepancy can be obtained by consideration of the physics of the flow field. As R decreases, the exhaust jet does not penetrate as far into the external stream and thus curves rearward with a higher curvature. This results in the jet being closer to the body and producing more of an induced effect. In addition, any viscous effects existing in the area directly behind the jet due to flow separation will be increased. Therefore, consideration of the physical flow field indicates that as R decreases, the method becomes less realistic due to the neglect of viscous and separation effects behind the jet. These results are encouraging if the trends with angles of attack are considered. The predicted lift curve scope ($d(L/T)/d\alpha$) for all four values of R agree very well with the experimental values, even though the lift curve slopes are quite different for each of the R values as shown in Figures 8-2 through 8-5. It should also be noted that the aspect ratio (length/width) of the jet is 9.8 which is considerably outside the range of the model data base.

The rectangular jet model and subsequent computer code, as described in reference 8.0-1, was developed for NASA and the Navy based primarily on data from tests on a flat plate. The computer code sent from NASA was inserted into the VAPE code under a previous Navy contract without verification on complete V/STOL configurations. Under the current contractual effort, this code has been verified against experimental data with the subsequent discovery of two major problems in the code: (1) It is applicable to zero degree angle of attack cases only, and (2) the solution algorithm is inefficient and difficult to use in its current form.

The first problem has been corrected during this contractual effort and results are be presented. The second problem is more difficult to solve since it effects the overall logic of the code. Currently, in the rectangular jet code (RJC), the jet coordinates and the effects of the jet on the overall configuration are both determined in the jet coordinate system. This system assumes the origin is at the jet exit and the axis orientation are a function of the angle of attack, the yaw angle, and the jet injection angle. This coordinate system, as defined in the RJC, has the z axis positive upwards with a 90 degree injection angle being in the positive z direction. The model then requires that the coordinates of the total configuration be transformed into this jet exit coordinate system. This is inefficient since there are several times as many body coordinates as there are jet coordinates. Also, the jet direction is assumed positive in the jet coordinate system which requires that the configuration be inverted during the transformation. These problems could be solved by reprogramming the routine to better fit the VAPE system.

The above discussion indicates that the current rectangular jet method can be used for jets which are within the specified boundaries given in Section 3.3 and produce reasonable results. The method should be reprogrammed to increase its generality and efficiency, and it should be evaluated against more jet configurations. In addition, in the future, the data base should be increased to enlarge the range of applicability of the method.

REFERENCES:

8.0-1 Thames, F.C.: "Development of an Analytical Model to Predict Induced Effects of Aspect Ratio 4.0 Rectangular Nozzles in a Subsonic Crossflow," Vought Report No. 2-53110/9R-52268.

SCALE = 1.8
PITCH = 20.0
YAW = 55.0
ROLL = 20.0

ORIGINAL PAGE IS
OF POOR QUALITY

FIGURE 8-1 V/STOL MODEL WITH RECTANGULAR JET

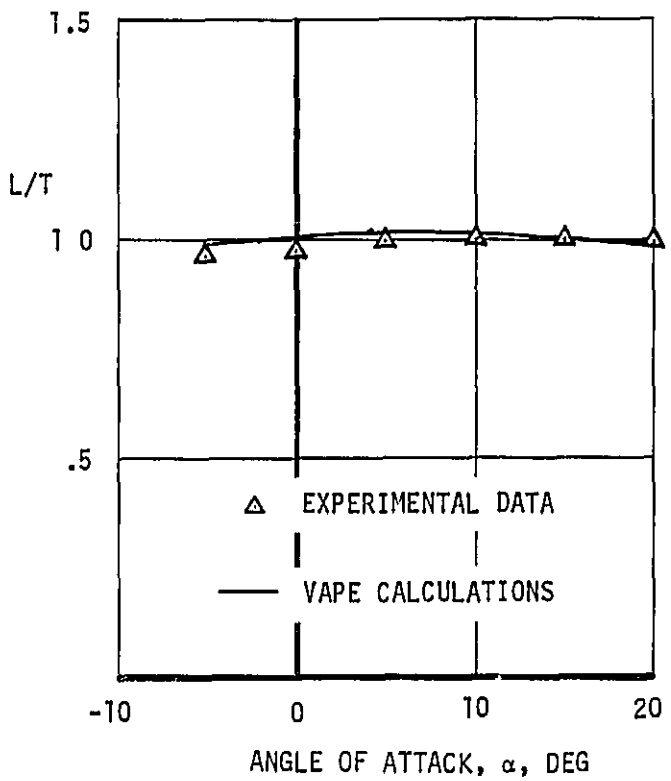

FIGURE 8-2 COMPARISON OF VAPE CALCULATED LIFT-TO-THRUST VALUES TO EXPERMENTAL DATA FOR THE RECTANGULAR JET MODEL OF NASA TND-3213, R = 20.0

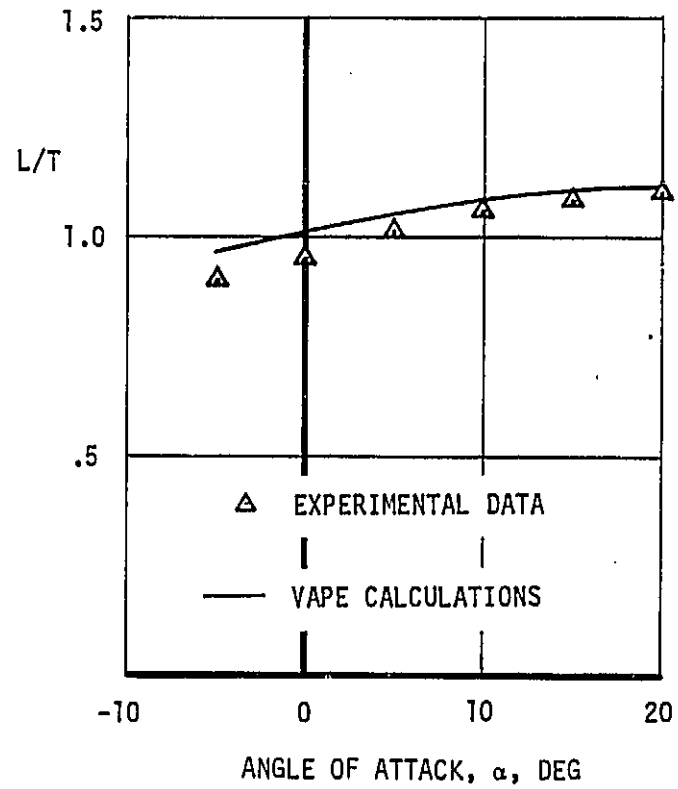

FIGURE 8-3 COMPARISON OF VAPE CALCULATED LIFT-TO-THRUST VALUES TO EXPERIMENTAL DATA FOR THE RECTANGULAR JET MODEL OF NASA TND-3213, R = 10

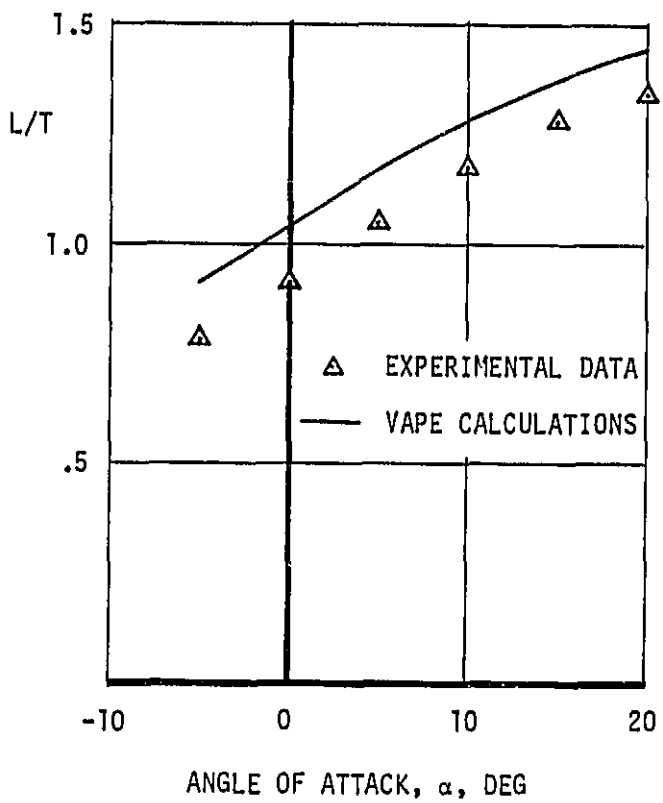

FIGURE 8-4 COMPARISON OF VAPE CALCULATED LIFT-TO-THRUST VALUES TO EXPERIMENTAL DATA FOR THE RECTANGULAR JET MODEL OF NASA TND-3213, R = 6.0

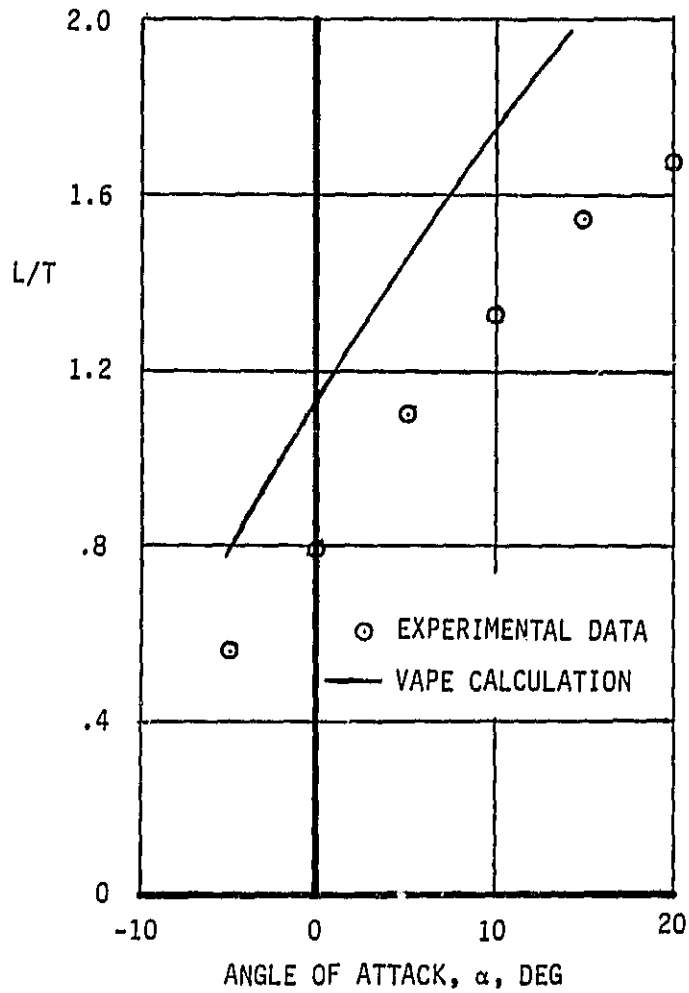

FIGURE 8-5 COMPARISON OF VAPE CALCULATED LIFT-TO-THRUST VALUES TO EXPERIMENTAL DATA FOR THE RECTANGULAR JET MODEL OF NASA TND-3213, R = 4.0

9.0 V/STOL AIRCRAFT CORRELATIONS

The validation of a computer program the size and complexity of VAPE requires direct comparison between calculated and experimental data. Throughout this study, as discussed in previous sections, comparisons of VAPE predicted data against experimental data for rather simple configurations have been presented. In addition to these comparisons, it was decided to try and analyze two more complicated configurations. The two configurations selected were both tested in the AMES 40 x 80 foot wind tunnel. The experimental data base was fairly comprehensive and the geometry was defined which would help reduce model formulation requirements. The configurations selected were: (1) the Grumman tilt-nacelle model, reference 9.0-1, and (2) the General Dynamics STOL fighter model, reference 9.0-2. The details of the analysis performed are given in the next two subsections. These studies were instructive, but were limited due to time and budget constraints. Further work should be done on both of these configurations to best determine how to use VAPE on these type of aircraft.

REFERENCES:

9.0-1 Anonymous: "Full-Scale Tests of Grumman Design 698-411 Tilt Nacelle V/STOL Model at the NASA-Ames Research Center," prepared under contract to Naval Air Systems Command, Contract No. N-00019-80-C-0015, Report No. 698-33, Dec. 1981.

9.0-2 Howell, G.A., Crosthwait, E.L., and White, M.C.: "Evaluation of Pressure and Thermal Data From a Wind Tunnel Test of a Large-Scale Powered STOL Fighter Model,": NASA CR-166170, June 1981.

9.1 TILT NACELLE CONFIGURATION

The Grumman tilt nacelle configuration is described in reference 9.1-1 along with the experimental data for several nacelle deflection angles. This configuration is quite complex and required careful modeling. The details of the model were obtained from wind tunnel model design drawings and should be accurate. Several items which were felt to be of significance to the overall air flow were excluded from the mathematical model of this configuration to reduce complexity. These items included:

- The model strut support system which simulated large landing gear struts and connected the model to the tunnel support system.
- The longitudinal strakes mounted on the lower fuselage.
- The vane control system mounted in the fan slipstream.

The basic geometry of this configuraion is shown in Figure 9.1-1 which shows a panel model generated for input to VAPE. This figure demonstrates several features. First, the inlet is paneled to permit inlet velocities to be specified. The nacelle is shown at the 40 degree deflection analyzed during this study. Secondly, the part span flap is deflected 5 degrees. The 40 degree nacelle deflection was originally chosen because it was essentially halfway through the deflection envelope. More deflection angles need to be analyzed in the future to better understand how to apply VAPE to this type of configuration.

The flap deflection was a source of concern when the model was first formulated. Since this type of flap configuration had never been run through VAPE, it was not known how the potential flow program would react to the discontinuities at the flap ends. Therefore, a simple study was conducted which used only the wing geometry. Two cases were formulated, one with the wing as shown in Figure 9.1-1, and one where the flap was blended into the wing so that no discontinuities existed. This latter case is not quite correct, but has been used in the past in vortex lattice and lifting line codes to simulate flap deflections. The results are presented in Figures 9.1-2 through 9.1-11. The lift and moment comparisons are presented in Figures 9.1-2 and 9.1-3. As can be observed, there is very little difference. Span loading comparisons are presented in Figures 9.1-4 through 9.1-6, again showing very good agreement. The chordwise pressure comparisons for an angle of attack of zero are presented in Figures 9.1-7 through 9.1-11, showing very good agreement. These results indicate that the actual flap deflection modeled in the VAPE system with the flap end discontinuities is working correctly and is not presenting any problems. Even the discontinuities in span loading at the flap ends are predicted. This data will also be used later to help understand the full case solutions.

The full configuration was then analyzed with the inviscid VAPE code to see how well the calculated results would agree with the experimental values. A total of seven runs were made on VAPE with the configuration, all at the same nacelle deflection angle of 40 degrees. For all of these runs, the inlet velocity values were obtained using corrected airflow values obtained from Figures 3-4 and 3-10 of reference 9.1-1. These corrected airflow values were used to determine a uniform distribution of velocity across the inlet face. This uniform flow will not be realized in real life

and is a possible source of error. However, this technique has been used successfully in the past and so was used in this case to simplify the problem.

The Weston jet method was used with the jet originating point taken to be the end of the nacelle nozzle.

The results of the first case are compared to experimental data in Figure 9.1-12 for lift coefficient. In this comparison, the direct power effects were removed from the experimental data (Figure 2-36 of reference 9.1-1). As can be observed in Figure 9.1-12, the comparison in terms of lift curve slope, C_L is fairly good, but there is a sizable difference in the actual C_L level. The model was studied in detail and several attempts were made to improve the correlations which will be discussed later. However, the basic shift in the C_L level remained. A possible explanation for this shift can be obtained by considering the effect the nacelle deflection angle has on the aircraft. Figures 9.1-13 and 9.1-14 present the predicted chordwise pressure distribution at two inboard wing stations directly behind the nacelle. If these are compared to the wing alone curves in Figures 9.1-7 and 9.1-8, it can be observed that the chordwise loading on the wing in the presence of the nacelle has changed considerably from the clean wing case. The leading edge pressure peak on the upper surface has disappeared. In fact, the wing has a download in this area, whereas on the clean wing case, there was an upload. This would imply that the nacelle is producing a downwash flow field on the wing. If the flow is attached to the nacelle, which it must be in potential flow, then a downwash field on the wing would be expected. If this deduction is true, the large lift coefficient in the experimental data cannot be explained. The only way that the wing can produce the lift coefficient at zero angle of attack that the experimental data indicates is with an upwash field imposed on the majority of the wing, a contradiction. Consider the data shown in Figure 9.1-15 which shows lift coefficient with direct power effects removed versus nacelle deflection angle. The curve increases up to slightly beyond 20 degrees and then becomes essentially constant at 30 degrees. If the nacelle were to be considered as a lifting body, then it would be expected to see the lift continue to increase throughout the angle of attack shown in this figure. This could very well indicate that at approximately 20 to 25 degrees, a separation on the leeward side of the nacelle is formed and becomes "stable" at 30 degrees (i.e. the separation lines remain the same). If this were to occur, then the flow over the inboard wing would no longer be a downwash and could very well become an upwash. Grumman personnel have stated that separation did exist at 40° of deflection, thus this theory gives a reasonable explanation to an experimental result.

Several runs were made to investigate the effect of other items on this model. First, what effect would be induced by considering the effect of wind tunnel walls on the model. No wall effects were supposedly used in reducing the experimental data, therefore, there should still remain some small effect of the bounding effect of the walls on the flow field. Figure 9.1-16 shows the configuration with a model of the 40 x 80 foot wind tunnel walls included. This configuration was run at zero angle of attack for two conditions: (1) the wind tunnel walls only to determine their effect, and (2) with the STOL ground plane module included to determine the effect of the jets impinging on the ground plane. The results of these two cases are shown in Figure 9.1-17. The wind tunnel walls produced an increase in lift coefficient of approximately .16 and the ground plane added another .06. Both of these cases ran with no problems. This shows an additional capability of VAPE to determine wind tunnel wall effects of V/STOL aircraft with the power effects and wall jet effects included.

The tilt Nacelle model is a good test case for VAPE because it illuminates the area where further work is required. For example, a viscous capability for bodies is need so that separation locations can be predicted. Further work should also be done in modeling of nacelles, i.e. how should a nacelle for a large bypass ratio fan be modeled.

REFERENCES:

9.1-1 Anonymous: "Full-Scale Tests of Grumman Design 698-411 Tilt Nacelle V/STOL Model at the NASA-Ames Research Center," prepared under contract to Naval Air Systems Command, Contract No. N00019-80-C-0015, Report No. 698-33, Dec. 1981.

FIGURE 9.1-1 VAPE INPUT PANELING FOR TILT NACELLE CONFIGURATION

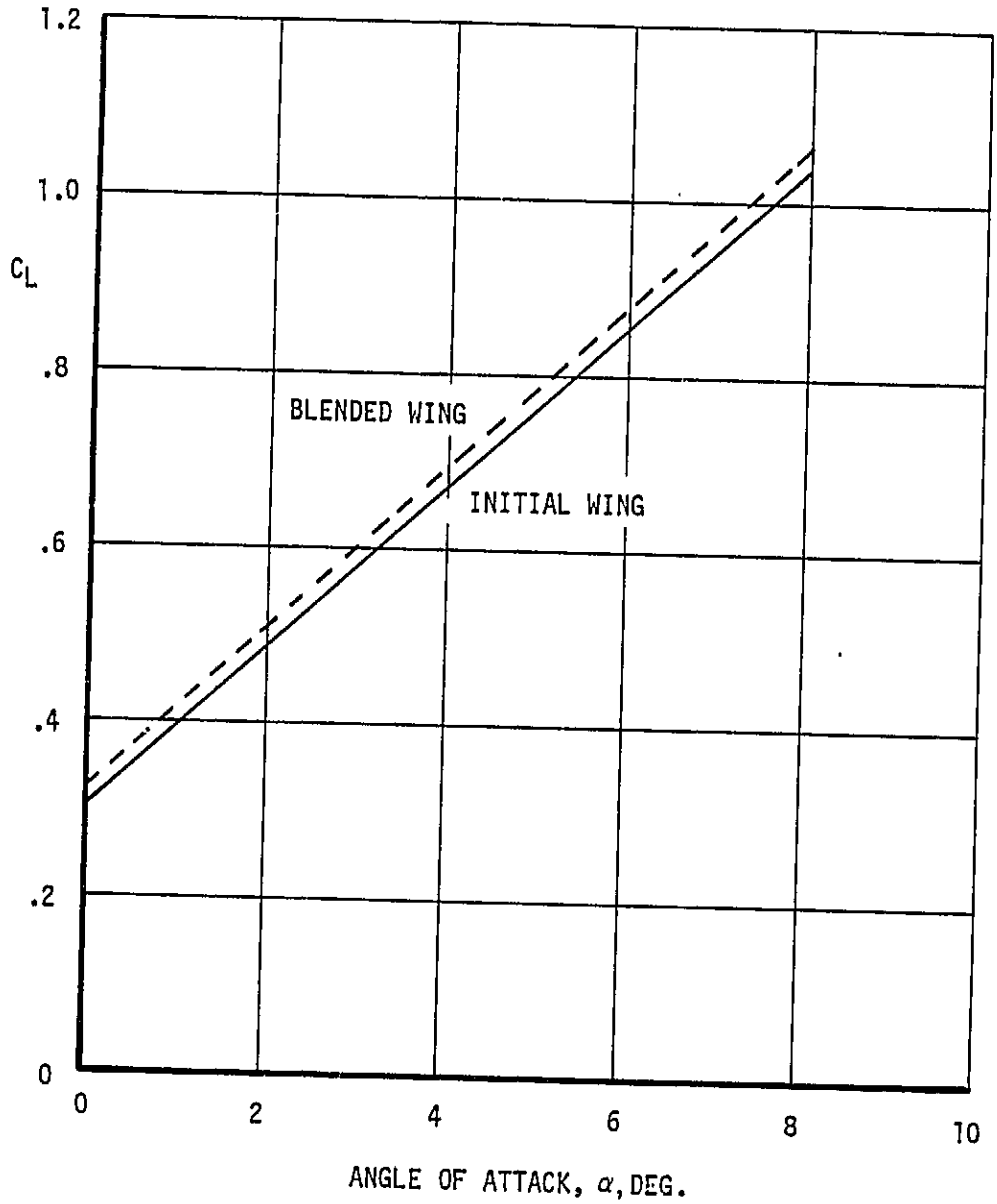

FIGURE 9.1-2 COMPARISON OF VAPE CALCULATED LIFT CURVES ON THE INITIAL PART SPAN FLAPPED WING AND THE BLENDED WING

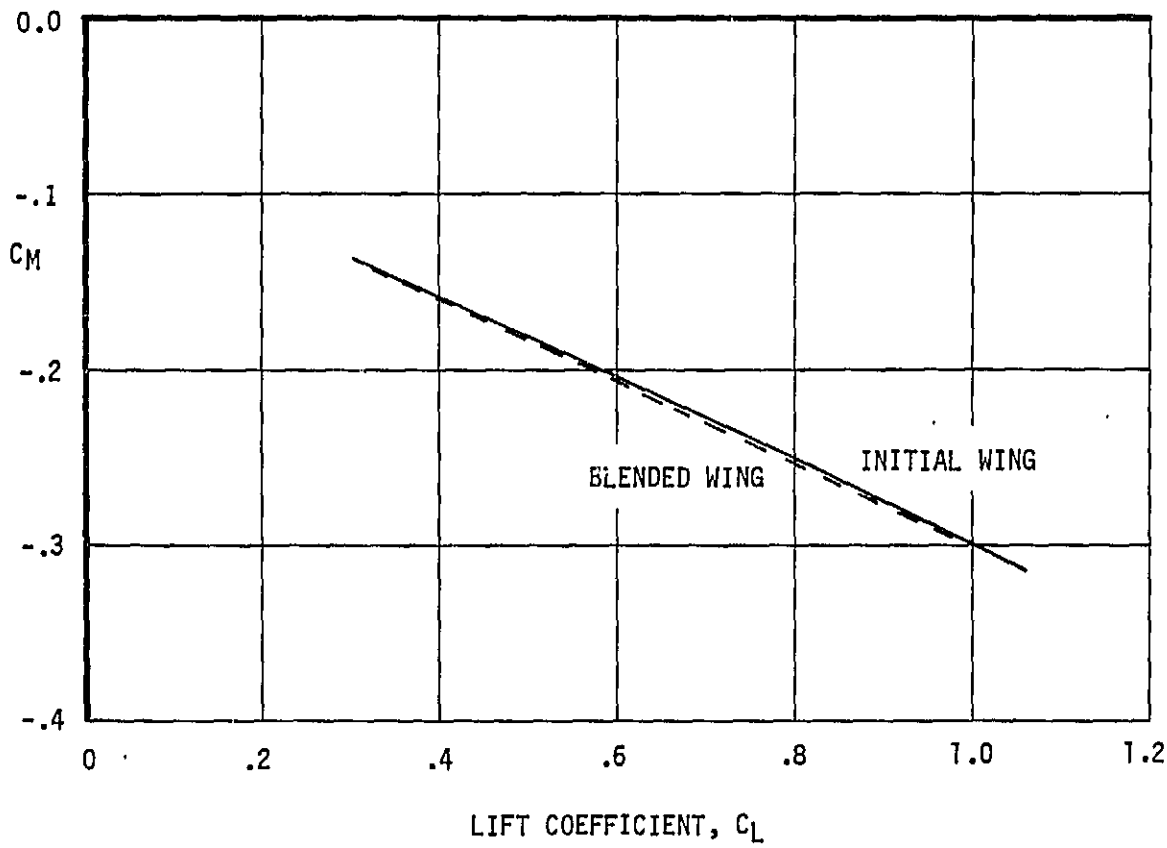

FIGURE 9.1-3 COMPARISON OF VAPE CALCULATED PITCHING MOMENTS ON THE INITIAL PART SPAN FLAPPED WING AND THE BLENDED WING

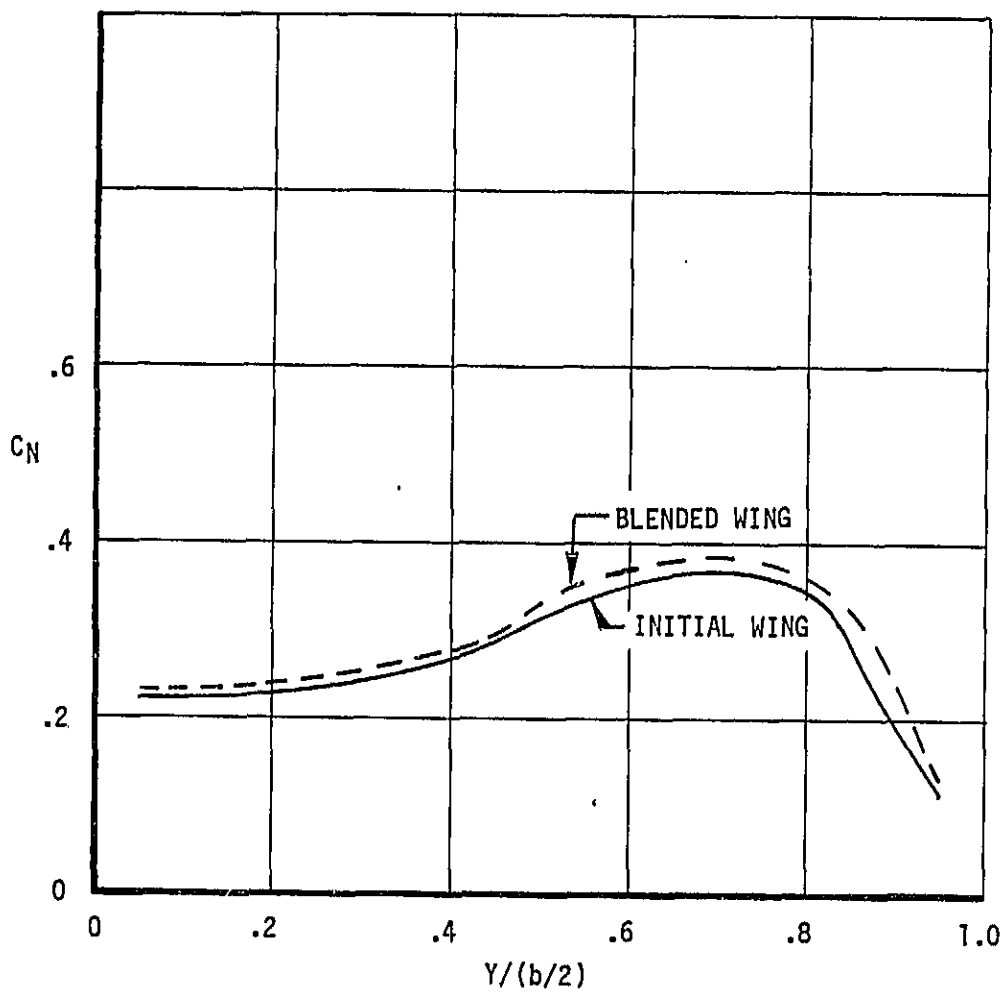

FIGURE 9.1-4 COMPARISON OF VAPE CALCULATED SPAN LOADING ON THE INITIAL PART SPAN FLAPPED WING AND THE BLENDED WING, $\alpha = 0^o$

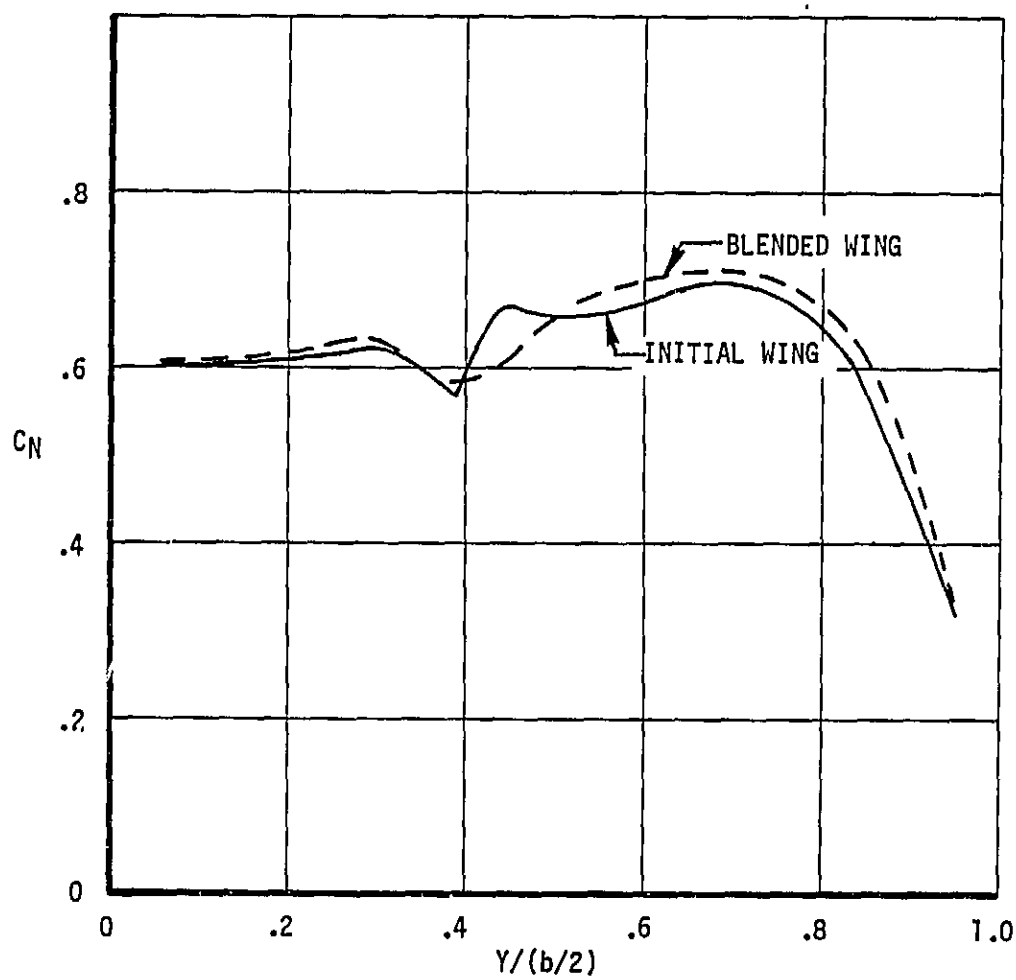

FIGURE 9.1-5 COMPARISON OF VAPE CALCULATED SPAN LOADING ON THE INITIAL PART SPAN FLAPPED WING AND THE BLENDED WING, $\alpha = 4^o$

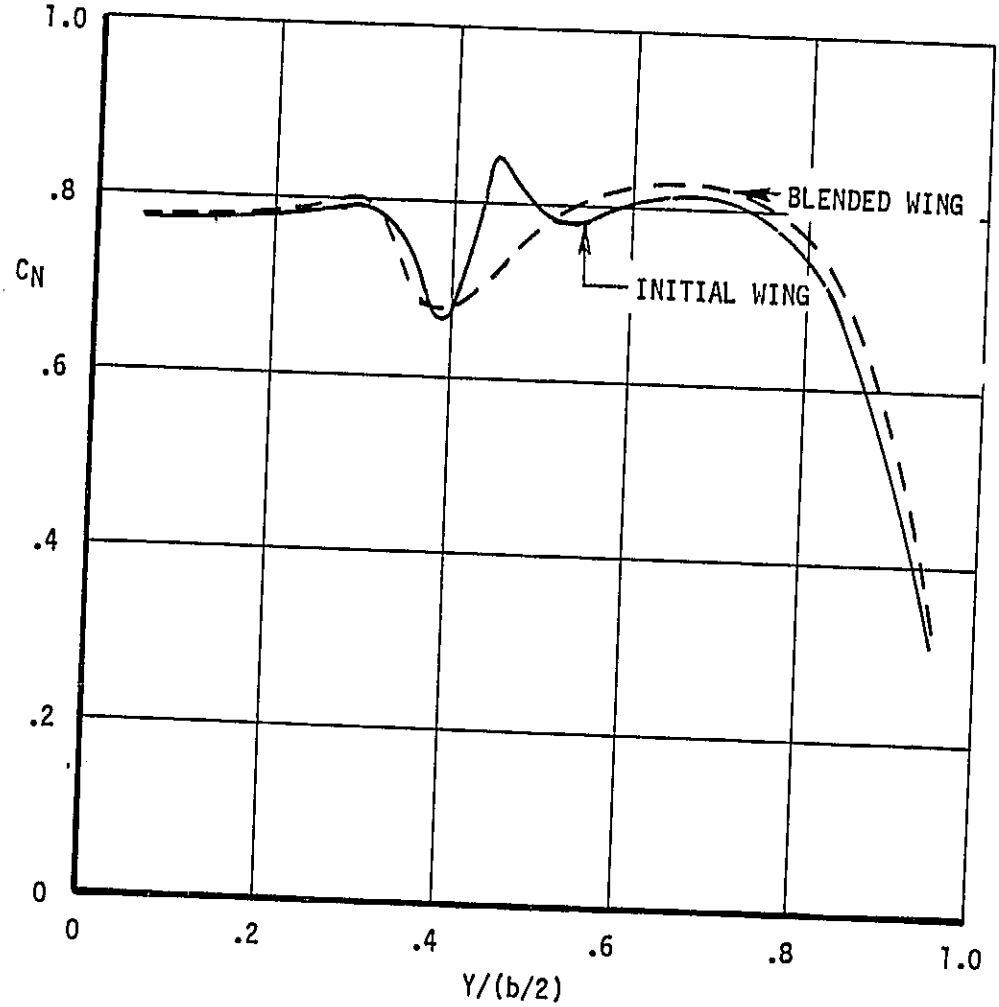

FIGURE 9.1-6 COMPARISON OF VAPE CALCULATED SPAN LOADING ON THE INITIAL PART SPAN FLAPPED WING AND THE BLENDED WING, α = 8°

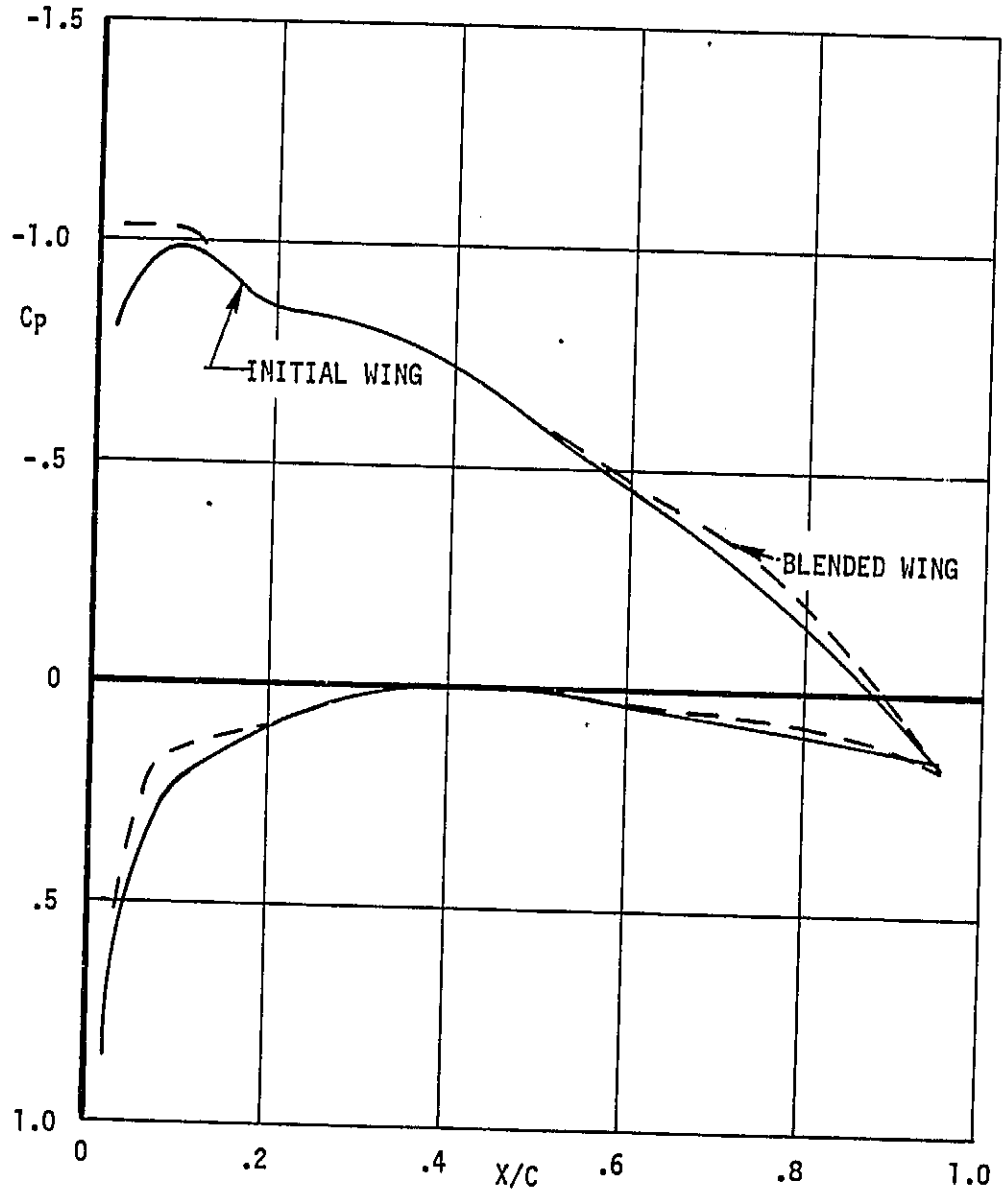

FIGURE 9.1-7 COMPARISON OF VAPE CALCULATED CHORDWISE PRESSURE COEFFICIENTS ON THE INITIAL PART SPAN FLAPPED WING AND THE BLENDED WING, $\alpha = 4^{o}$, $\eta = .385$

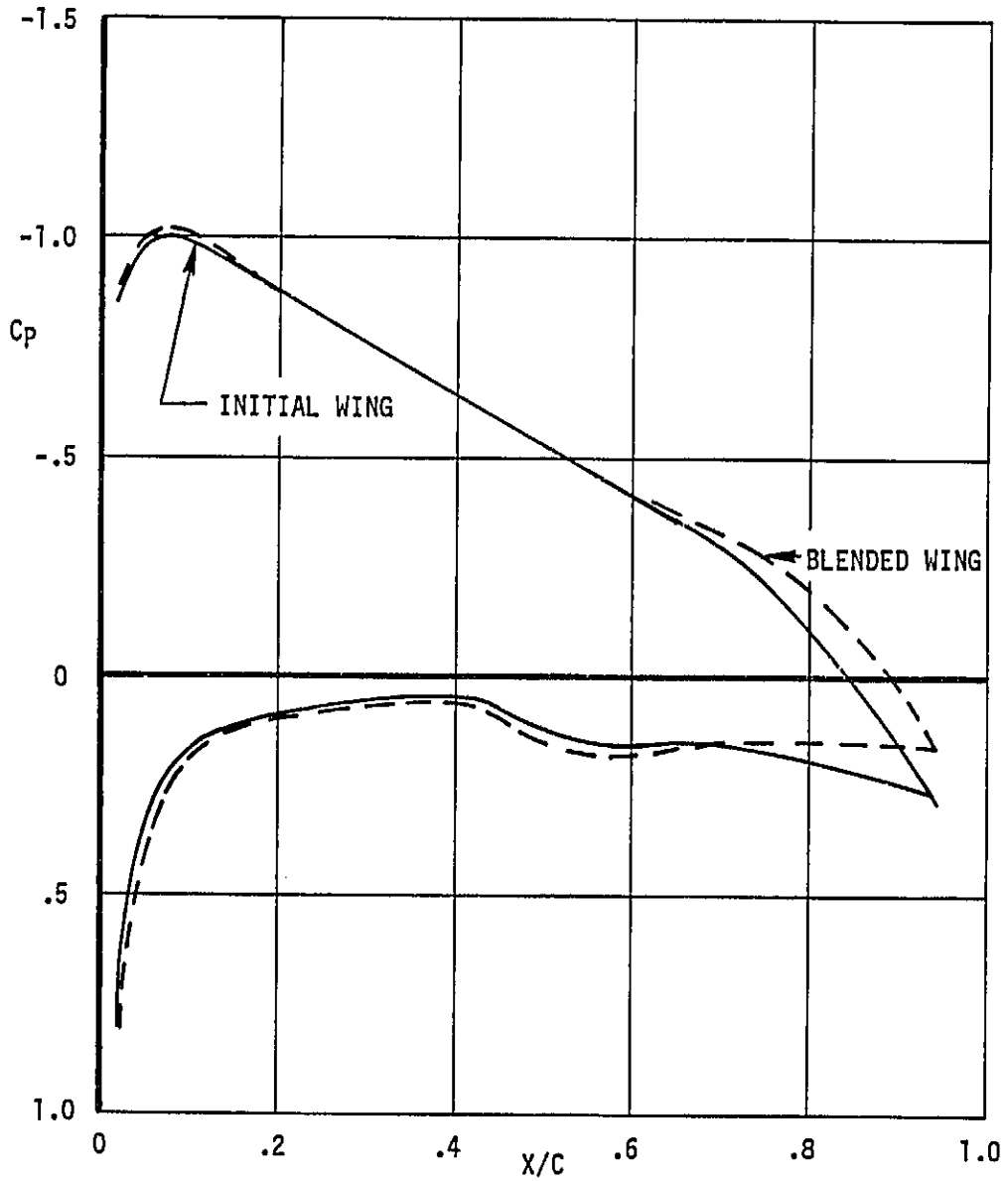

FIGURE 9.1-8 COMPARISON OF VAPE CALCUALTED CHORDWISE PRESSURE COEFFICIENTS ON THE INITIAL PART SPAN FLAPPED WING AND THE BLENDED WING, $\alpha = 4^{o}$, $\eta = .527$

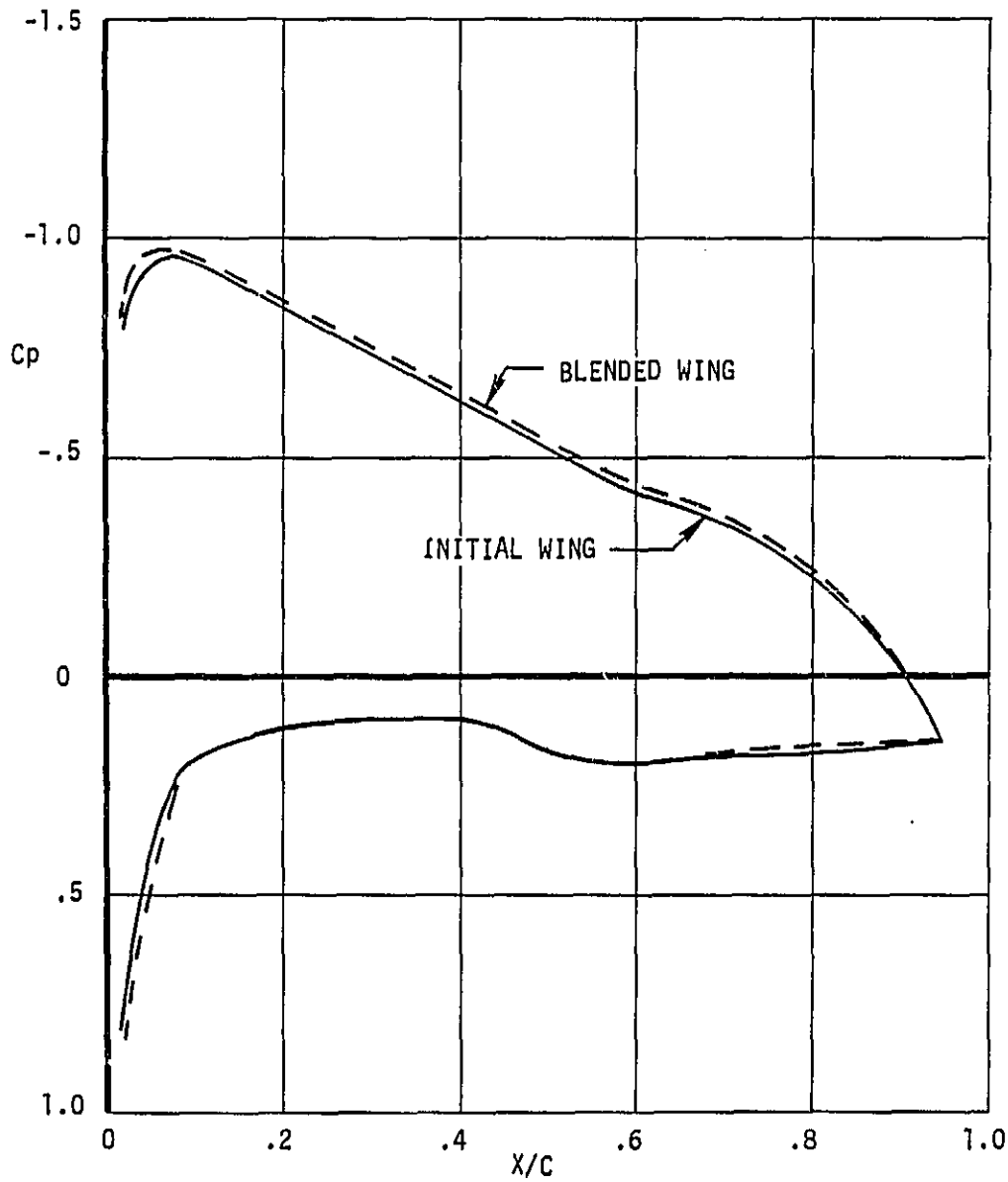

FIGURE 9.1-9 COMPARISON OF VAPE CALCULATED CHORDWISE PRESSURE COEFFICIENTS ON THE INITIAL PART SPAN FLAPPED WING AND THE BLENDED WING. $\alpha = 4^{o}$ $\eta = .73$

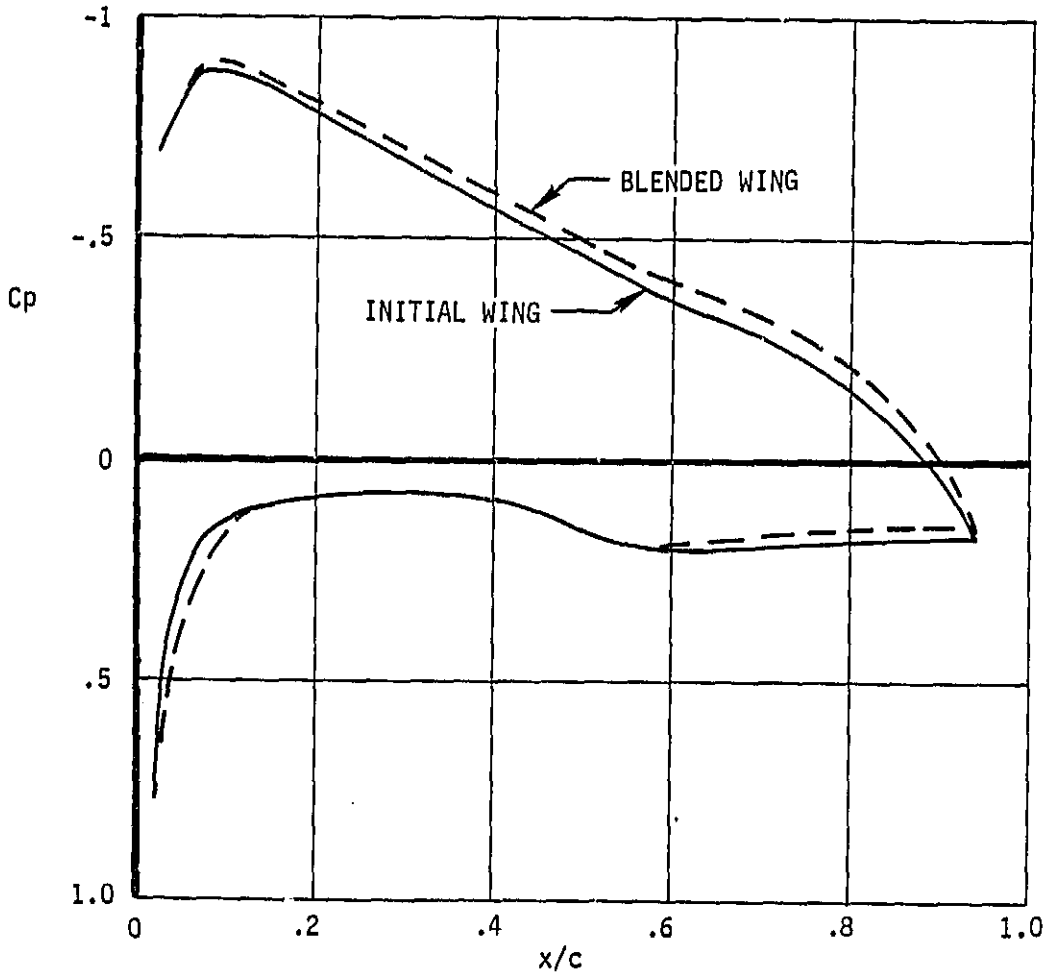

FIGURE 9.1-10 COMPARISON OF VAPE CALCULATED CHORDWISE PRESSURE COEFFICIENTS ON THE INITIAL PART SPAN FLAPPED WING AND THE BLENDED WING $\alpha = 4^{o}$ $\eta = .83$

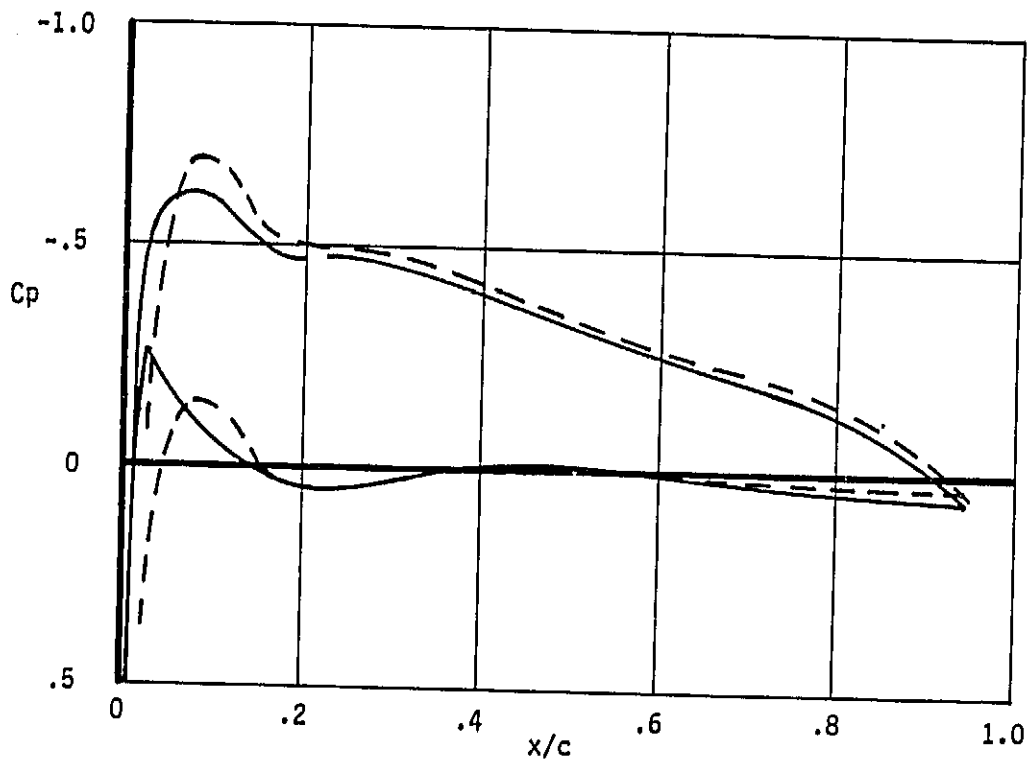

FIGURE 9.1-11 COMPARISON OF VAPE CALCULATED CHORDWISE PRESSURE COEFFICIENTS ON THE INITIAL PART SPAN FLAPPED WING AND THE BLENDED WING, $\alpha = 4^{o}$, $\eta = .95$

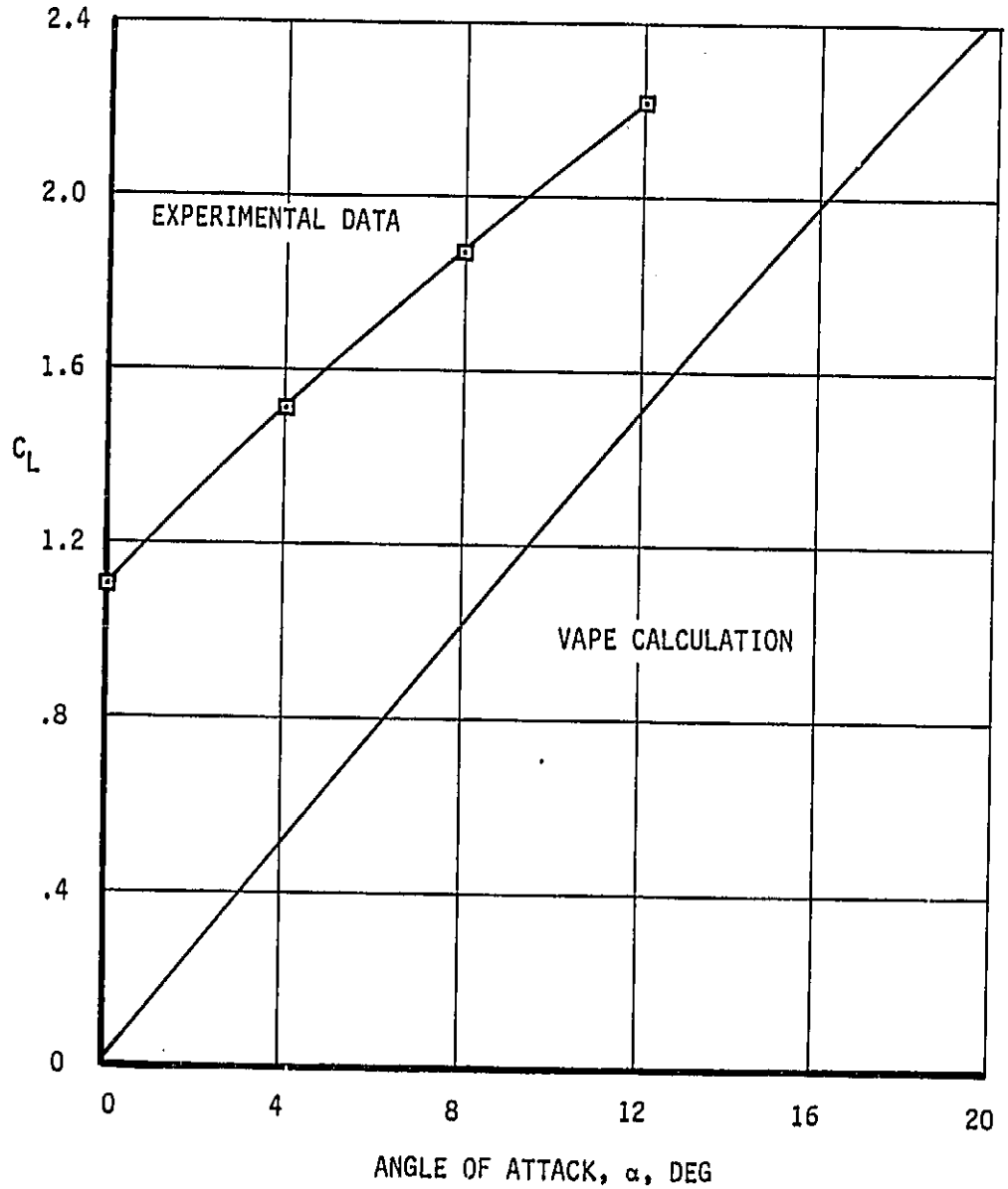

FIGURE 9.1-12 COMPARISON OF VAPE CALCULATED LIFT CURVE TO EXPERIMENTAL DATA FOR THE TILT NACELLE CONFIGURATION $\delta_{Nacelle} = 40^{o}$

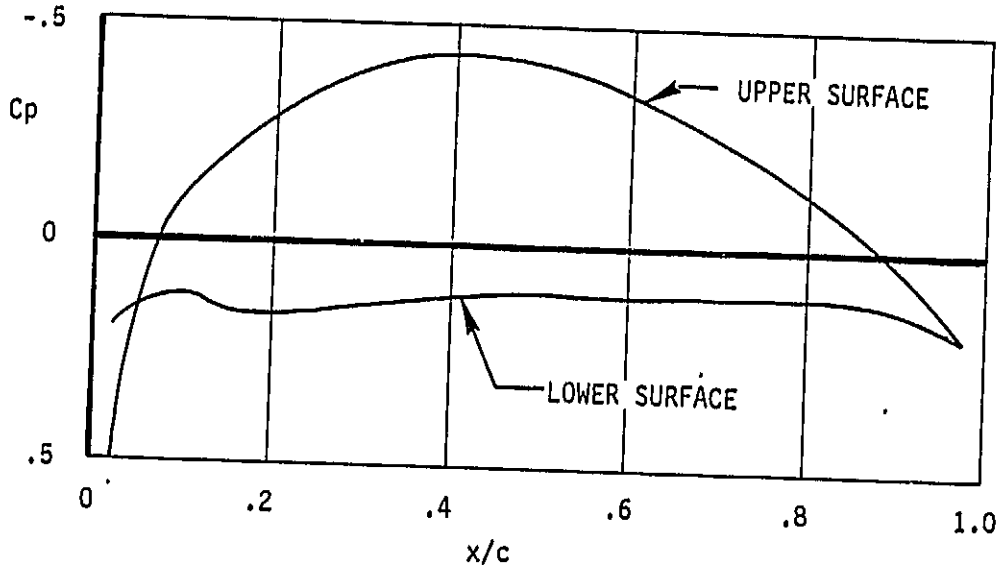

FIGURE 9.1-13 VAPE CALCULATED CHORDWISE PRESSURE DISTRIBUTION $\alpha = 4^{o}$ $\eta = .21$

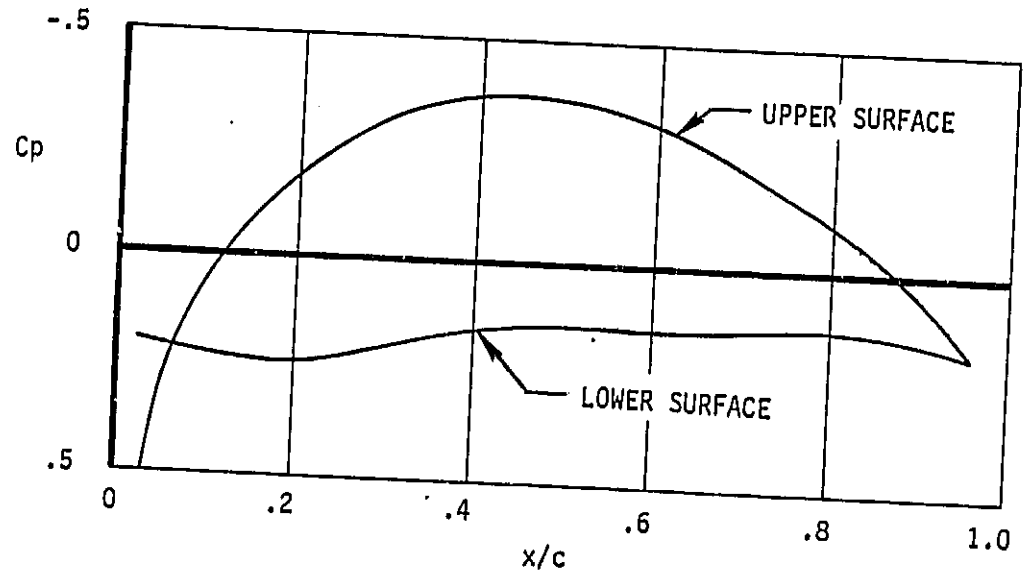

FIGURE 9.1-14 VAPE CALCULATED CHORDWISE PRESSURE DISTRIBUTION $\alpha = 4^{o}$ $\eta = .385$

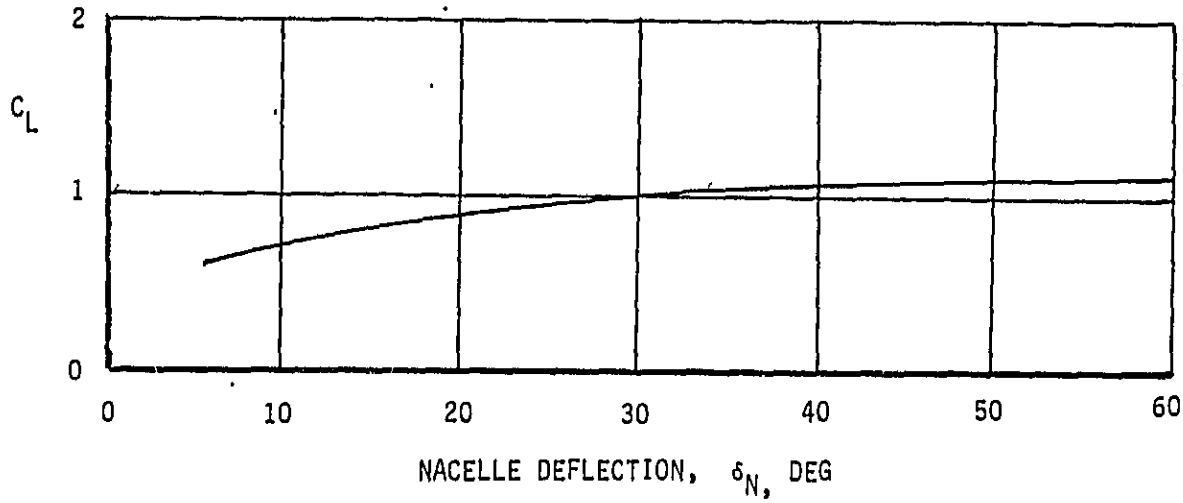

FIGURE 9.1-15 EXPERIMENTAL LIFT COEFFICIENT DUE TO NACELLE DEFLECTION

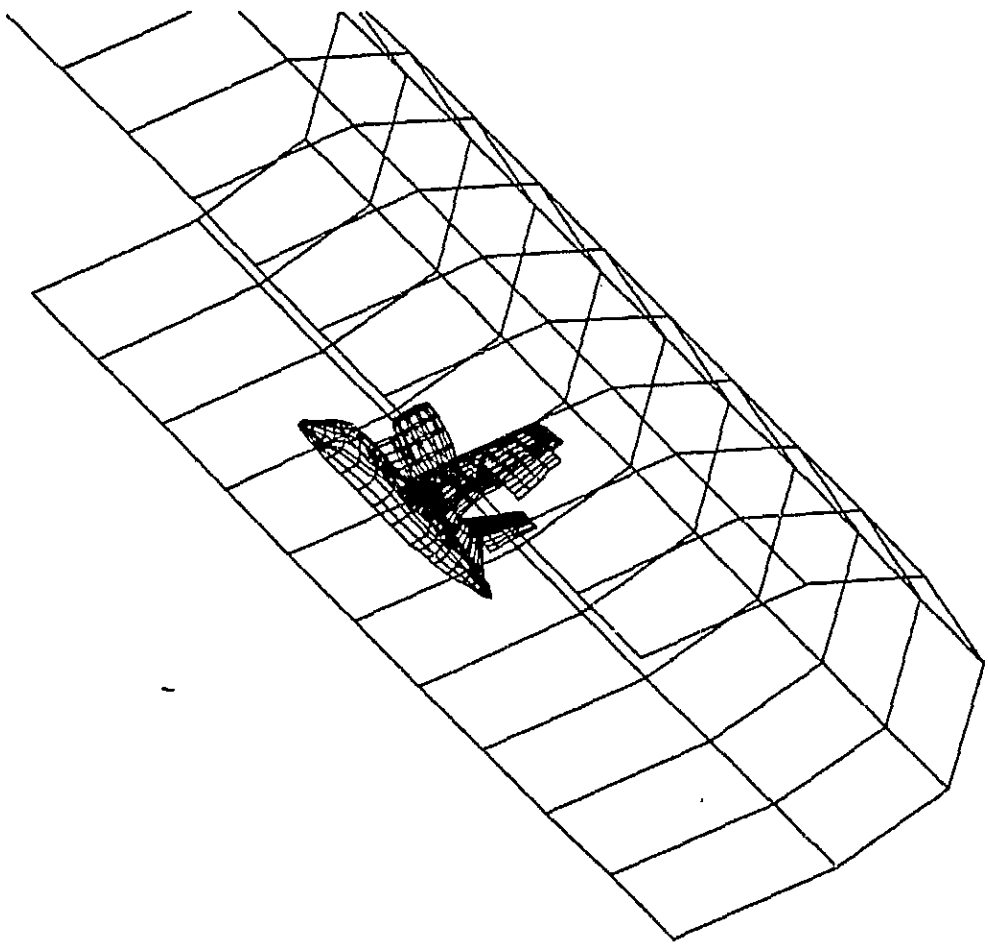

FIGURE 9.1-16 TILT NACELLE MODEL WITH AMES 40 x 80 FOOT WIND TUNNEL WALLS SIMULATED

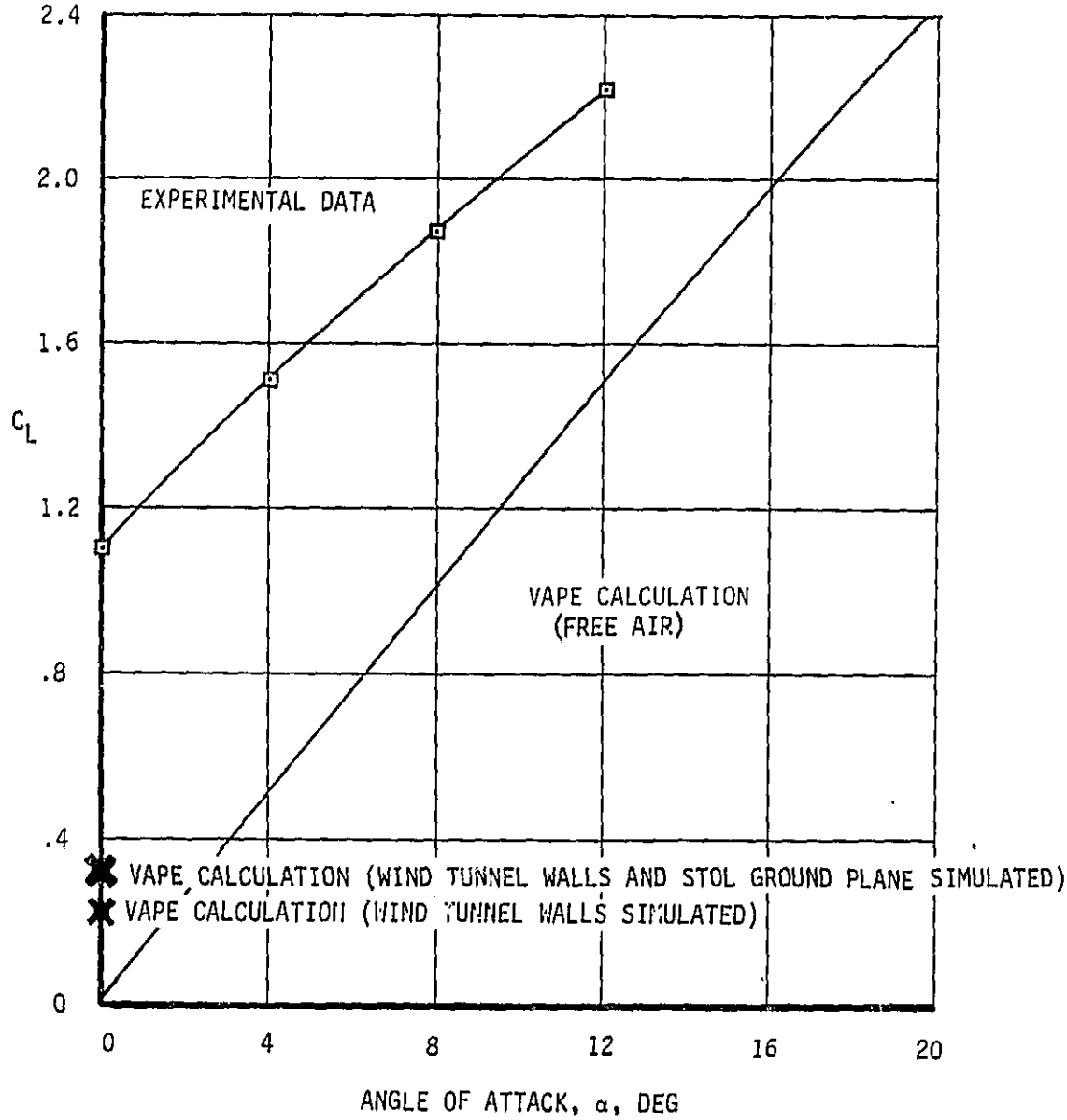

FIGURE 9.1-17 COMPARISON OF VAPE CALCULATED LIFT CURVE TO EXPERIMENTAL DATA FOR THE TILT NACELLE CONFIGURATION WITH THE AMES 40 x 80 FOOT WALLS SIMULATED, $\delta_{Nacelle} = 40^{o}$

9.2 STOL CONFIGURATION

The STOL fighter configuration of reference 9.2-1 was also modeled and some analysis work performed using the VAPE system. The analysis was however, limited due to budget and time constraints.

Figures 9.2-1 and 9.2-2 present pictures of the model as paneled for input to VAPE. This VAPE paneling was obtained by modifications to an existing PANAIR description.

This configuration was an extremely complicated case for VAPE due to the large nacelles and the strake inboard of the nacelles. Also, the thrust deflection device gives jet deflections which are at the edge of the VAPE applicability envelope. Therefore, the analysis of this configuration was begun with a simple case when the jet wake was modeled by a solid tube. This technique has been used successfully before, even though it ignores the jet entrainment. Figures 9.2-3 and 9.2-4 present the VAPE input model which was used. Figure 9.2-5 presents the VAPE predicted lift coefficients compared to experimental values. As can be observed, the C_{L_α} agreement is fair, but is less than the experimental data. The lift curve slope agreement is good. This case was then rerun with the 40 x 80 foot wind tunnel walls to see what effect they would have. Figure 9.2-6 shows this configuration, which was analyzed for zero angle of attack. The results, as shown in Figure 9.2-5, indicate only a very small effect. The reason for the predicted lift being lower in this no-power case has not been determined. Unfortunately, the scope of the contract did not permit further analysis was performed on this configuration to determine what produced this discrepancy or to determine the power effects. It is recommended that such work be pursued in future efforts.

REFERENCES:

9.2-1 Howell, G.A., Crosthwait, E.L., and White, M.C.: "Evaluation of Pressure and Thermal Data From a Wind Tunnel Test or a Large-Scale, Powered STOL Fighter Model," NASA CR-166170, June 1981.

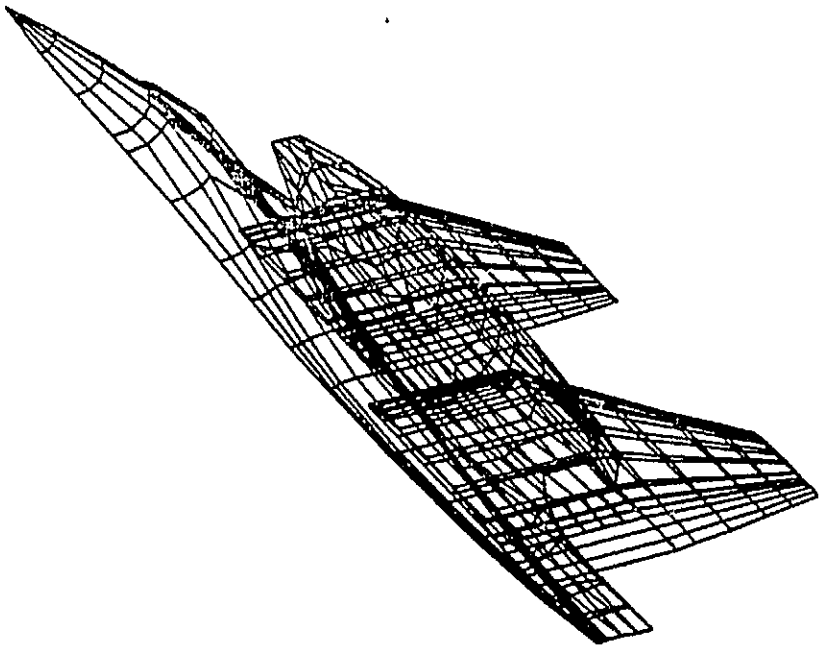

FIGURE 9.2-1 V/STOL FIGHTER MODEL PANELING FOR VAPE

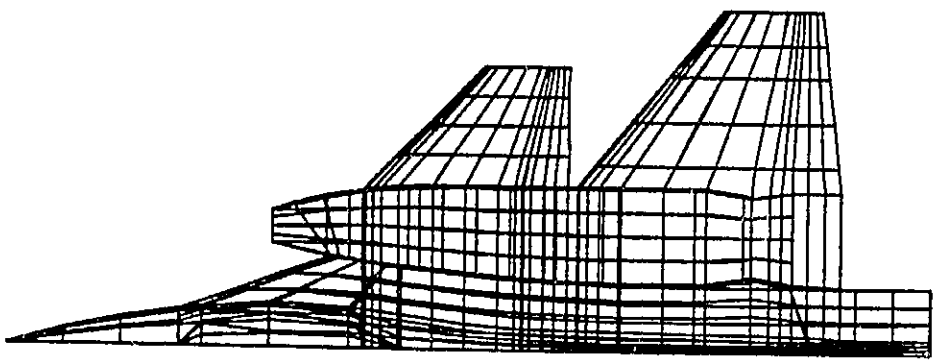

FIGURE 9.2-2 V/STOL FIGHTER MODEL PANELING FOR VAPE, TOP VIEW

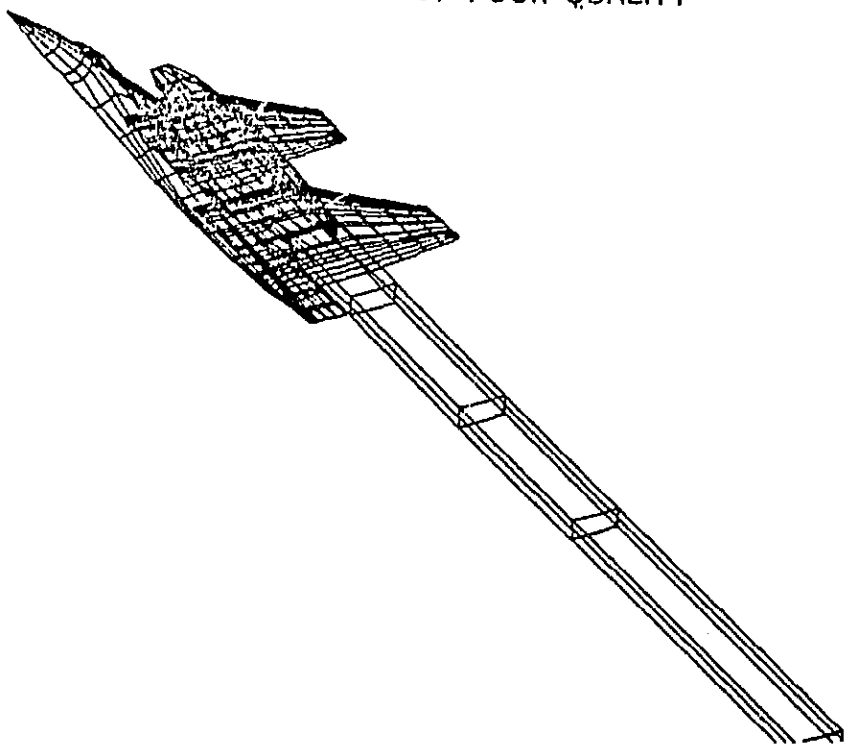

FIGURE 9.2-3 V/STOL FIGHTER MODEL PANELING INCLUDING JET EXHAUST MODEL

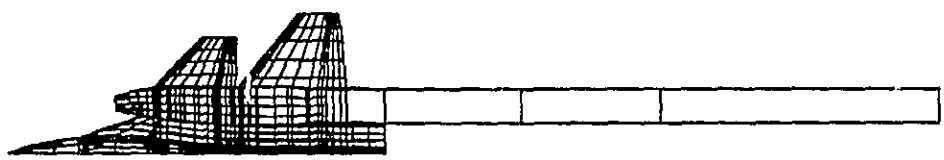

FIGURE 9.2-4 V/STOL FIGHTER MODEL PANELING INCLUDING JET EXHAUST MODEL, TOP VIEW

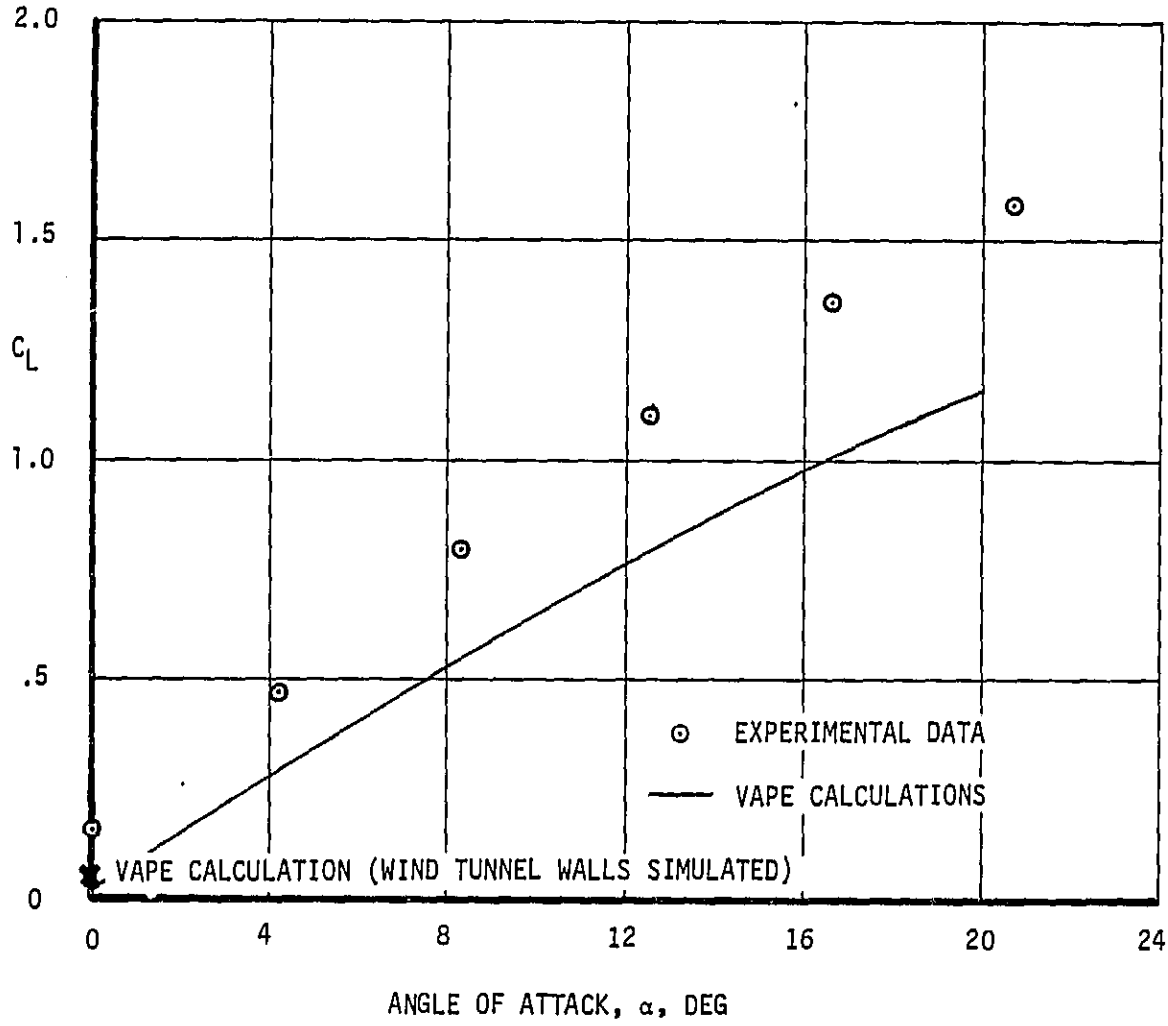

9.2-5 COMPARISON OF VAPE CALCULATED LIFT CURVE TO EXPERIMENTAL DATA FOR STOL FIGHTER MODEL, POWER OFF.

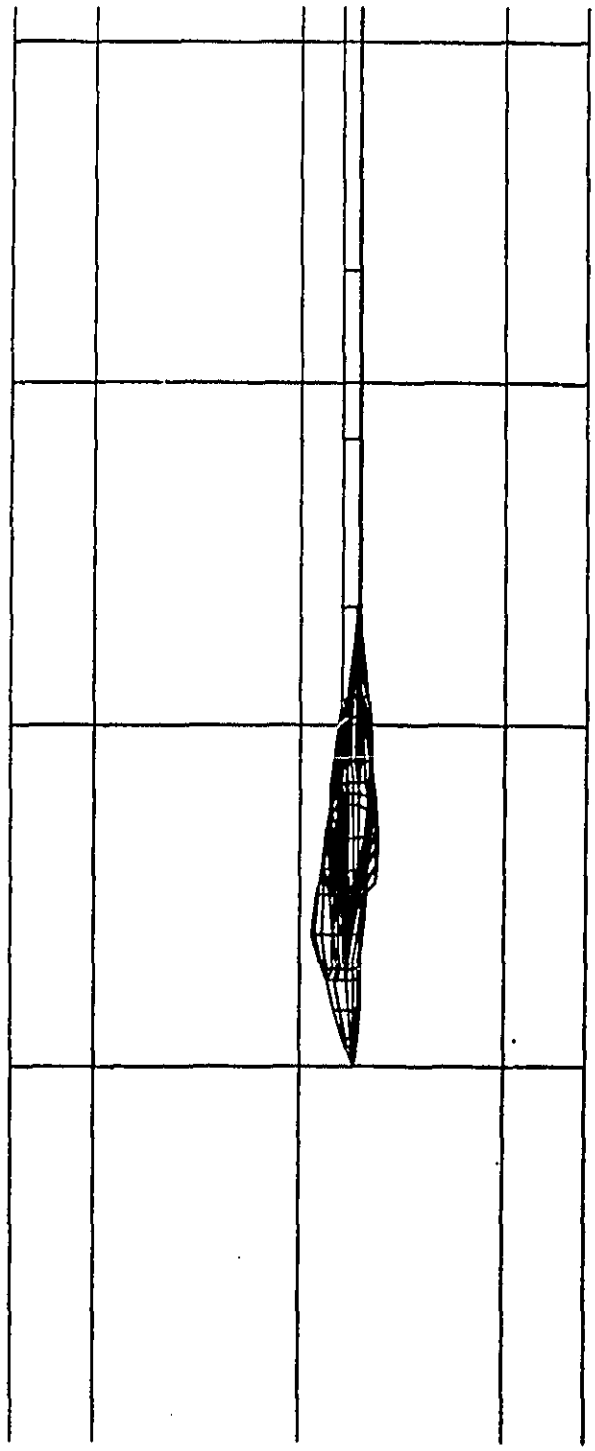

FIGURE 9.2-6 STOL FIGHTER MODEL WITH 40 x 80 FOOT WIND TUNNEL WALLS SIMULATED

10.0 CONCLUSIONS

The VAPE system, initially developed for the Navy, has the potential for being developed into a useable computational tool for analysing V/STOL configurations in the transition region of flight.

This contract effect has improved the VAPE system by the addition of a boundary layer procedure to determine the viscous effects on the lifting surfaces of the configurations. The program has also been validated with experimental data for several configurations. The viscous modification produces results which agree very well with previous NASA results.

The STOL model was substantiated by using NASA experimental data for a STOL configuration the agreement was found to be very good, even when the aircraft was very close to the ground.

The analysis of the rectangular jet model has shown that the current model worked fairly well within its rather limited scope. Additional work is needed on the rectangular jet model to improve both its efficiency and its applicability envelope.

The applicability of VAPE to VATOL configurations was studied and limitations of the current program for these configurations were found.

The analysis of two complex configurations indicate that some discrepancies between prediction and experiment exist. These cases need further work in order to better understand and correct these discrepancies.

In summary, the following have been accomplished during the course of the contract.

(1) A viscous effects option for lifting surfaces has been added to VAPE.

(2) This viscous option has been verified by comparisons of calculated data to experimental data.

(3) The STOL model was verified.

(4) VAPE was evaluated for use on VATOL model and recommendations made.

(5) The rectangular jet model was evaluated and improvements suggested.

(6) Two complex V/STOL models were modeled and analyzed.

The contract has resulted in both an improved VAPE system and in better understanding the codes uses and limitations. The modular system employed in VAPE will permit continued improvements to enhance its accuracy, ease of use and applicability.

11.0 RECOMMENDATIONS

The VAPE system is a large computer code which will continually be updated and improved as new V/STOL technologies develop. This code which began several years ago as a simple combination of the Hess potential flow code and the Wooler Jet method has been expanded to include three different jet codes, an inlet analysis code and a viscous approximation method. All of these additions have been performed in a modular manner and thus can be modified, improved or replaced as required. Continued use of this code by engineers involved in design and analysis will illuminate areas of applicability not currently envisioned. In addition, limitations, problem areas and needed improvements will also be identified.

In the course of this contract several areas where additional work is recommended have been identified. The more important items are listed below, not necessarily in order of importance:

- Improve rectangular jet code
  This code needs to be reprogrammed to better fit the VAPE System. Included in this should be a generalization of the jet and vortex curve definitions, using equations instead of table look ups.

- Extend jet models to include lower jet deflections, including zero degrees jet deflection. This improvement is necessary to properly analyze vehicles in the cruise mode and at the upper end of transition.

- Improve the STOL model by the addition of a vortex, off the ground, to model the upwash due to separation. This condition will improve the STOL model by more realistically describing the physical flow field.

- Investigate the nacelle modelling to determine the best way of analyzing the fan type Nacelles,
  The current limitation to one fan exit may be adequate, but a study should be performed to determine what is the best simulation approach.

- Study the tilt nacelle model to determine why the large lift discrepancies exist,
  The difference shown in lift coefficient for the forty degree deflection case is probably due to separation as explained in the text. Additional runs should be made at lower nacelle deflections to try and verify the method. In addition, further study of this problem will improve the user's understanding of the VAPE system and its applicability to unusual configurations.

- Do additional analysis on the STOL fighter model, including adding power effects. This configuration is a difficult one to analyze due to its complex geometry. Additional studies will improve the user's ability to model and analyze future blended supersonic shapes in the V/STOL flight regime.

- Include a technique for simulating the first order separation effects on both lifting and non-lifting surfaces in VAPE. This requires being able to predict the separation lines on all the surfaces and being able to adequately model the separation region using a potential flow model. Existing methods should be examined and new ones developed if necessary.

In addition, other areas of improvement exist in terms of modelling and input simplification. Also, graphical output can be added since the data sets required are already created. This would enhance the user's ability to visualize the flow field and its effects.